AFML-TR-77-163
PART II

LEVEL

A054023

FRACTURE MECHANICS FOR STRUCTURAL ADHESIVE BONDS, PHASE II
FINAL TECHNICAL REPORT

T. R. Brussat and S. T. Chiu, Lockheed-California Company, and
S. Mostovoy, Materials Research Laboratory, Inc., Glenwood, Illinois 60425

Lockheed-California Company
A Division of Lockheed Corporation
Burbank, California 91520

AUGUST 1978

DDC

DEC 4 1978

F

Final Report July 1977—June 1978

NOTICE

When Government drawings, specifications, or other data are used for
any purpose other than in connection with a definitely related Government
procurement operation, the United States Government thereby incurs no
responsibility nor any obligation whatsoever; and the fact that the govern-
ment may have formulated, furnished, or in any way supplied the said
drawings, specifications, or other data is not to be regarded by implica-
tion or otherwise as in any manner licensing the holder or any other person
or corporation, or conveying any rights or permission to manufacture, use,
or sell any patented invention that may in any way be related thereto.

This technical report has been reviewed and is approved for
publication.

WILLIAM B. JONES, JR., Ph.D.   T. J. REINHART, JR., Chief
Project Monitor   Composite & Fibrous Matls Branch
                                    Nonmetallic Materials Division

FOR THE COMMANDER

J. M. KELBLE, Chief
Nonmetallic Materials Division

"If your address has changed, if you wish to be removed from our mailing
list, or if the addressee is no longer employed by your organization please
notify _____, WPAFB, OH 45433 to help us maintain a current
mailing list."

Copies of this report should not be returned unless return is required
by security considerations, contractual obligations, or notice on a specific
document.

Final rept. 1 Jul 77-30 Jun 78 on
phase 2,

REPORT DOCUMENTATION PAGE	READ INSTRUCTIONS BEFORE COMPLETING FORM

1. REPORT NUMBER AFML-TR-77-163-PT-2	2. GOVT ACCESSION NO.	3. RECIPIENT'S CATALOG NUMBER

4. TITLE (and Subtitle) FRACTURE MECHANICS FOR STRUCTURAL ADHESIVE BONDS, PHASE II - FINAL REPORT	5. TYPE OF REPORT & PERIOD COVERED 1 July 1977 - 30 June 1978
	6. PERFORMING ORG. REPORT NUMBER LR-28652

7. AUTHOR(s) T. R. Brussat, S. T. Chiu, S. Mostovoy	8. CONTRACT OR GRANT NUMBER(s) F33615-75-C-5224

9. PERFORMING ORGANIZATION NAME AND ADDRESS LOCKHEED-CALIFORNIA COMPANY Burbank, California 91520	10. PROGRAM ELEMENT, PROJECT, TASK AREA & WORK UNIT NUMBERS 486U-00-09

11. CONTROLLING OFFICE NAME AND ADDRESS Air Force Materials Laboratory/(MBC) Air Force Systems Command Wright-Patterson Air Force Base, Ohio 45433	12. REPORT DATE August 1978
	13. NUMBER OF PAGES

14. MONITORING AGENCY NAME & ADDRESS(if different from Controlling Office)	15. SECURITY CLASS. (of this report) UNCLASSIFIED
	15a. DECLASSIFICATION/DOWNGRADING SCHEDULE

16. DISTRIBUTION STATEMENT (of this Report)

17. DISTRIBUTION STATEMENT (of the abstract entered in Block 20, if different from Report)

18. SUPPLEMENTARY NOTES

19. KEY WORDS (Continue on reverse side if necessary and identify by block number)

Fracture Mechanics	Crack Propagation
Adhesive Bonds	Fatigue Testing
Test Specimens	Bonded Joints
Mode I, Mode II	Finite Element Analysis

20. ABSTRACT (Continue on reverse side if necessary and identify by block number)

Research results are presented of crack propagation tests and fracture mechanics analysis of laboratory joints and specimens bonded with FM-73 adhesive and containing bondline cracks. New baseline specimens and tests are developed, analyzed, and used for Mode I and mixed-mode fracture mechanics testing of adhesives. Baseline test data are reported for FM-73 including increasing load (fracture toughness) tests in laboratory air and sustained-load, hot-water-immersed tests. Results of fatigue crack growth tests are presented at two stress ratios, two environments, and three cyclic frequencies

DD FORM 1473 EDITION OF 1 NOV 65 IS OBSOLETE

20. ABSTRACT, Continued

for three different baseline specimen geometries and three different mixes of
Modes I and II. Fracture mechanics prediction methodology is demonstrated using
results of nine da/dN tests of structural joint specimens immersed in hot water.
Two different finite element analysis procedures are used to calculate strain
energy release rate as a function of crack size. Then the baseline data en-
able crack growth rate estimation. Multiple cracking is considered based on
measurements of final crack sizes on the fracture surfaces of the failed
specimens. The estimated crack growth rates correlate well with the experimental
data.

PREFACE

This document describes the research conducted for the Air Force
Materials Laboratory (AFML) to fulfill the Phase II objectives of
Contract F33615-75-C-5224. The Structural Methods Group of Lockheed-
California Company had primary responsibility for the project. Materials
Research Laboratory (MRL) was the major subcontractor and performed the
experimental specimen development and baseline testing.

The support and cooperation of Dr. W. B. Jones, the responsible AFML
technical monitor, is greatly appreciated.

TABLE OF CONTENTS

LIST OF ILLUSTRATIONS

LIST OF ILLUSTRATIONS (Continued)

LIST OF TABLES

SECTION I

INTRODUCTION AND SUMMARY

1. <u>INTRODUCTION</u>

This contract began in June 1975, initially as a 27-month effort. The objective was to develop and experimentally demonstrate the fracture mechanics methodology required to predict the growth of bondline flaws in adhesively bonded primary aircraft structural components in service.

The first phase of this work is reported in Reference 1*. Fracture mechanics test specimens were developed, baseline data generated, predictions made of the growth of bondline flaws in structural-type joints, and fatigue tests conducted on these joints with preexisting bondline flaws. All test specimens were bonded using 7075-T6 bare aluminum adherends, phosphoric acid anodize surface treatment, and BR-127A primer, as used in the PABST program. However, the adhesive used was AF-55S, not the eventual PABST selection, FM-73m.

The project reported herein was initiated 1 July 1977 as Phase II of this contract. The objective of this project was to extend the Phase I results to be directly applicable to the fuselage structure being developed in the PABST program. The approach was similar to that of Phase I. The main new aspects planned were:

- Use of FM-73m adhesive.

- Development and use of a new Mode I specimen, the Width-Tapered Beam (WTB) specimen, which can be machined from large area bonded panels.

---

*Reference 1. Brussat, T. R., Chiu, S. T. and Mostovoy, S. "Fracture Mechanics for Structural Adhesive Bonds - Final Report," AFML-TR-77-163, Part I, October 1977.

1

- Processing and bonding all the specimens in the test program in one continuous operation. This tends to minimize extraneous fabrication variables and maximize the validity of analyzing the data to estimate the effects of test variables. (Unfortunately it became necessary to deviate from this plan and bond additional specimens for retest, as discussed in Section IV.)

2. SUMMARY OF PHASE I RESULTS

Results and conclusions from Phase I of this research, reported in Reference 1, set the direction for the Phase II effort. Therefore, the key Phase I results are reviewed here, as follows.

Fracture mechanics methodology was developed and experimentally demonstrated for the prediction of the growth of bondline flaws in an adhesively bonded structure. This work was considered to be an initial step toward providing the technology required to assess the influence of possible preexisting bondline flaws on the structural integrity of aluminum adhesively bonded fuselage structures.

Test procedures and analytical relationships were developed for the Cracked Lap Shear (CLS) specimen. The ratio $\mathcal{G}_I/\mathcal{G}$ for this specimen was found to be about 0.2, which is typical of many structural applications involving large area bonds. (The exact value of $\mathcal{G}_I/\mathcal{G}$ depends upon relative adherend thicknesses and whether or not the specimen is side notched.) The value of $\mathcal{G}$ is independent of crack length, which simplifies the monitoring of tests. The specimen can be machined from large area bonded plates which are cured under exactly the same conditions as used for the structure, a feature not possible with the Mode I Contoured Double Cantilever Beam (CDCB) specimen. The CLS specimen as used is very long to maximize the applicability of a mathematical analysis which ignores end effects. Side notching was a successful way to increase the stresses in the bondline so as to induce bondline cracking prior to metal failure. As a result of the work reported in Reference 1, the use of the CLS specimen was recommended for mixed Mode I and Mode II fracture mechanics testing of structural adhesives.

Increasing-load tests of 48 CDCB specimens bonded with AF-55S adhesive resulted in a mean $\mathcal{G}_{Ic}$ value of 2.24 kJ/m^2 (12.78 lb/in). Limited increasing

load data from side-notched CLS specimens suggested that the addition of large amounts of $\mathscr{G}_{II}$ loading does not significantly reduce the critical value of $\mathscr{G}_I$ at the onset of crack instability. Because this high value of $\mathscr{G}_{Ic}$ is maintained for mixed-mode loading, a structure bonded with AF-55S adhesive exhibits a very high resistance to crack growth in the adhesive layer when subjected to a monotonically increasing load in room temperature air. However, in pure Mode I, fatigue crack propagation of bondline cracks can occur at values of $\Delta\mathscr{G}_I/\mathscr{G}_{Ic}$ of 0.1 or less, and the Mode II component has a definite detrimental effect on da/dN. Therefore, fatigue (and also environmentally induced crack growth) tend to be the critical conditions for the adhesive system. A recommendation was made that greater emphasis be placed on fatigue and environmental effects in the fracture mechanics testing of adhesives.

Mode I stress corrosion cracking data for AF-55S adhesive and BR-127A primer in $333^{\circ}K$ ($140^{\circ}F$) water seemed to show a strong dependence on adherend surface treatment method. Specimens prepared by FPL etch failed near the metal/primer interface. Specimens prepared by the Phosphoric Acid Anodize process failed cohesively within the adhesive, and the crack growth rates were up to three orders of magnitude slower at the same sustained value of $\mathscr{G}_I$. A confident estimate of the threshold value of $\mathscr{G}_{ISCC}$ could not be obtained because of practical limitations on test time.

The most important loading variable in the propagation of a bondline crack seemed to be $\mathscr{G}_I$, the Mode I component of strain energy release rate. However, fatigue testing of CDCB and CLS specimens showed a significant effect of $\mathscr{G}_{II}$ on da/dN. When da/dN data were plotted as functions of $\Delta\mathscr{G}_I$ only, the CLS data were segregated to the left of the CDCB data (that is, at higher da/dN values for the same value of $\Delta\mathscr{G}_I$). Based on these data, an effective strain energy release rate, $\Delta\mathscr{G}_{eff}$, was defined as follows to account for the interaction of $\mathscr{G}_I$ and $\mathscr{G}_{II}$ on the fatigue crack growth rate in AF-55S adhesive:

$$\Delta\mathscr{G}_{eff} = (1 + \frac{2\mathscr{G}_{II}}{\mathscr{G}})\Delta\mathscr{G}_I \tag{1}$$

The empirical relationships between da/dN and $\Delta \mathscr{G}_I$ obtained from Mode I testing could then be extended to mixed Modes I and II by replacing $\Delta \mathscr{G}_I$ with $\Delta \mathscr{G}_{eff}$. It was recognized that, for other adhesives, a slightly modified definition of $\Delta \mathscr{G}_{eff}$ may be needed, but the same general approach was expected to apply. In future testing of other adhesive systems, a recommendation was made to test both pure Mode I specimens and mixed-mode CLS specimens in fatigue and establish a specific definition of $\Delta \mathscr{G}_{eff}$ for use in data interpolation.

The slope of the plot of log (da/dN) versus log ($\Delta \mathscr{G}_{eff}$) for adhesives was observed to be much steeper than that for metallic materials. This means that small changes in stress cause large changes in crack growth rate. Furthermore, small errors in estimated stress cause large errors in estimated crack growth life. This makes it difficult to design for finite life. Thus, an estimated value of $\Delta \mathscr{G}_{Ith}$, the no-growth threshold, was identified as an important design parameter.

At the same time, it was recognized in Reference 1 that crack growth threshold data are expensive to obtain because of the long test times required. This is even more true in adhesives than in metals because the adhesive is time dependent (so high-frequency values of $\Delta \mathscr{G}_{Ith}$ may be misleading), and the increment of crack growth required for a confident measurement of da/dN is substantially longer in adhesives than in metals. Therefore, the recommendation was made to estimate $\Delta \mathscr{G}_{Ith}$ by linearly extrapolating the da/dN curve downward in log-log space to a crack growth rate of 1 mm per year (1 in. per 25 years). This procedure tended to give a usable threshold value for AF-55S by virtue of the steepness of slope of the da/dN curve.

The cyclic frequency effect on da/dN (particularly in laboratory air) was shown to be stronger for bondline cracks in AF-55S adhesive than is typical for cracks in metal. Thus, laboratory testing at high cyclic frequency (say, 30 Hz) was seen to have at least two drawbacks. First, the use of da/dN curves obtained at high frequency for prediction of crack growth in service at a slower frequency would be unconservative. Secondly, because the metal da/dN properties do not significantly improve with increasing

4

frequency, testing at high frequency may cause metal failure before the bond-line crack growth data can be obtained. For the Phase I research with AF-55S, a cyclic frequency of 3 Hz was believed to be a good compromise between the inapplicability of results obtained at high frequency and the costliness of testing at low frequency. Past work on other adhesive systems had indicated that the frequency effect in laboratory air can be negligible in the range $0.1 \text{ Hz} \leq f \leq 3 \text{ Hz}$. Further study of time/frequency/environment interaction effects and extended-time da/dN testing of adhesives was recommended to determine general guidelines for selection of cyclic test frequencies.

Crack growth rates in AF-55S from fatigue tests in 333°K (140°F) water were significantly faster than in laboratory air. Some fatigue testing in the extremes of the anticipated service environment was therefore recommended to obtain applicable baseline data for prediction.

Even with a preflaw in the adhesive layer, there was a tendency for bonded thin-sheet structure to fail in the adherend. The following means were used in the simulated structural tests to increase the tendency for the bondline crack to propagate without adherend yielding:

- Increase the adherend thickness

- Increase $\mathcal{K}_I$ by increasing the induced bending moment at the crack tip

- Load in fatigue rather than by a single increasing load

- Use a warm, moist environment

The use of these means was successful in that 9 of the 12 simulated structural specimens bonded with AF-55S adhesive failed by fatigue crack growth in the bondline.

The bonded structural single lap joints exhibited very little sensitivity to initial flaw size. Some specimens were unflawed, some had an initial across-the-width bondline flaw, and some had flaws only partially across the width. Despite these differences, the lives of all thick adherend specimens tested in laboratory air were within a factor of 2.0 of one another, and (except for one specimen which failed prematurely due to an inadvertent machining flaw in the metal doubler) the lives of the thin adherend specimens tested in 333°K (140°F) water were within a factor of 1.21 of one another.

For the single lap joint geometry, the stress concentration at the gap of the joint is high, so a small flaw originating there grows rapidly at first and then decelerates. This was seen as the reason that the crack growth life-times were so insensitive to flaw size. It was recognized that there may be other bonded structural configurations with flaw size sensitivity more similar to that of conventional metal structure with cracks in the metal. Therefore, further consideration of flaw sensitivity was recommended to learn more about the importance of the initial size of bondline flaws.

Since the cracks could not be visually monitored, two methods of flaw growth monitoring were used in the structural tests of Reference 1, a direct contact ultrasonic method and a compliance method. The ultrasonic method utilized transducers in direct contact with the specimen. The compliance method measured periodically the opening displacement of the gap of the joint and compared it to finite-element-computed displacement estimates for a series of assumed crack lengths. The compliance method was more reliable and less expensive to use than the ultrasonic method, but the information on flaw shape and location obtained ultrasonically could not be obtained by the compliance method.

A fracture mechanics method for predicting the growth of bondline flaws was demonstrated and evaluated. A finite element analysis of the structural single lap joint specimens was used to compute bending and axial stresses. From these, approximate values of $\mathscr{G}_I$, $\mathscr{G}_{II}$, and $\Delta \mathscr{G}_{eff}$ were estimated. Crack growth in the adhesive layer was then estimated using the baseline da/dN data. Calculations for the thick adherend specimens were completed after testing. However, those for the thin adherend specimens were done prior to testing. The predicted crack growth lives were about twice the actual lives. In the prediction, the assumption was made that only one crack would grow, but in the actual specimens, two cracks propagated simultaneously in the same fracture surface. It was suggested that this might account for the factor of 2 error in the prediction; however, in light of the sensitivity of the adhesive crack growth process to small variations in estimated stress, it was felt that larger errors than a factor of 2 could reasonably be expected for crack growth life predictions.

6

Continued efforts were recommended to apply linear elastic fracture mechanics theory for predicting the growth of bondline cracks in structural adhesive joints. As a continuation of the work reported in Reference 1, the research reported herein was recommended to extend the above results to be applicable to the PABST program, using the selected PABST adhesive, FM-73m. It was anticipated that this work would demonstrate the generality of the baseline testing and analytical methods of Reference 1 and provide data specifically applicable to the PABST program.

Finally, Reference 1 pointed out the need for further research to extend MIL-A-83444 to apply it to bondline flaws. These future efforts would include development of criteria for initial flaw size and type, and evaluation of the impact of such criteria on the design of bonded structure.

3. THE PHASE II PROGRAM

The primary objective of the Phase II program was to extend the results and conclusions of Phase I to be directly applicable to PABST. To do this, it was necessary to:

(1) Demonstrate that the fracture mechanics methodology will work when FM-73m adhesive is used:

- That baseline testing is still possible with the same or with improved specimens and test conditions.

- That the accuracy of the analytical methods is maintained.

- That the conclusions and recommendations from Reference 1 apply to FM-73m adhesive as well as to AF-55S.

(2) Provide data for the application of fracture mechanics methodology to PABST structure:

- FM-73m adhesive baseline data

- Conditions applicable to PABST anticipated service environment

- Definition of criticality of various conditions for this adhesive

7

While accomplishing the above, the validity of test comparisons was increased by bonding all specimens as large area bonded panels using standard industry bonding practices.

Specimen development work on the three baseline test specimens used is described in Section II of this report. This includes a finite element analysis of the cracked lap shear (CLS) specimen, experimental compliance calibrations and fatigue feasibility tests on the width-tapered beam (WTB) specimen, and establishment of da/dN data analysis methods for the uniform double cantilever beam (UDCB) specimen. In addition, a four-point bend test procedure for the CLS specimen was developed, and two specimens were tested.

Baseline test results are reported in Section III. Increasing-load (fracture toughness) tests in laboratory air and sustained-load tests in $333^\circ K$ ($140^\circ F$) water were conducted on CLS and WTB specimens. The emphasis, however, was on da/dN testing, covering the following conditions:

- Two stress ratios: R = 0.1 and 0.6.

- Two environments: laboratory air and $333^\circ K$ ($140^\circ F$) deionized water.

- Three specimen geometries: CLS, WTB and UDCB.

- Three cyclic frequencies: f = 0.3 Hz, 3 Hz, and 15 Hz.

Not all combinations were tested. The baseline fatigue tests that were conducted are summarized in Table 9 of Section III.

Section IV demonstrates the use of fracture mechanics methodology in the estimation of crack growth in the structural specimens. A surface preparation problem on the first set of structural specimens led to premature failures in the primer-metal interface, necessitating the testing of a second set of specimens. Five of these were tested with improved results. As in Reference 1, a finite element analysis was used to estimate strain energy release rate as a function of crack size, and the baseline da/dN data were then used to obtain crack growth estimates. This time, however, the analysis also considered multiple cracking.

In Section V, conclusions and recommendations from this Phase II research are presented and compared to those of Phase I as reported in Reference 1.

8

SECTION II

SPECIMEN DEVELOPMENT

Three different baseline specimens were tested in this program, the combined Modes I and II Cracked Lap Shear (CLS) specimen, axially loaded and in uniform bending, and two pure Mode I specimens, the Width-Tapered Beam (WTB) and the Uniform Double Cantilever Beam (UDCB) specimen. A great deal of development work on the CLS specimen had been conducted during Phase I of this contract and is reported in Reference 1. However, estimation of $\mathscr{G}_I$ required an assumption that needed to be checked by an independent method, such as a finite element analysis. The details and results of this analysis are presented in Subsection 1.

The WTB specimen was introduced for use in Phase II testing as a replacement for the standard Mode I CDCB specimen. In bonding the CDCB specimen during Phase I, it had been difficult to achieve a consistent bondline quality and bondline thickness of 0.13 to 0.20 mm (0.005 to 0.008 in.). The source of the problem was the low viscosity of AF-55S adhesive at the cure temperature, $394^{\circ}K$ ($250^{\circ}F$). The bondline in the CDCB specimen is only 13 mm (0.5 in.) wide, and at standard cure temperatures and pressures used for bonding aircraft structure, most of the adhesive flows out and escapes. Thus, it was necessary to use shims or lower bonding pressures to obtain a reasonable bondline thickness in these specimens. The resulting inconsistencies led to variations in $\mathscr{G}_{IC}$ but appeared not to affect fatigue crack growth rates. Nevertheless, these inconsistencies detracted from the validity of the data and from their applicability to large-area bonded structures.

The viscosity of FM-73m at cure temperature is as low or perhaps even lower than that of AF-55S. Therefore, use of the narrow CDCB specimen was abandoned in favor of the WTB, a Mode I configuration that can be machined from a large-area bonded panel. Specimen development tests were performed to

9

demonstrate that the WTB specimen could be tested, instrumented, and analyzed. Experimental compliance calibration was used to determine the functional dependency of $\mathcal{G}$ upon applied load P and crack length a, using specimens of various crack lengths bonded with AF-55S. The da/dN data obtained in pre-cracking those specimens provided a comparison of the pure Mode I da/dN properties of large-area bonded panels and the narrow CDCB specimens, both bonded with AF-55S and tested in laboratory air at R = 0.1 and f = 3.0 Hz. Analysis of the compliance data resulted in the loading holes being moved axially toward the crack tip in order to achieve an approximately constant $\mathcal{G}$, independent of crack length. This altered loading hole location was used on all the FM-73m WTB specimens tested in the program. Development of the WTB specimen is summarized in Subsection 2.

The WTB specimen is up to 63 mm (2.5 in.) wide, and crack tunnelling occurs. Because of the tunnelling, there was some uncertainty about the accuracy of analysis of the WTB specimen, which is based on compliance measurements of specimens with straight (Teflon tape) crack fronts. Therefore, the primary Mode I data were confirmed using the UDCB specimen. The analysis of this specimen, which has been presented previously, is summarized in Subsection 3.

1. <u>CLS SPECIMEN</u>

1.1 <u>Analysis and Test Procedures for Axial Tension Loading (Reference 1)</u>

The long cracked lap shear (CLS) specimen is shown in Figure 1. Because of its resemblance to typical bonded structures, it provides baseline data that are relevant to structures. Also, since axial loading of the CLS specimen leads to predominantly Mode II stresses at the crack tip, pre-dictions for a structure exhibiting an intermediate mode ratio can be ob-tained by simple interpolation between baseline results from an axially loaded CLS specimen and those from a pure Mode I specimen.

Analysis of test data from this specimen requires a capability to estimate the crack length and the Mode I and Mode II components of strain energy release rate. The crack length is monitored indirectly by means of a measured separation between the two adherends. A theoretical expression
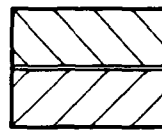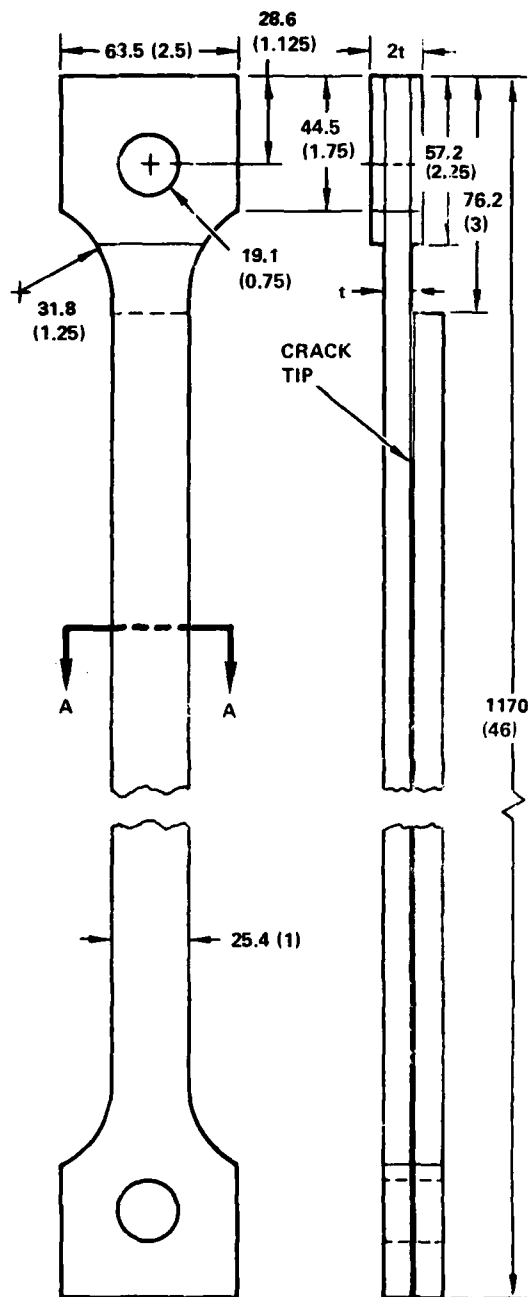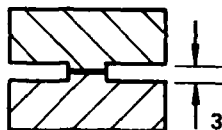
10
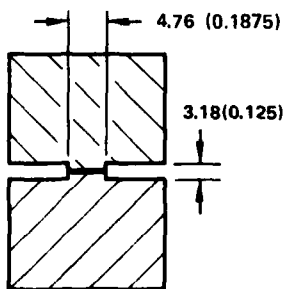
Figure 1.   Cracked Lap Shear (CLS) Specimen

11

relating this separation to the crack length is obtained in Reference 1 from
a beam-theory analysis of the specimen. The strain energy release rate com-
ponents are estimated from the calculated virtual change δW in strain energy
due to a virtual crack extension δa; that is

$$\mathcal{G} = \lim_{\delta a \to 0} \left(\frac{\delta W}{b_N \delta a} \right) \tag{2}$$

where b_N is the width of the bondline.

A schematic of the specimen under axial load is shown in Figure 2. In
general, it may be side notched, so that the width b_N of the bondline may
be less than the nominal width of the metal adherends. Also the adherend
materials, thicknesses, and cross-sectional shapes may differ from one
another. Let $(EI)_2$ and $(EA)_2$ denote the bending and tensile stiffnesses
of the loaded single adherend on the right-hand end of the specimen. Like-
wise let $(EI)_0$ and $(EA)_0$ denote the bending and tensile stiffnesses of the
two-layer beam at the left-hand end of the specimen. Let y_2 be the location
of the centroid on the right-hand end, and let y_0 be the location (measured
from the same reference axis) of the stiffness-adjusted centroid of the two-
layer beam on the left-hand end.
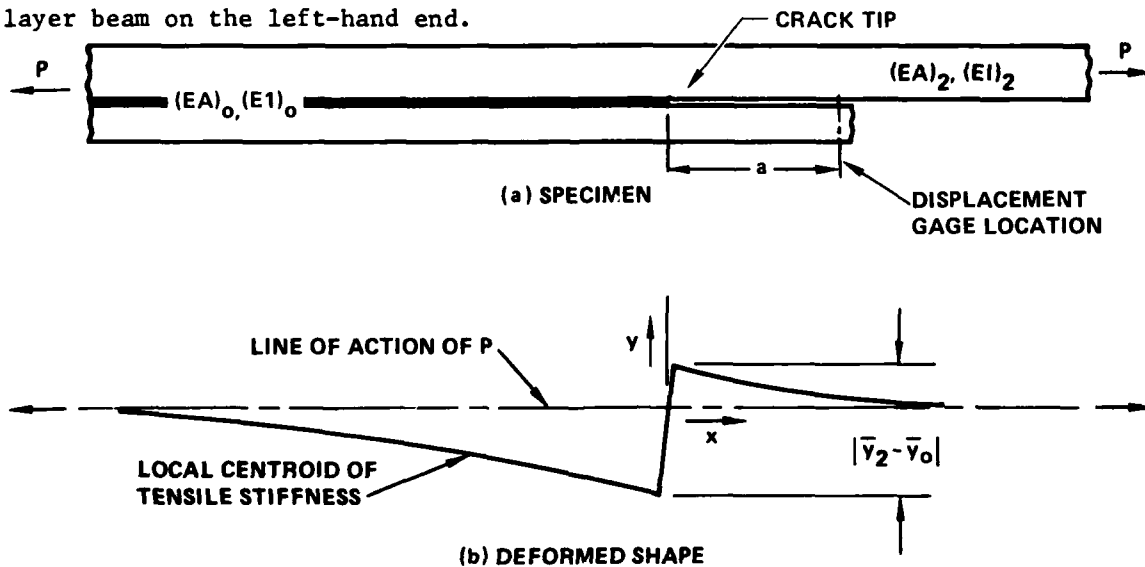
Figure 2. CLS Specimen and Its Deformed Shape

On the left-hand end of the specimen, the applied tensile load P distributes proportionally between the two adherends, while on the right-hand end, P is carried in adherend 2. As shown, the adhesive layer terminates at a crack tip. In addition to the obvious Mode II crack tip loading, there is a significant Mode I component due to the eccentricity of the load path at the crack tip.

In the test a displacement gage is placed a distance "a" to the right (Figure 2) of the crack tip. The separation of the two adherends is monitored as the measure of crack length, and is obtained from the beam-theory solution as

$$\Delta(a) = \frac{(\bar{y}_2 - \bar{y}_o)\lambda_o}{\lambda_2 + \lambda_o} \left(e^{-\lambda_2 a} + \lambda_2 a - 1 \right) \tag{3a}$$

where

$$\lambda_2 = \sqrt{P/(EI)_2} \tag{3b}$$

$$\lambda_o = \sqrt{P/(EI)_o} \tag{3c}$$

The total strain energy release rate due to a tensile load P is calculated using Equation (2). The result is

$$\mathscr{G} = \mathscr{G}_I + \mathscr{G}_{II} = \frac{P^2}{2b_N(EA)_2} \left[1 - \frac{(EA)_2}{(EA)_o} \right] \tag{4}$$

The Mode I component, $\mathscr{G}_I$, is caused by the induced bending moment at the crack tip. The assumption is made in Reference 1 that $\mathscr{G}_I$ due to the induced bending moment is equivalent to $\mathscr{G}_I$ due to a remotely applied uniform bending moment, calculated using Equation (2), and is given by

$$\mathscr{G}_I = \frac{2M^2}{7b_N(EI)_2} \left[1 - \frac{(EI)_2}{(EI)_o} \right] \tag{5}$$

When an expression for the induced crack-tip bending moment, available from the beam-theory solution, is substituted into (5), the result is

$$\mathscr{G}_I = \frac{2(\bar{y}_2 - \bar{y}_o)^2 P^2}{7b_N(EI)_o} \left[\frac{\sqrt{(EI)_o/(EI)_2} - 1}{\sqrt{(EI)_o/(EI)_2} + 1} \right] \tag{6}$$

1.2 Finite Element Analysis

Finite element analyses were conducted to calculate the Mode I and Mode II components of the strain energy release rate for the long Cracked Lap Shear (CLS) specimen. The objective was to independently check the accuracy of the assumptions that were necessary in obtaining the algebraic solutions, Equations (4) and (6).

The utilization of special crack-tip finite elements has been useful in obtaining stress intensity factors for crack problems directly by the finite element method. However, the problem of a CLS specimen with axial loading is geometrically nonlinear. Such nonlinear problems can be solved using a differential stiffness approach available in the Calac-NASTRAN finite element analysis system, but not when specialized crack elements are used, because the approach requires an additional geometric matrix which is not available for these elements. Therefore, a two-step procedure was adopted. The first step was a nonlinear analysis of the entire specimen using standard elements to obtain the bending moment distribution. The second step was a linear analysis of a region around the crack tip using the special crack tip element, in order to determine directly the stress intensity factor components. The boundary conditions for the second model were obtained from the results of the first.

The linear model of the crack-tip region is shown in Figure 3(a). A singular crack-tip membrane element was used to model the adherends in the crack-tip region, and quadrilateral membrane elements were employed elsewhere. The adhesive was not modeled, because the solution being sought was the strain energy release rate for the geometrically equivalent homogeneous cracked body.

14
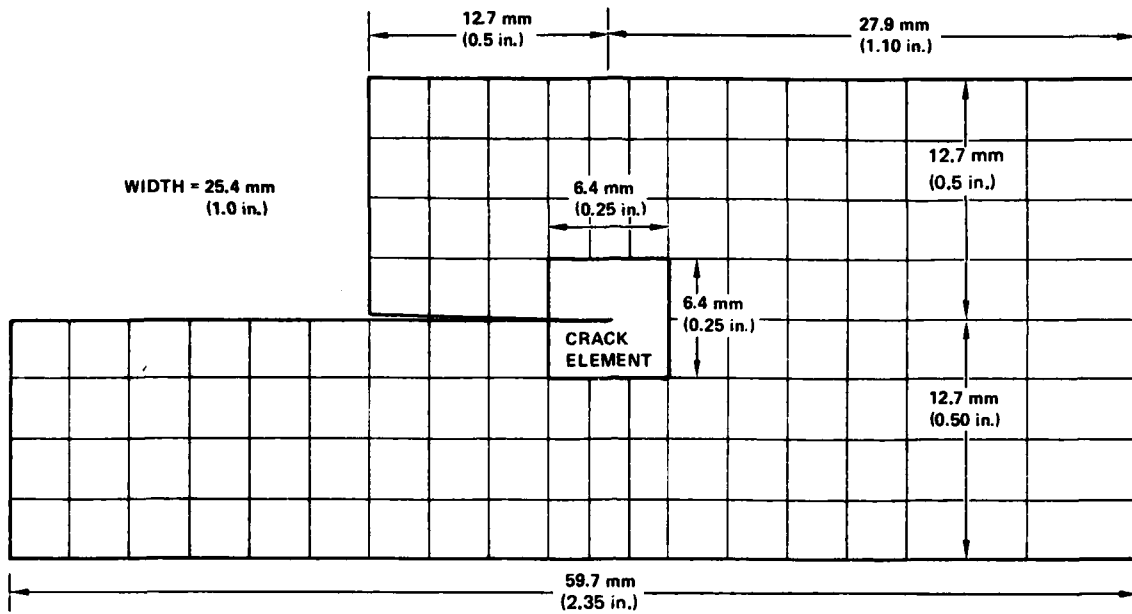
(a) FINITE ELEMENT GRID

	LOADS			BENDING MOMENTS	
	kN	kip		Nm	in-lb
P_{11}	57.826	13.000	M_1	55.10	487.7
P_{12}	00.685	0.154	M_2	28.90	255.8
P_{21}	14.139	3.179	M_3	29.88	264.5
P_{22}	0.523	0.118			
P_{31}	43.681	9.810			
P_{32}	0.634	0.143			
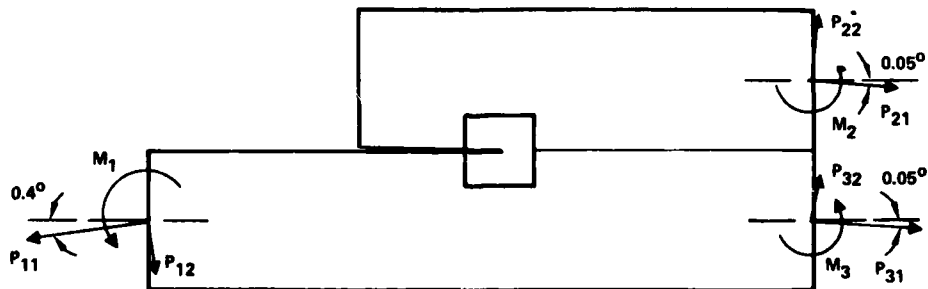
(b) BOUNDARY CONDITIONS OBTAINED FROM NONLINEAR ANALYSIS, AXIAL LOADING

Figure 3.   Crack Tip Region of the CLS Specimen

15

A closed-form stress intensity solution is available from beam theory for the CLS specimen in pure bending, so this loading condition was used to test the finite element model. The solutions for the Mode I and Mode II components of strain energy release rate are shown in Table 1.

A second test case for the model was a combined bending-tension load. The applied bending moment, $M = 95.91$ Nm (848.9 in-lb), was equal to the induced moment at the crack tip calculated for a pin-loaded CLS specimen with an axial load P of 57.827 kN(13.0 kip). The results given in Table 1 show a good correlation between the finite element and algebraic solutions, indicating that the linear model can be accurate for estimating $\mathscr{G}_I$ and $\mathscr{G}_{II}$.

Having gained confidence in the linear finite element model of the crack-tip region, it was used to analyze the axially-loaded CLS specimen. The bending moments, loads and element rotations obtained from the nonlinear analysis of the entire specimen were applied to the linear model as shown in Figure 3(b). Results are compared to the approximate analytical results in Table 2. The results match closely, even though the bending moment at the crack tip results, not from pure applied bending alone, but rather a combination of applied moments and eccentrically applied loads. This confirms the approximate analytical solution for the equal-adherend-thickness CLS specimen in tension.

1.3 Four-Point Bend Test of CLS Specimens

Late in the research program, a decision was made to check and improve the formula for interpolating between the da/dN data for the axially loaded CLS specimen ($\mathscr{G}_I/\mathscr{G} = 0.2$) and the pure Mode I specimens by testing a specimen with an intermediate value of $\mathscr{G}_I/\mathscr{G}$.

For this purpose, two CLS specimens were shortened to a length of 0.6 m (2 ft.) and cyclically loaded in symmetric four-point bending as shown schematically in Figure 4. The test fixture was such that the compressive actuator load, Q, was transmitted to the specimen through a rocker arm which contacted the specimen at the two inner support points. The symmetry of the support point locations and the rotational freedom of the rocker arm assured equal loads of magnitude Q/2 at each support point. Thereby, a

TABLE 1.

FINITE ELEMENT MODEL TEST CASES

Test Case Description	Calculated Quantity	Algebraic Solutions	Finite Element Solutions
Pure Bending	$\mathscr{G}_I/\mathscr{G}$	0.571	0.570
	$\mathscr{G}_{II}/\mathscr{G}$	0.429	0.430
	$\mathscr{G}/\mathscr{G}_{ALG}$	1.000	1.009
Combined Tension – Bending: P = 57.827 kN (13 kip) M = 95.91 Nm (848.9 in-lb.)	$\mathscr{G}_I/\mathscr{G}$	0.206	0.200
	$\mathscr{G}_{II}/\mathscr{G}$	0.794	0.800
	$\mathscr{G}/\mathscr{G}_{ALG}$	1.000	1.021

TABLE 2.

STRAIN ENERGY RELEASE RATES, CLS SPECIMEN IN TENSION

	Algebraic Solution [1]	Finite Element Solution [2]
$\mathscr{G}_I/\mathscr{G}$	0.206	0.218
$\mathscr{G}_{II}/\mathscr{G}$	0.794	0.782
$\mathscr{G}/\mathscr{G}_{ALGEBRAIC}$	1.000	1.025

NOTES: (1) The algebraic solution is calculated based on M = 95.91 Nm (848.9 in.-lb) and P = 57.83 kN (13.00 kip). The same loading condition is used in Table 1.

(2) Loading condition shown in Figure 4. Note that on the left-hand side M_1 = 55.10 Nm (487.7 in-lb) and P_1 = 57.83 kN (13.00 kip).
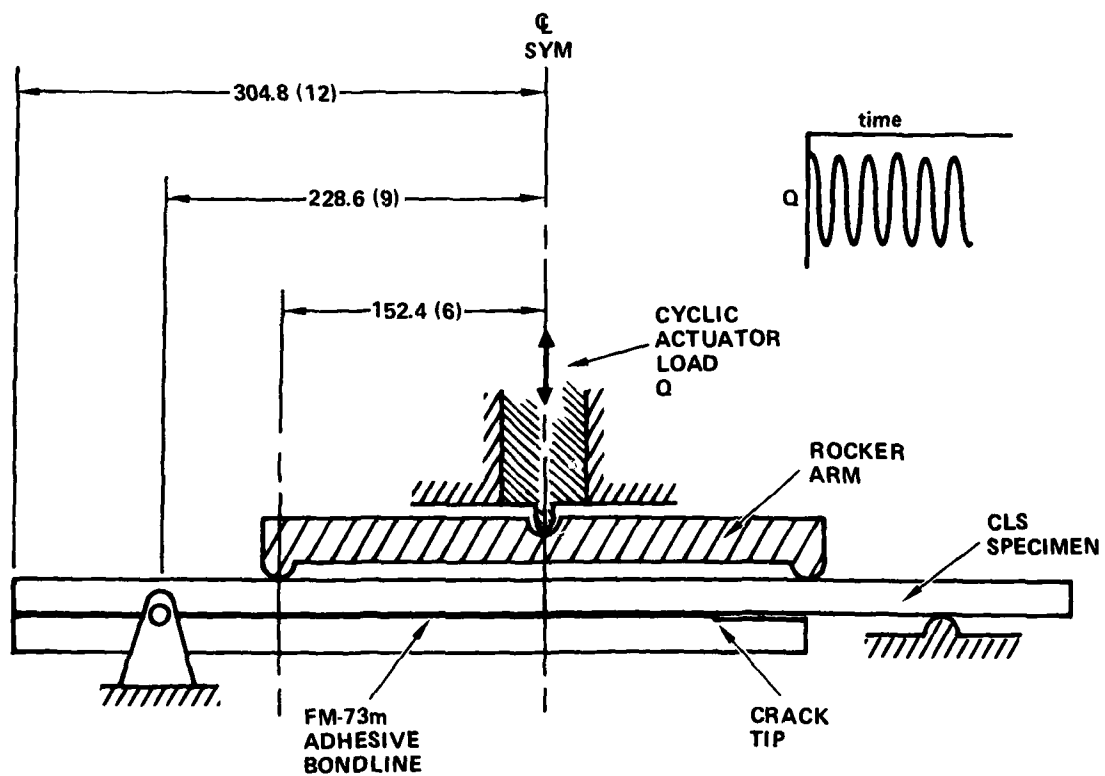
DIMENSIONS IN mm (in.)

Figure 4.   Symmetric Four-Point Bend Loading of a CLS Specimen

18

uniform bending moment and zero shear forces were obtained throughout the central region between the two inner supports. For uniform bending, the strain energy release rate is independent of crack length. $\mathscr{G}_I$ is calculated from Equation (5), and $\mathscr{G}_{II}$ is equal to $0.75\,\mathscr{G}_I$.

Both specimens were fatigue tested in laboratory air at f = 1 to 3 Hz. Crack length was monitored visually using a traveling microscope. The data are included in Figure 16 of Section III. Specimen CB-202 was tested at constant cyclic load magnitude, and the crack grew at nearly a constant rate for 4 in., verifying the assumed crack length independence of $\mathscr{G}$.

2. WIDTH TAPERED BEAM (WTB) SPECIMEN

In Phase I of this program all baseline Mode I data were obtained on the standard contoured double cantilever beam (CDCB) specimen. Despite its advantages a problem persisted in achieving a consistent bondline quality and thickness. The source of the problem was the tendency for the AF-55S adhesive to flow at cure temperature. The bondline in the CDCB specimen is only 12.7 mm (0.5 in.) wide, and at standard cure temperatures and pressures used for large-area bonds in structures, much of the adhesive flows out and escapes. Thus, it was necessary to use shims or lower bond pressures to obtain a bondline of reasonable thickness in these specimens. The resulting inconsistencies in the specimens led to variations in $\mathscr{G}_{IC}$ values and uncertainties about the applicability of the baseline da/dN data to large area bonded structure.

Like AF-55S, FM-73m adhesive flows readily at cure-temperature. Therefore the width-tapered beam (WTB) specimen, Figure 5, was designed for Mode I baseline testing in Phase II. Like the CDCB specimen, the WTB specimen consists of two cantilever beams, contoured to vary the bending stiffness so as to provide a crack-length-independent value of $\mathscr{G}_I$. In this specimen, however, the beam height is constant and the width is tapered. Thus, it is possible to bond two large plates face to face and machine the specimens from the laminate.

19
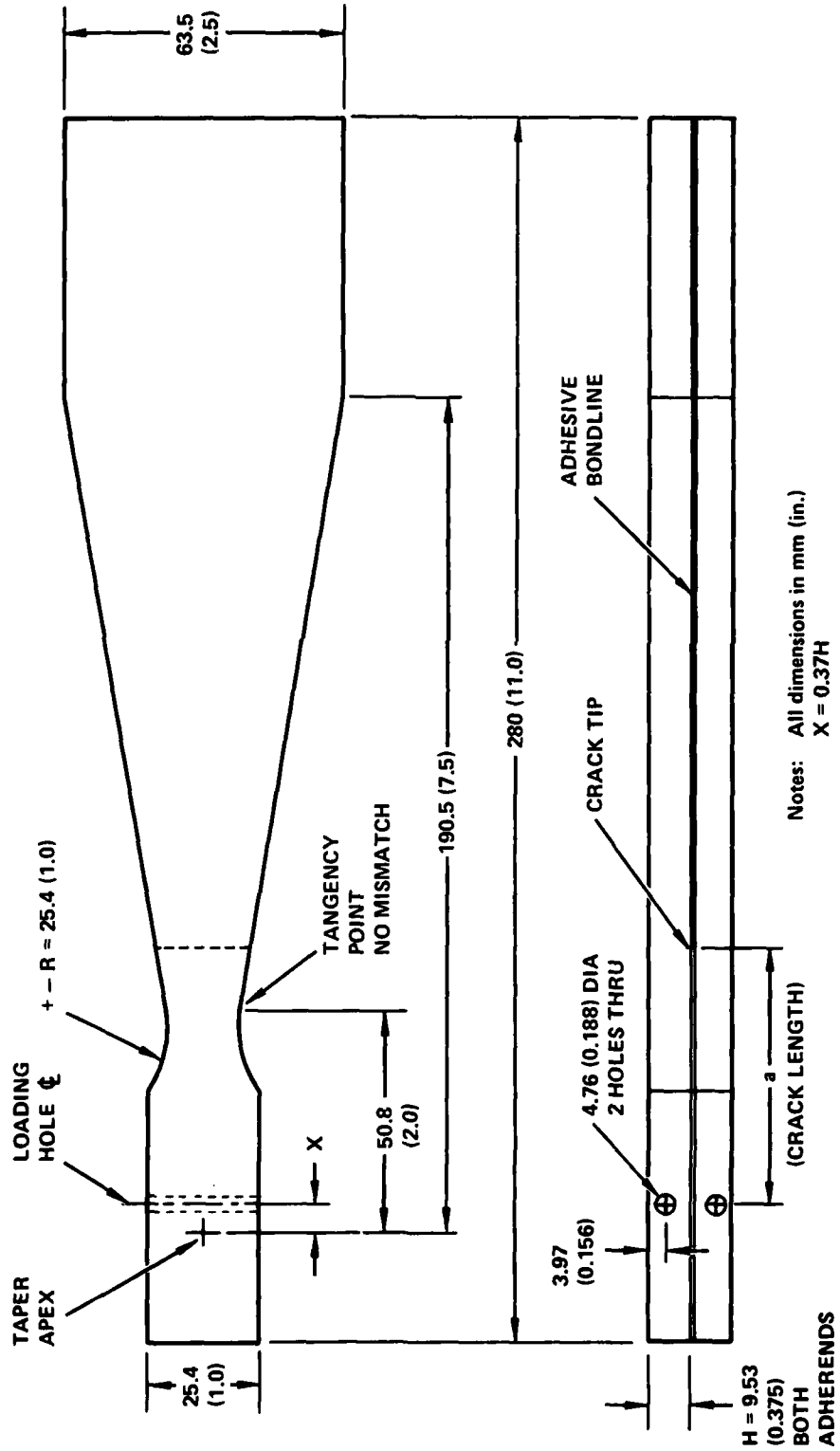
Figure 5. Width Tapered Beam (WTB) Specimen

20

2.1 Initial Compliance Calibration Tests and Analysis: X = 0

Eleven WTB specimens bonded with AF-55S adhesive were prepared with Teflon tape bondline preflaws at selected crack length locations. The original specimen geometry was the same as shown in Figure 5, except that X = 0; that is, the centerline of the loading holes coincided initially with the apex of the linear taper of the width, B. (Later the loading holes were moved, as discussed below). The taper is such that $(a + X)/B \equiv k = 3$, and it begins (after an initial untapered segment) at a distance of 50.8 mm (2.0 in.) from the apex.

The strain energy release rate applicable to these specimens is related to the load P and the derivative of compliance C and is given by

$$\mathscr{G}_I = \frac{P^2}{2B} \frac{dC}{da} \tag{7}$$

If each adherend were to behave as an ideal beam of thickness H and modulus E, built in at the crack tip, the compliance derivative would be

$$\frac{dC}{da} = \frac{24}{EH^3} \frac{a^2}{B} \tag{8}$$

and $\mathscr{G}_I$ would be

$$\mathscr{G}_I = \frac{12P^2}{EH^3} k^2 \tag{9}$$

Thus, for ideal built-in beam adherends, the value of $\mathscr{G}_I$ would be independent of crack length.

In the actual WTB specimen, the bending of the adherends can be expected to approximate that of ideal beams, but a finite initial rotation and initial displacement will occur at the crack tip in violation of the ideal built-in-beam end conditions. This can be handled by adding a constant length increment, βH, to the crack length. One can choose to modify the crack length

21

term either in the expression for compliance or in the expression for its derivative. Here the latter was chosen and Equation (8) was rewritten as

$$\frac{dC}{da} = \frac{24}{EH^3} \frac{(a + \beta H)^2}{B} \tag{10}$$

If β is non-zero, $\mathscr{G}_I$ as given by Equation (7) will no longer be crack length independent. Suppose, however, that the specimen is modified by moving the loading holes a selected distance X closer to the crack tip as shown in Figure 5, so that

$$B = (a + X)/k \tag{11}$$

If X is selected to be equal to βH, then $\mathscr{G}_I$ is made to be crack length independent. This can be seen by combining Equations (7), (10) and (11) and thereby recovering Equation (9).

If the loading hole location X is arbitrary, the general expression for compliance, found by integrating Equation (10), can be written as follows:

$$C = C^* + \frac{24k}{EH^3} [F(a) - F(a^*)] \tag{12}$$

where a* is the crack length at the start of the tapered segment of the specimen (thus, a* + X = 50.8 mm (2.0 in.)); C* is the compliance at a = a*; and the function F(a) is given by

$$F(a) = \frac{(X + a)^2}{2} - 2(X - \beta H)(X + a) + (X - \beta H)^2 \ln(X + a) \tag{13}$$

22

Initially in the calibration specimens, the loading hole centerline coincided with the apex of the taper, so that X = 0. Table 3 gives the calibration data. The crack lengths are based on the visible location of the Teflon tape. These data were used to obtain the following least-squares best-fit values of the constants β and C*:

$$\beta = 0.37$$

$$C^* = 1.422 \text{ mm/kN} \ (0.249 \text{ in/kip})$$

Using these values in Equation (12), values of calculated compliance were found for each data point and the error was expressed in terms of a discrepancy in crack length.

To achieve constant $\mathcal{C}$, the loading holes were moved a distance X = 0.37H closer to the crack tips for recalibration. This is considered significant since it exceeds the largest crack length discrepancy given in Table 3.

TABLE 3. WTB COMPLIANCE DATA, LOADING HOLES AT TAPER APEX (X = 0)

Spec. No.	Crack Length[1]		Measured Compliance		Calculated Compliance[2]		Crack Length Discrepancy	
	mm	in.	mm/kN	in/kip	mm/kN	in/kip	mm	in.
A2-2	51.8	2.04	1.43	0.250	1.490	0.261	0.31	0.012
A5-2.5	63.5	2.50	2.35	0.411	2.324	0.407	-0.11	-0.005
A6-3	76.2	3.00	3.63	0.635	3.403	0.596	-1.09	-0.043
A7-3.5	88.9	3.50	4.94	0.865	4.659	0.816	-1.37	-0.054
A8-4	101.6	4.00	6.34	1.110	6.093	1.067	-1.12	-0.047
A9-4.5	114.3	4.50	8.18	1.432	7.703	1.349	-2.32	-0.091
A10-5	128.0	5.04	9.71	1.700	9.644	1.689	-0.31	-0.012
A12-6	152.0	6.00	13.62	2.385	13.60	2.382	0.74	0.029
A14-7	178.0	7.00	18.04	3.160	18.42	3.225	0.69	0.027

NOTES: (1) Crack lengths based on visible location of embedded teflon tape.
(2) Calculated from Equation (12) with β = 0.37 and C* = 1.422 mm/kN (0.249 in/kip).

Adhesive: AF-55S
Adherends: 7075-T6 Aluminum plate, H = 9.83 mm (0.387 in.)

2.2 Second Compliance Calibration Tests and Analysis: Constant ⚹

Duplicate sets of compliance measurements are shown in Table 4 for the loading holes located at X = 0.37H. The crack lengths are different from those listed in Table 3 for two reasons. First, they are smaller by 3.64 mm (0.143 in.) because they are measured from the new loading hole locations. Secondly, they are the lengths of cracks observed visually during loading, not the visually observed teflon tape locations used previously.

As previously, these data were analyzed to estimate the best-fit values of C* and β in Equation (12). The calculated best-fit value of β was 0.34.

TABLE 4. WTB COMPLIANCE DATA, LOADING HOLES AT X = 0.37H

| Specimen Number | Crack Length [1] | | Measured Compliance | | | |
| | | | Run 1 | | Run 2 | |
	mm	(in.)	mm/kN	(in/kip)	mm/kN	(in/kip)
A2-2	45.2	(1.78)	1.18	(0.207)	1.17	(0.205)
A5-2.5	57.7	(2.27)	2.00	(0.351)	1.91	(0.334)
A6-3	71.6	(2.82)	3.19	(0.558)	3.16	(0.554)
A7-3.5	84.8	(3.34)	4.47	(0.783)	4.47	(0.782)
A8-4	99.1	(3.90)	5.89	(1.013)	5.78	(1.013)
A9-4.5	115.1	(4.53)	7.73	(1.353)	7.65	(1.340)
A10-5	125.5	(4.94)	9.11	(1.595)	9.16	(1.605)
A11-5.5	136.9	(5.39)	10.71	(1.875)	10.76	(1.885)
A12-6	147.6	(5.81)	12.53	(2.195)	12.53	(2.195)
A13-6.5	162.6	(6.40)	14.65	(2.565)	14.90	(2.610)
A14-7	175.8	(6.92)	17.19	(3.010)	17.33	(3.035)

[1] Crack Lengths listed are those observed visually during loading.

However, $\beta = 0.37$ can be used without significant additional error in the data fit, so the new loading hole location $X = 0.37H$, was retained. Figure 6 compares the measured data with values computed using $\beta = 0.37$ and $C^* = 1.55$ mm/kN (0.271 in/kip).

With $\beta H = X$, Equation (9) is a valid expression for strain energy release rate.

2.3 Third Compliance Calibration Tests and Analysis: Slightly Variable $\mathscr{G}$

Compliance measurements taken on the Instron test machine and shown in Table 4 were eventually confirmed on the servo hydraulic machine, as shown in Table 5. The compliance data listed in Table 5 were then reexamined for a possible variability, previously overlooked, of the strain energy release rate ($\mathscr{G}$) with crack length.

Based on an initial analysis of the compliance data in Table 4 taken on the Instron machine, $\mathscr{G}$ appeared to be approximately constant, any trends being obscured by data scatter. Unfortunately, small scatter errors are always magnified by algebraic differentiation, and in the use of compliance data to estimate $\mathscr{G}$, two derivatives of the measured displacement are required:

$$\mathscr{G} = \frac{P^2}{2B} \frac{dC}{da} = \frac{P^2}{2B} \frac{\partial^2 \delta}{\partial P \, \partial a} \tag{14}$$

Therefore, relatively small errors in measured displacements (δ), loads (P), or crack lengths (a) can lead to much larger errors in estimated $\mathscr{G}$.

In another attempt to compute $\mathscr{G}$ for various crack lengths, Equation (7) is written in incremental form:

$$\frac{\mathscr{G}}{P^2} = \frac{1}{2B} \frac{\Delta C}{\Delta a} \tag{15}$$
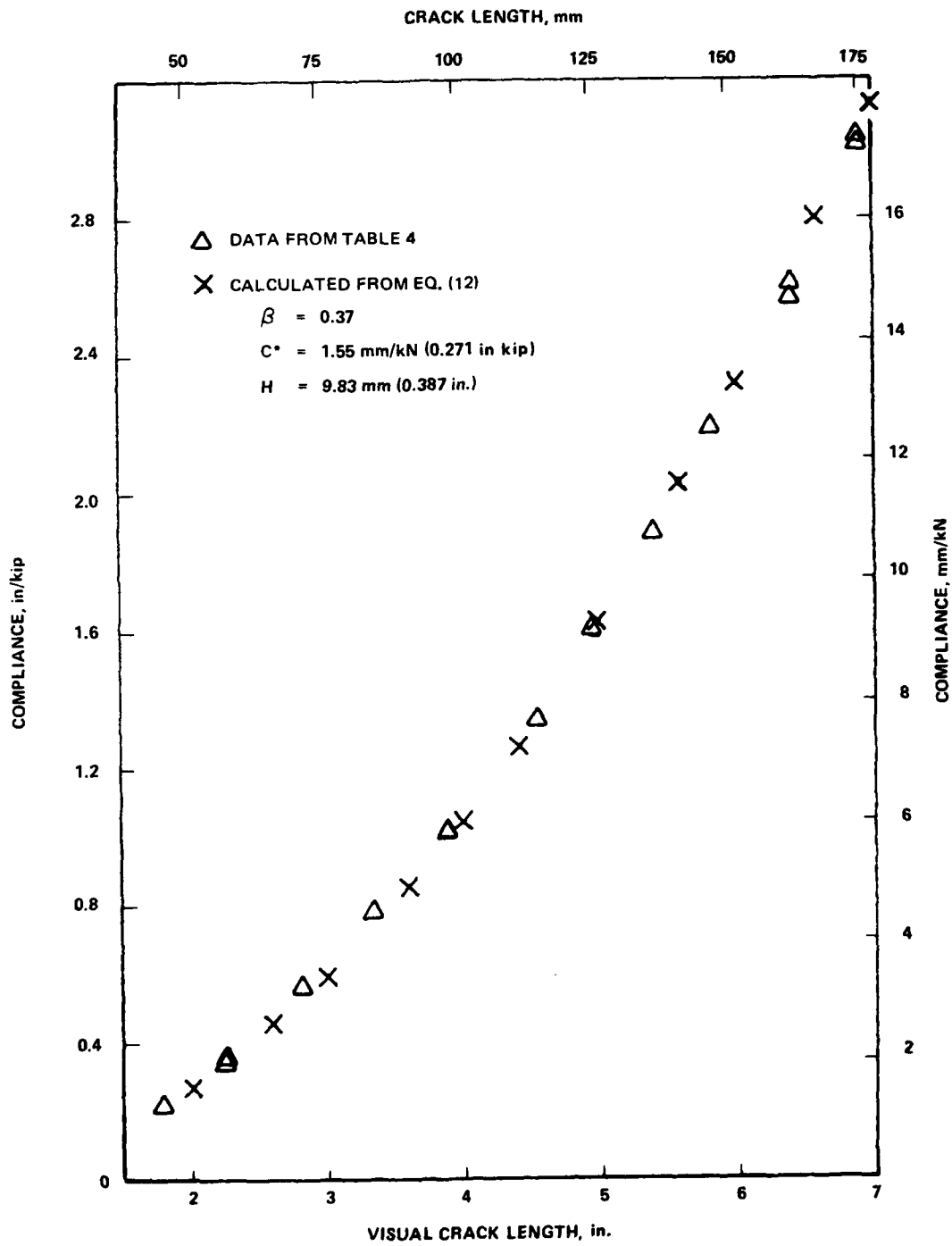
25

Figure 6. Compliance of WTB Specimens with X = 0.37H

26

TABLE 5. WTB COMPLIANCE DATA FROM TWO TEST MACHINES

(H = 9.83 mm (0.387 in.) a/b = 3 with holes 3.68 mm (0.143 in.) from taper apex)

Crack Length mm (in.)	Measured Compliance (Averaged)			
	LVDT[1] In Instron Test Machine		Kaman[2] In Servo Hydraulic Test Machine	
	mm/kN	(in/kip)	mm/kN	(in/kip)
45.2 (1.78)	1.18	(0.206)	1.23	(0.216)
57.7 (2.27)	1.96	(0.343)	1.98	(0.346)
71.6 (2.82)	3.18	(0.556)	3.15	(0.551)
84.8 (3.34)	4.47	(0.783)	4.30	(0.753)
99.1 (3.90)	5.78	(1.013)	5.77	(1.011)
115.1 (4.53)	7.74	(1.356)	7.67	(1.344)
125.5 (4.94)	9.14	(1.600)	9.14	(1.600)
136.9 (5.39)	10.74	(1.880)	10.71	(1.876)
147.6 (5.81)	12.53	(2.195)	12.51	(2.190)
162.6 (6.40)	14.77	(2.587)	14.63	(2.562)
175.8 (6.92)	17.26	(3.023)	17.13	(3.000)

(1) Linear variable differential transformer calibrated to
    ±12.7 mm (0.500 in.)

(2) Eddy current type displacement gage calibrated to
    ±12.7 mm (0.500 in.)

The data in Table 5 were examined three times using Equation (15), with three different nominal sizes of the increment Δa. The averages of the corresponding compliance measurements on the Instron and servo-hydraulic machines were used. For each incremental computation, B was assigned the value of the width at the midpoint of the increment.

The geometric mean value of $\mathscr{G}/P^2$ computed in this manner was 1.63 J/m^2 per kN^2 (0.184 lb/in per kip^2) regardless of increment size. Figure 7 shows the deviations of the computed values from the mean. For the smallest nominal increment size, 10.4 mm (0.41 in.) $\leq \Delta a \leq$ 16.0 mm (0.63 in.) shown as open circle symbols, trends with crack length are not discernable. However, for the larger two increment sizes, 21.8 mm (0.86 in.) $\leq \Delta a \leq$ 30.2 mm (1.19 in.) and 32.5 mm (1.28 in.) $\leq \Delta a \leq$ 43.3 mm (1.71 in.), a downward trend in $\mathscr{G}$ is apparent as the crack length increases.

It is useful to define normalizing constants for strain energy release rate, load and crack length as follows:

$$\mathscr{G}_o = 0.1751 \text{ kJ/m}^2 \text{ (1.0 lb/in)} \tag{16a}$$

$$P_o = 4.4482 \text{ kN (1.0 kip)} \tag{16b}$$

$$A_o = 25.4 \text{ mm (1.0 in.)} \tag{16c}$$

The following equation for $\mathscr{G}$ was obtained:

$$\mathscr{G}/\mathscr{G}_o = 165 \left[\left(1 + \frac{0.57H}{a} \right) \frac{P}{P_o} \right]^2 \left(\frac{0.387 \ A_o}{H} \right)^3 \tag{17}$$

Equation (17), shown as a solid line in Figure 7, properly displays the downward trend in $\mathscr{G}$ with crack length and provides a better fit to the incrementally-determined data points for $\mathscr{G}$.

An equation for compliance is obtained by substituting for $\mathscr{G}$ from Equation (17) into Equation (14) and integrating once with respect to crack length. The resulting equation is as follows:
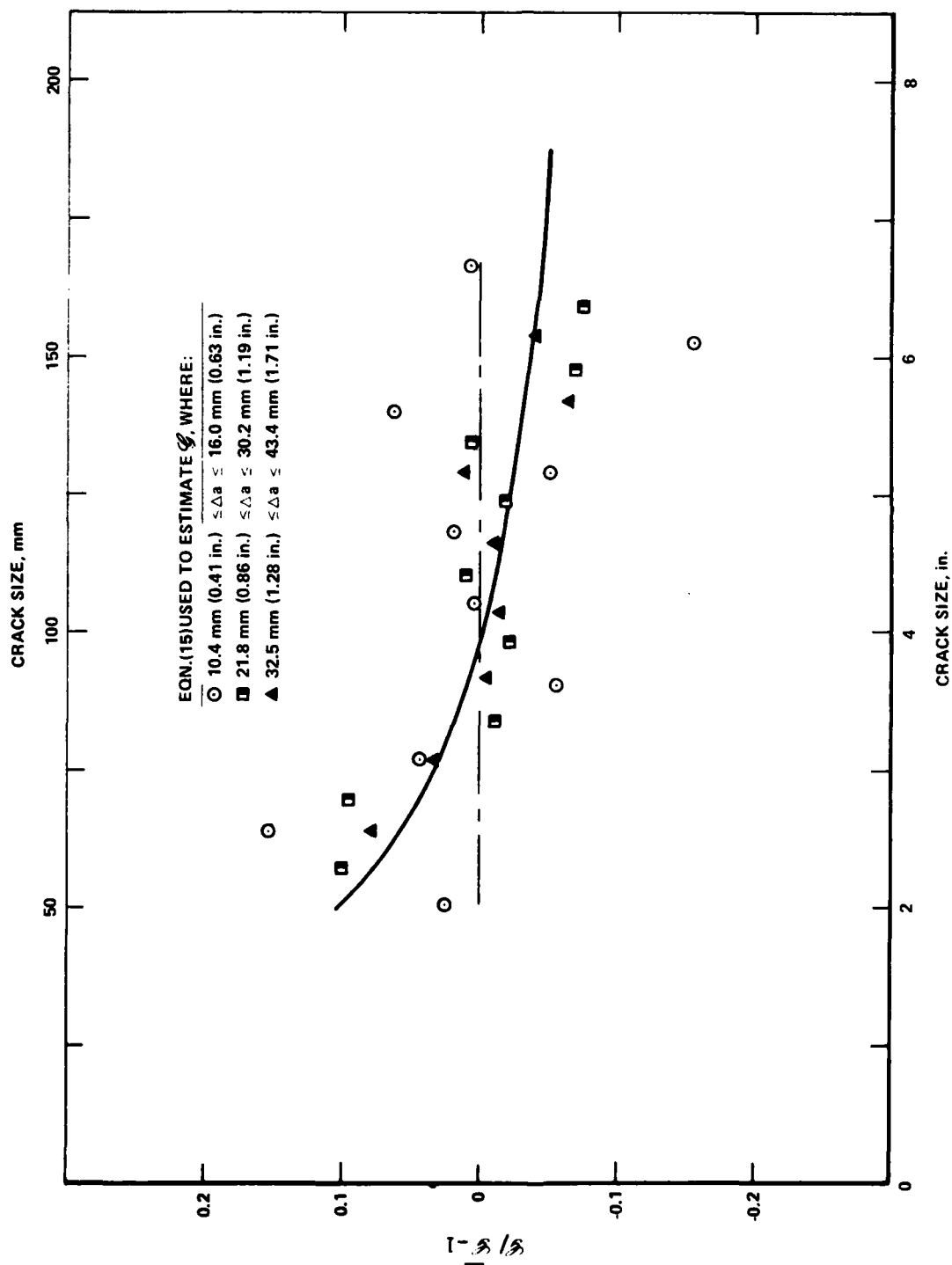
28

Figure 7. Deviations of Estimated $\mathscr{G}$ from the Geometric Mean, $\overline{\mathscr{G}}$

$$\frac{C - C(0)}{C_o} = 0.11 \left(\frac{0.387 \, A_o}{H}\right)^3 \left[0.5 \left(\frac{a}{A_o}\right)^2 + 0.583 \, \frac{a}{A_o}\right.$$

$$\left. + 0.11132 \, \ell n \left(\frac{a}{A_o}\right) - 0.069212 \, \frac{A_o}{a}\right] \tag{18}$$

where the normalizing constant for compliance is defined by

$$C_o = 5.71 \text{ mm/kN} \quad (1.0 \text{ in/kip}) \tag{19}$$

and the best-fit value of C(0) is -0.473 mm/kN (-0.0828 in /kip). In Table 6, the compliance as computed from Equation (18) is compared with the measured data points. The error of the fit is comparable in magnitude to the error of agreement between the corresponding measurements in the Instron and servo-hydraulic machines.

Equations (17) and (18) are a somewhat more accurate data fit than Equations (9) and (12), and may be useful when comparing WTB data taken at extremely different crack lengths. For most data analysis purposes, however, either set of equations can be used, since most often the difference is obscured by data scatter.

2.4 Compliance Measurement on the WTB Specimens

Separate compliance measurements from an Instron mechanical testing machine and an electrohydraulic closed-loop machine were virtually the same as shown in Table 5.

The test equipment used to determine compliance in the Instron consisted of a standard load cell, an LVDT displacement measuring coil with a range of ±12.7 mm (0.5 in.), and an x-y chart recorder. Calibration cf the coil preceded measurements in all cases, and problems of nonlinearity were minimized by using the coil in a very linear part of its range. Compliance values were obtained by slope measurement once it was assured that the mechanical load train was aligned to give a reasonably straight-line trace.

TABLE 6.

ACCURACY OF EQUATION (18) FOR ESTIMATING COMPLIANCE OF WTB SPECIMENS

a/A$_o$	C/C_o Measured	C/C_o From Equation (18)	Percent Difference
1.78	0.2110	0.20836	+1.27
2.27	0.3445	0.35283	-2.36
2.82	0.5535	0.54538	+1.49
3.34	0.7680	0.75740	+1.40
3.90	1.0120	1.01853	-0.64
4.53	1.3500	1.35314	-0.23
4.94	1.6000	1.59418	+0.37
5.39	1.8780	1.87990	0.10
5.81	2.1925	2.16658	1.20
6.40	2.5745	2.60193	-1.05
6.92	3.0115	3.01728	-0.19

A$_o$ = 25.4 mm (1.0 in.)

C$_o$ = 5.71 mm/kN (1.0 in/kip)

When measurements were taken in the closed-loop machine, the displacement gage used was of the noncontacting eddy current type (range, +12.7 mm (0.5 in.)). Since this machine is designed for computer control, the entire calibration record for this gauge was fitted with a polynomial and stored for use to reduce the compliance record. Compliance records in this test machine were obtained as follows: The cyclic amplitude was fixed so that the load excursion in one cycle ranged from 44.5 to 356 N (10 to 80 lb). Loading was accomplished by the computer which considers 64 load-displacement data pairs during loading only and calculates compliance from a least-squares fit to all the data. This was judged to be satisfactory when successively truncating the data points used in the fit did not significantly change the result.

2.5 Comparison of da/dN Data from CDCB and WTB Specimens

A da/dN curve is presented in Reference 1 for Pure Mode I cyclic loading of CDCB specimens bonded with AF-55S adhesive. As mentioned, the applicability of these data to large-area bonded structure could be questioned since different bonding procedures had to be used on the CDCB specimens to prevent excessive squeeze-out of the adhesive. On the other hand, the WTB specimen is machined from a large-area bonded panel and is therefore applicable to a structure.

WTB specimens bonded with AF-55S were da/dN tested prior to their use in compliance calibration tests. The loading holes were located at the apex of the taper (X = 0 in Figure 5), so Equations (7) and (10) had to be used to estimate $\mathscr{G}$, which varied with crack size.

For convenience in discussing and using the data, best-fit straight lines in log-log space are used in Reference 1, of the form

$$\frac{da/dN}{a_o} = C_a \left(\frac{\Delta \mathscr{G}_I}{\mathscr{G}_o}\right)^n \tag{20}$$

where C_a and n are the best-fit constants and

$$a_o = 0.0254 \ \mu \ (10^{-6} \ \text{in.}) \tag{21a}$$

$$\mathscr{G}_o = 0.1751 \ \text{KJ/m}^2 (1.0 \ \text{lb/in}) \tag{21b}$$

The data are plotted in Figure 8. Note that the crack growth rate is consistently slower in the WTB specimens than was reported in Reference 1 for the CDCB specimens.
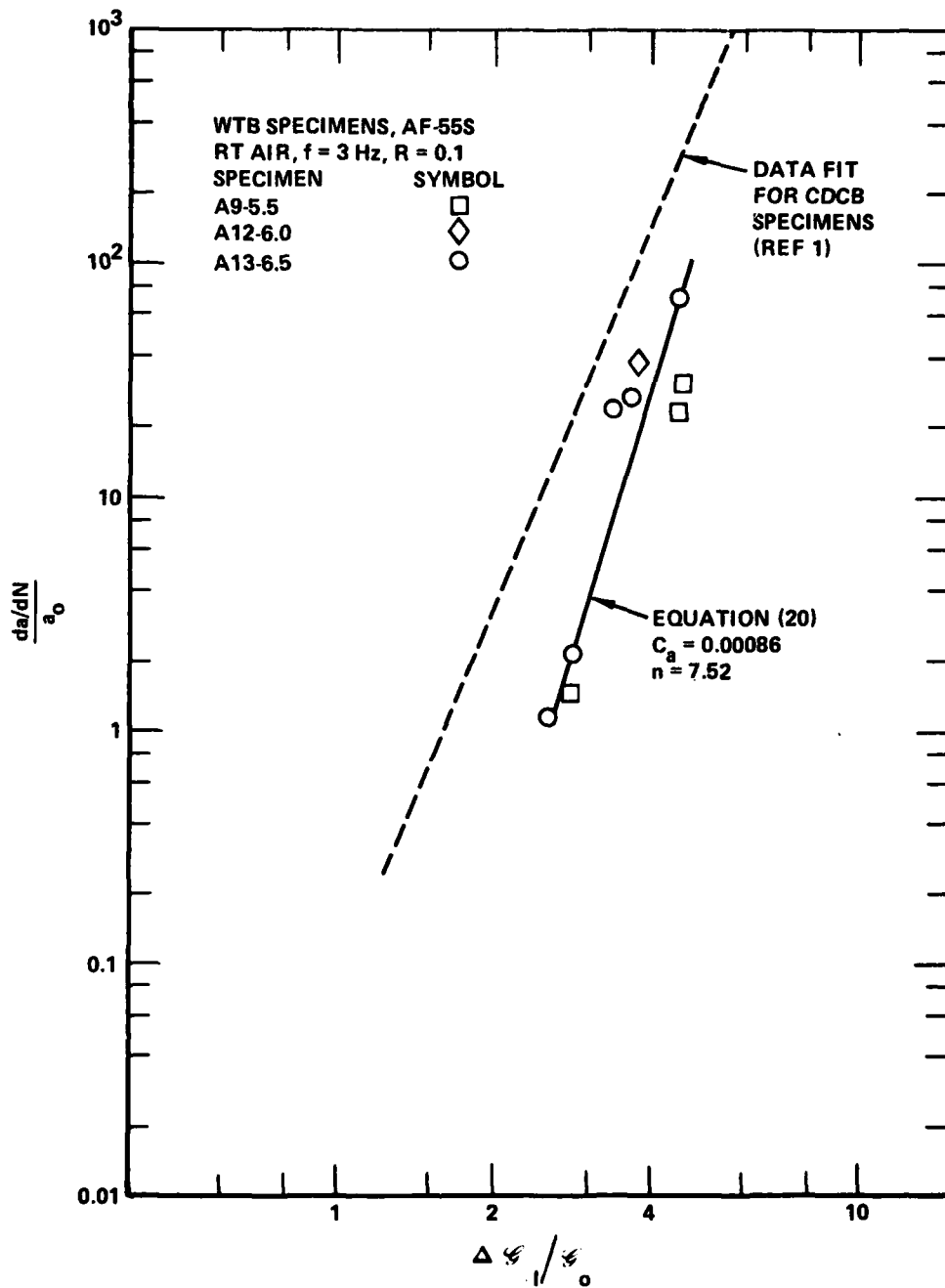
Figure 8. Comparison of Pure Mode I da/dN Data on AF-55S Adhesive From WTB and CDCB Specimens

The uniform beam (UDCB) specimen discussed in the next subsection was introduced into this program to help substantiate the analysis of the WTB specimen. As shown in Section III, matching da/dN data were obtained for FM-73m on WTB and UDCB specimens. Because of this verification of the WTB analysis, one is led to conclude from Figure 8 that da/dN data from the CDCB specimen are conservative when applied to bondline cracks in large-area bonded structures.

2.6 Crack Tunnelling in Fatigue

Inspection of the fracture surface of WTB specimen W-106 after da/dN testing shows that the crack front is not straight across as assumed in the compliance analysis. Instead, the crack tunnels, such that the crack length at mid-width is 2 to 7.6 mm (0.08 to 0.3 in.) longer than at the edges. The average tunnelling depth is about 3.8 mm (0.15 in.). Thus, it is expected that compliance-measured crack lengths will be about 1.9 mm (0.075 in.) longer than those visually measured.

The effect may be consistent for all crack lengths; if so, there would be no major discrepancy between "actual" da/dN values and those measured by compliance. Further, crack tunnelling is not expected to significantly effect the value of $\mathcal{G}$.

However, the degree of tunnelling may vary with magnitude of applied $\Delta \mathcal{G}_I$. If so, there may be a period of transient da/dN following a major change in the load magnitude.

3. THE UDCB SPECIMEN

The development of the uniform double cantilever beam (UDCB) specimen is described in Reference 2*. The strain energy release rate (for a fixed load magnitude, P) increases with crack length (a).

---

*Reference 2. Mostovoy, S., Crosley, P. B. and Ripling, E. J. "Use of Crack-Line Loaded Specimens for Measuring Plane-Strain Fracture Toughness" J. of Materials, Vol. 2, No. 3, ASTM, 1967.

The compliance, C, depends upon the bending stiffnesses of the two adherends, $(EI)_1$ and $(EI)_2$, and the average adherend thickness (H), and is given by

$$C = 1/3 \left[\frac{1}{(EI)_1} + \frac{1}{(EI)_2} \right] \left[(a + 0.6H)^3 + H^2a \right] \tag{22}$$

thus

$$\frac{dC}{da} = \left[\frac{1}{(EI)_1} + \frac{1}{(EI)_2} \right] \left[(a + 0.6H)^2 + \frac{H^2}{3} \right] \tag{23}$$

Crack length is determined from measured compliance by means of Equation (22). $\mathscr{G}$ is determined from Equation (23) by substitution for dC/da into Equation (7).

Although the analysis of the UDCB specimen is straightforward, fatigue testing can be more difficult than for the constant dC/da specimens. One of the major difficulties is in reducing the "a" versus "N" data to a $\Delta \mathscr{G}_I$ - da/dN curve. This is difficult because even at constant load, both $\Delta \mathscr{G}_I$ and da/dN increase rapidly during each small increment of crack growth.

The best data have been obtained when the fatigue load magnitude is held constant for a substantial increment of crack growth (50 mm (2.0 in.) or more), and numerous (a, N) pairs are obtained within each increment. For data thus obtained, two methods of data reduction were tried and compared, a polynomial fit method and an incremental method.

In the polynomial fit method of data reduction, a polynomial of the form

$$a = \sum_{o}^{2n} c_i N^i \tag{24}$$

is fitted to the raw data and differentiated once to obtain da/dN. These $(\Delta \mathscr{G}_I, da/dN)$ pairs are calculated and plotted for all except the first n and

last n values of "a" for which (a, N) pairs were originally obtained. (The ends of the curve are deleted because 2n degrees of freedom are used up in obtaining the data fit).

In the incremental method, successive (a, N) pairs are selected from the raw data such that the crack grows approximately 10 mm (0.4 in.) during each increment. The value of $\Delta\mathscr{G}_I$ is calculated for each selected (a, N) pair. Then the average value of $\Delta\mathscr{G}_I$ for the increment is plotted against the average crack growth for the increment.

Data from a UDCB specimen were reduced by both methods and compared in Figure 9. Despite the unusual dip in the da/dN curve caused by data scatter, the two data reduction methods correlate. This means that either can be used.
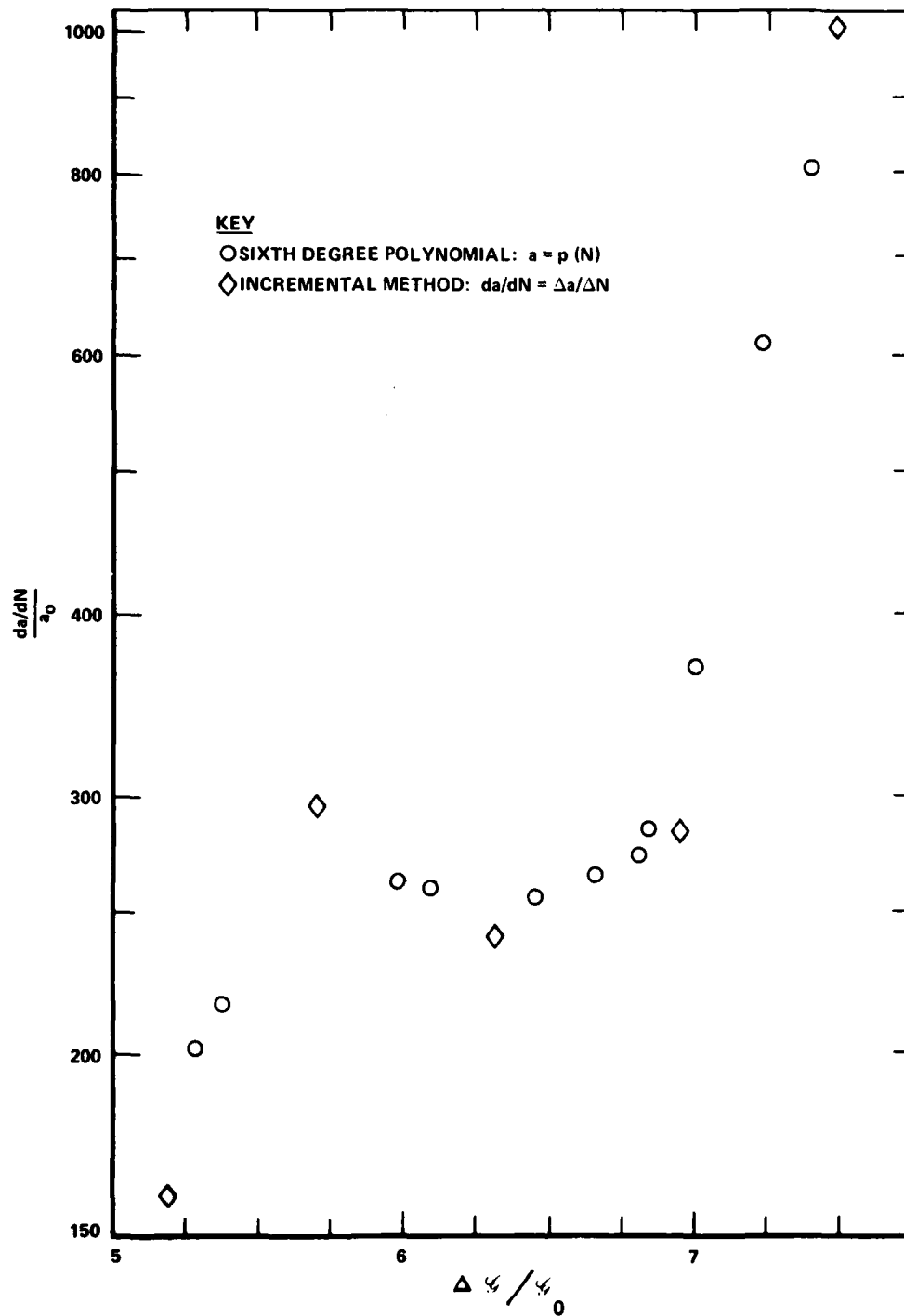
Figure 9. Comparison of Data Reduction Methods for da/dN on UDCB Specimen UB-9

37

SECTION III

BASELINE TEST RESULTS

1. STATIC TEST DATA

1.1 $\mathscr{G}_{IC}$ Test Data

Sixteen WTB specimens were $\mathscr{G}_{IC}$ tested prior to fatigue and sustained-load testing. The crack length when tested was approximately 56 mm (2.2 in.), and two measurements of critical load were made. The average $\mathscr{G}_{IC}$ value for the two measurements is given for each specimen in Table 7. After fatigue testing, $\mathscr{G}_{IC}$ tests were performed on two of these specimens and two UDCB specimens. These results are also shown in Table 7. The average $\mathscr{G}_{IC}$ value for these 36 tests was 2.38 kJ/m^2 (13.58 lb/in), compared to 2.24 kJ/m^2 (12.78 lb/in) for 48 AF-55S CDCB specimens reported in Reference 1.

1.2 Mixed-Mode Toughness Tests

A side-notched CLS specimen, C-110, was $\mathscr{G}_C$ tested. Critical values of $\mathscr{G}$ in three succesive tests of this specimen were 9.00 kJ/m^2 (51.4 lb/in), 9.12 kJ/m^2 (52.1 lb/in), and 9.65 kJ/m^2 (55.1 lb/in). Corresponding values of the Mode I component are 2.12 kJ/m^2 (12.13 lb/in), 2.15 kJ/m^2 (12.28 lb/in), and 2.28 kJ/m^2 (13.00 lb/in), which are within the scatterband of the $\mathscr{G}_{IC}$ data listed in Table 7.

1.3 Sustained Load Test Data

Three WTB specimens and one CLS specimen were subjected to sustained load for periods of two to eight months while immersed in 333°K (140°F) deionized water. Crack length was measured during the test by unloading and reloading

38

TABLE 7. $\mathcal{G}_{IC}$ MEASUREMENTS FOR FM-73m ADHESIVE

| Specimen Number | Initial Tests, $a/A_o \doteq 2.2$ | | | After Fatigue Testing | | |
| | P_{CRIT}/P_o | | $\mathcal{G}_{IC}/\mathcal{G}_o$ (Avg.) | a/A_o | P_{CRIT}/P_o | $\mathcal{G}_{IC}/\mathcal{G}_o$ |
	1	2				
W-101	0.264	0.248	13.9	--	--	--
W-102	0.2472	0.2472	12.9	7.29	0.267	13.3
W-103	0.246	0.244	12.7	--	--	--
W-104	0.240	0.242	12.3	--	--	--
W-105	0.2632	0.256	14.3	--	--	--
W-106	0.250	0.240	12.7	--	--	--
W-107	0.244	0.264	13.7	--	--	--
W-108	0.256	0.248	13.4	--	--	--
W-109	0.268	0.254	14.4	--	--	--
W-110	0.2552	0.243	13.1	--	--	--
W-111	0.2712	0.266	15.3	--	--	--
W-112	0.244	0.240	12.4	--	--	--
W-113	0.270	0.262	15.0	--	--	--
W-114	0.256	0.254	13.8	7.16	0.264	13.0
W-115	0.258	0.2704	14.8	--	--	--
W-116	0.264	0.258	14.4	--	--	--
UB-1	--	--	--			13.4
UB-2	--	--	--			11.4

Note: A_o, P_o and $\mathcal{G}_o$ defined in Equation (16).

MEAN $\mathcal{G}_{IC}$ = 2.38 kJ/m^2 (13.58 lb/in)

7075-T651 Aluminum adherends

FM-73m Adhesive

H = 9.55 min (0.379 in.)

to obtain compliance changes. This unloading and reloading is necessary because, although the displacement changes gradually under sustained loading, this change does not necessarily affect the compliance, nor is it indicative of crack growth.

The data are shown in Table 8. Limited data were obtained, because the cracks tended not to propagate. The high resistance of FM-73m to crack growth in hot water indicates that sustained loading is not likely to be a critical condition for this adhesive, primer, and surface treatment combination.

TABLE 8. DATA FOR SUSTAINED LOADING IN 333°K $(140^{\circ}$F) WATER

| Specimen Number | Dates | | P/P_o | γ_I/γ_o | Δt (Min) | $\Delta a/A_o$ | $\dfrac{da/dt}{a_o}$ (per min) |
	From	To					
W-101	12/19/77	2/20/78	0.100	2.0	87840	0	0
	2/20/78	3/5/78	0.150	4.5	18720	0	0
	4/4/78	8/6/78	0.180	6.48	178560	0.625	3.50
W-102	12/19/77	2/20/78	0.100	2.0	87840	0	0
W-103	2/20/78	3/5/78	0.150	4.5	18720	0	0
	4/4/78	8/6/78	0.180	6.48	178560	2.010	11.3
C-113	4/14/78	8/8/78	3.000	3.12	167040	0.05	0.3

A_o, P_o and γ_o defined in Equation (16); a_o in Equation (21).

Specimen W-102 removed and da/dN tested in 333°K $(140^{\circ}$F) water

2. FATIGUE CRACK GROWTH TEST DATA

Bondline crack growth data have been obtained in pure Mode I and mixed Modes I and II in two environments, two stress (R) ratios, and three cyclic frequencies.

Table 9 summarizes the number of data points obtained on the four types of baseline FM-73m specimens fatigue tested. Specimen numbers W-102 through W-115 are pure Mode I width tapered beam (WTB) specimens; UB-1 through UB-11 are pure Mode I uniform double cantilever beam (UDCB) specimens; C-102 through

TABLE 9. NUMBER OF CRACK GROWTH DATA POINTS, FM-73m ADHESIVE

Specimen Number[1]	Laboratory Air					Water Immerse, $333°K$ ($140°F$)			
	f = 3 Hz		f = 15 Hz		f = 0.3 Hz	f = 3 Hz		f = 0.3 Hz	
	R = 0.1	R = 0.6	R = 0.1	R = 0.6	R = 0.1	R = 0.1	R = 0.6	R = 0.1	R = 0.6
W-102[2]	--	--	--	--	--	--	4	--	5
W-104	3	2	--	--	--	--	--	--	--
W-105	--	6	--	--	--	--	--	--	--
W-106	7	--	--	--	--	--	--	--	--
W-107	--	4	--	--	--	--	--	--	--
W-108	--	--	--	--	--	--	--	2	--
W-111	--	--	--	--	--	6	8	--	--
W-112	2	--	--	--	--	--	--	--	--
W-114	5	3	--	--	--	--	--	--	--
W-115	--	--	--	--	4	--	--	--	--
UB-1	15	--	--	--	--	--	--	--	--
UB-2	2	--	--	--	--	--	--	--	--
UB-9	--	--	--	--	--	21	--	--	--
UB-10	--	--	--	--	--	--	12	--	--
UB-11	--	--	--	--	--	24	--	--	--
C-102	3	--	--	--	--	--	--	--	--
C-106	7	4	--	--	--	--	--	--	--
C-108[2]	--	--	--	--	--	6	--	--	--
C-110	3	--	--	--	--	4	7	8	--
C-111	5	1	2	3	--	--	--	--	--
C-115	--	--	--	--	--	5	--	1	--
C-116	--	7	--	--	--	--	--	--	--
CB-201	5	--	--	--	--	--	--	--	--
CB-202	4	--	--	--	--	--	--	--	--

NOTES: (1) Specimens W-XXX are Mode I width tapered beam (WTB) specimens; UB-X are Mode I uniform double centilever beam (UDCB) specimens; and C-XXX are long cracked lap shear (CLS) specimens).

(2) Specimens W-102 and C-108 were immersed in $333°K$ ($140°F$) water for 58 days and 106 days, respectively under sustained load and no load, respectively prior to fatigue testing.

C-116 are axially loaded mixed-mode (I and II) cracked lap shear (CLS) specimens; and CB-201 and 202 are CLS specimens subjected to four-point bending.

The da/dN data are plotted as log(da/dN) versus log($\Delta \mathcal{G}_I$) and fitted with straight lines of the form given by Equation (20).

2.1 Mode I da/dN Data In Laboratory Air

Figure 10 shows the Pure Mode I data for FM-73m from 4 WTB specimens tested in laboratory air at R = 0.1 and f = 3.0 Hz. The best-fit line for WTB specimens bonded with AF-55S from Figure 8 is shown for comparison. For this condition, no significant difference between the two adhesives can be ascertained.

Because the WTB is a new specimen configuration, the data plotted in Figure 10 were verified on the pure Mode I UDCB specimen. Results of this verification are plotted in Figure 11. The first UDCB data obtained gave three points far to the left of the best fit line for the WTB specimen, suggesting that data from the two specimen configurations conflicted. However, testing of Specimen UB-1 was continued, and all subsequent data points fell in a tight scatterband around the best-fit line for the WTB specimen. Unfortunately no explanation is available for the two different scatterbands of UDCB data.

The effect of stress ratio (R) is examined in Figure 12, where the data for R = 0.6 are plotted. These data are subject to more scatter than the R = 0.1 data, and the slope of the best fit line (n = 8.3) is substantially steeper. This slope is identical to the slope of the best-fit line for the AF-55S data generated on CDCB specimens at R = 0.6 and presented in Reference 1, but the da/dN values are lower than those of Reference 1 by a constant factor of 2.2. As Figure 8 showed, this magnitude of difference in da/dN can occur due to differences between the CDCB and WTB specimen configurations, and may not reflect any superiority of the FM-73m adhesive for this test condition.

The effect of slower cyclic frequency in laboratory air (0.3 Hz instead of 3.0 Hz) is shown in Figure 13. Only a few data points were obtained at f = 0.3 Hz, but the detrimental effect appears to be substantial, a factor of 3 at low da/dN values and a factor of 10 at higher da/dN values. The factor of 10 difference means that the growth rates per unit time were equal.
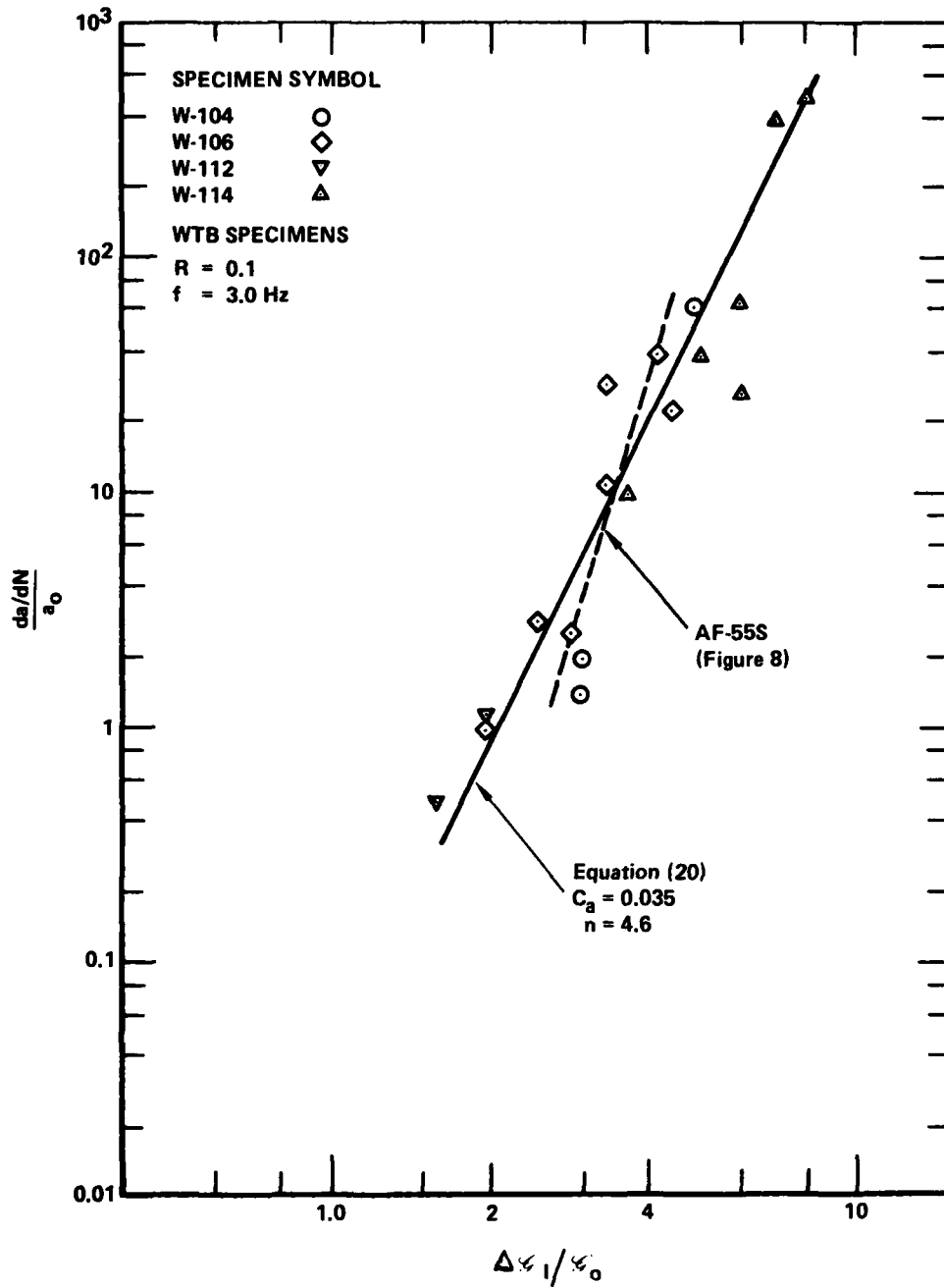
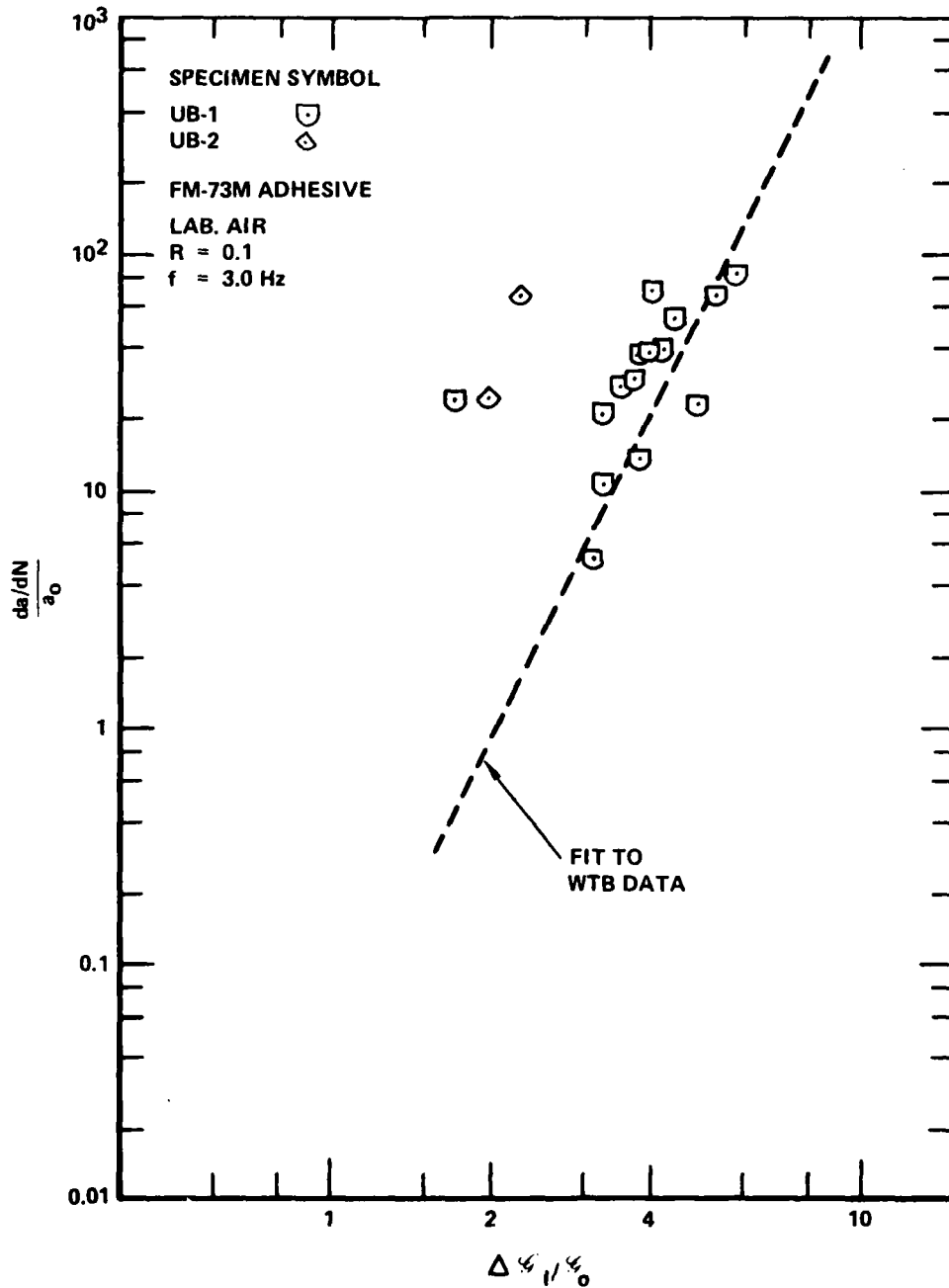Figure 10. Pure Mode I da/dN in Laboratory Air for FM-73m

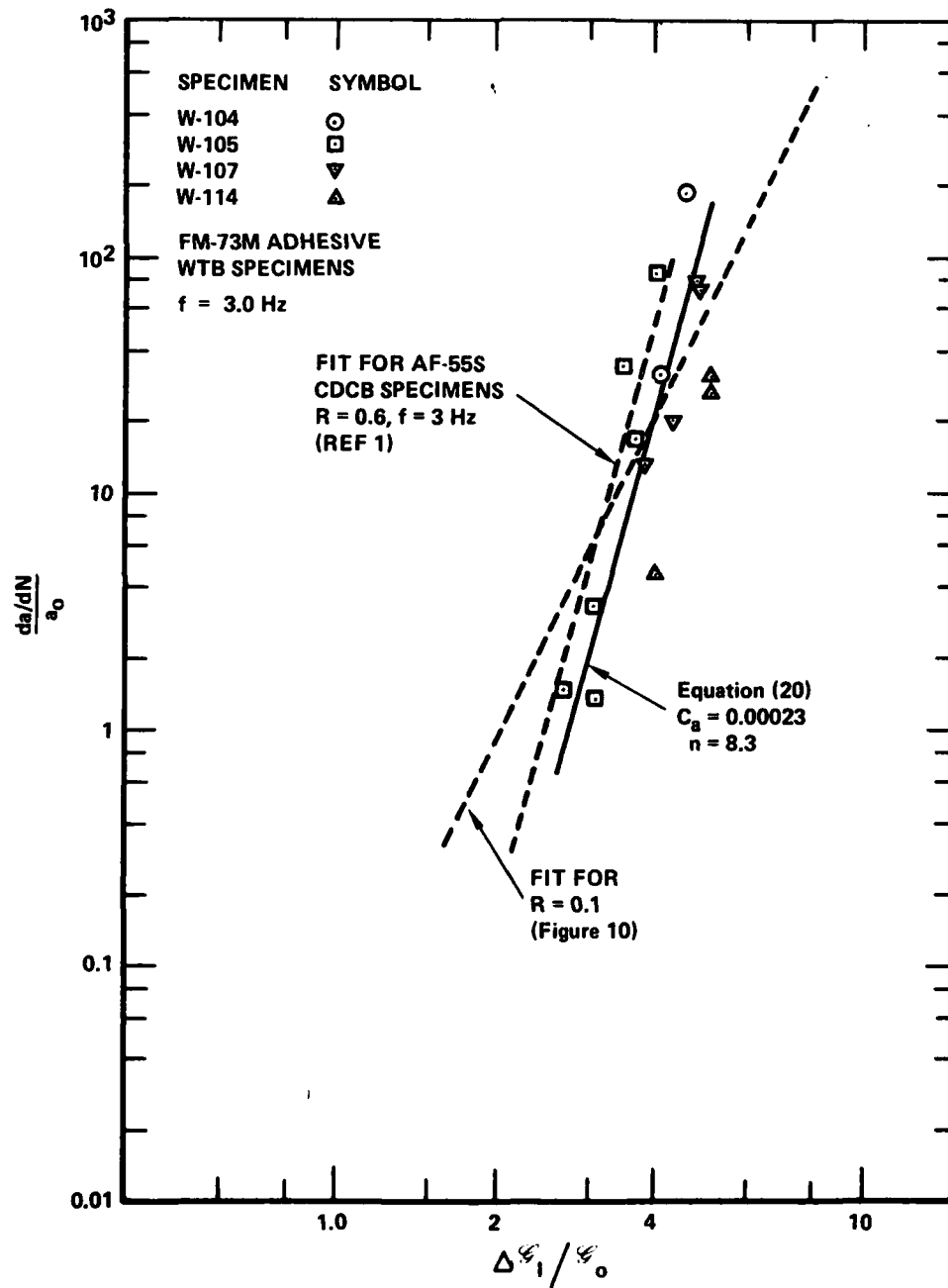Figure 11.   Verification of WTB Data Using UDCB Specimens
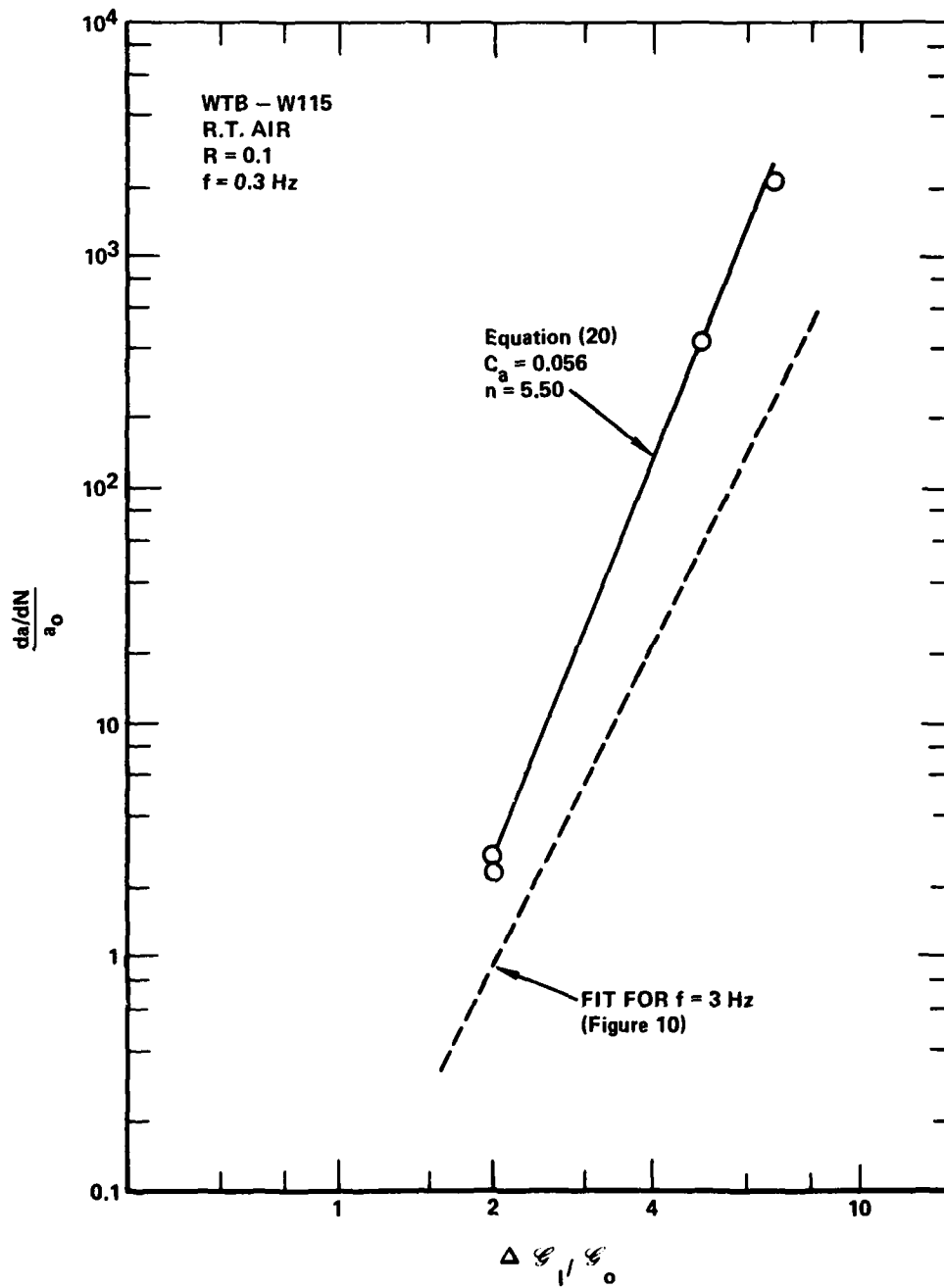
Figure 12. Pure Mode I da/dN in Laboratory Air at R = 0.6

Figure 13. Pure Mode I da/dN in Laboratory Air at R = 0.1 and f = 0.3 Hz

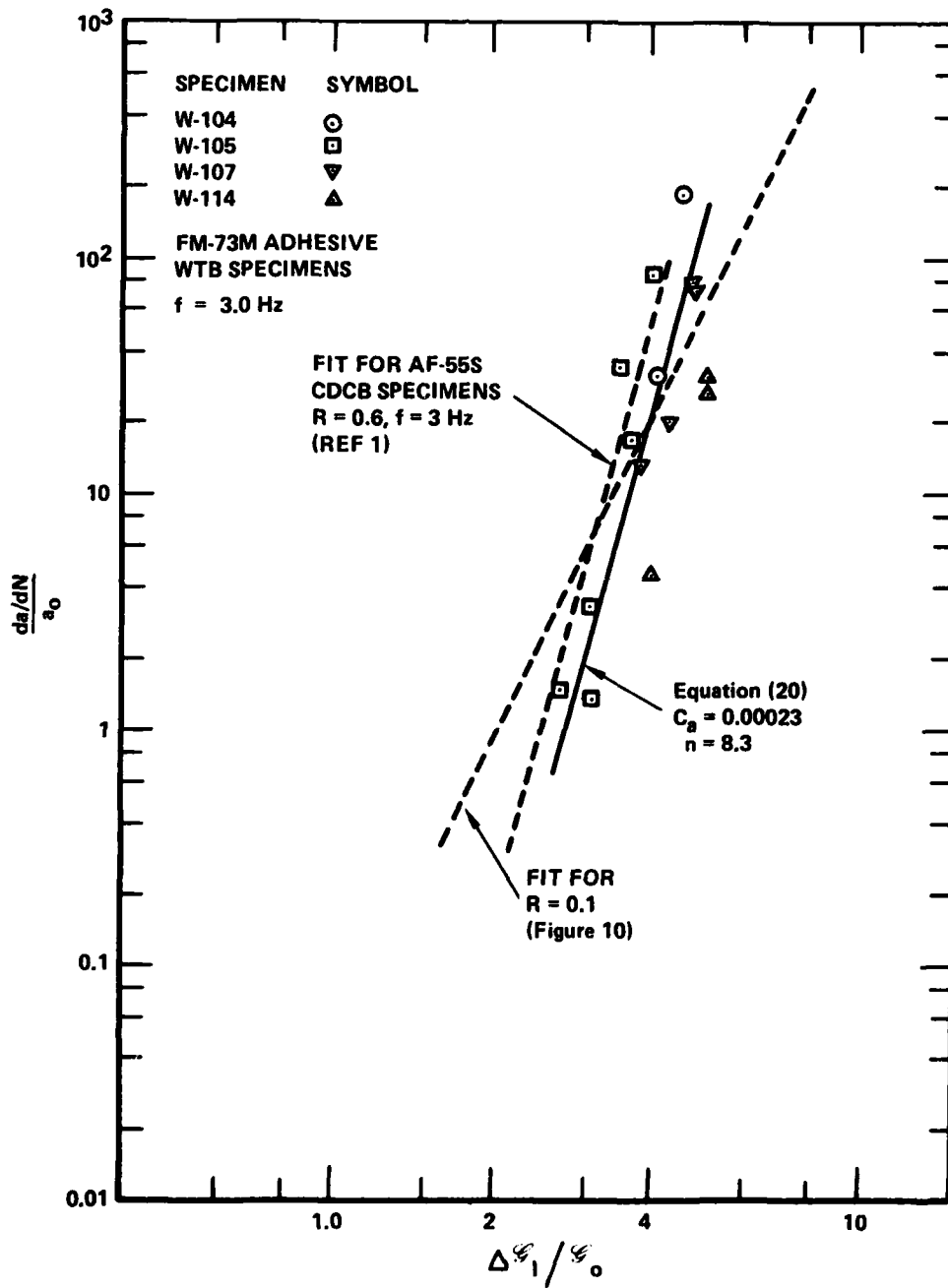Figure 12.   Pure Mode I da/dN in Laboratory Air at R = 0.6

45

2.2 Mixed Mode da/dN Data In Laboratory Air

Baseline da/dN data for mixed Modes I and II are presented in Reference 1 in terms of effective strain energy release rate, defined as:

$$\Delta \mathscr{G}_{eff} = \left(1 + \frac{2 \mathscr{G}_{II}}{\mathscr{G}}\right) \Delta \mathscr{G}_{I} \tag{25}$$

This definition was selected empirically, such that the Mode I and mixed mode da/dN curves for AF-55S were approximately coincident. Recall, however, that the pure Mode I data used in developing Equation (25) for AF-55S was from CDCB specimens. As shown in Figure 8, the use of WTB specimens machined from large-area bonded panels leads to a shift in the Mode I da/dN curve. Therefore, the Mode I and mixed mode da/dN curves for AF-55S will no longer correlate on the basis of $\Delta \mathscr{G}_{eff}$.

Figure 14 shows data from four axially loaded and two four-point-bend (CB) CLS specimens bonded with FM-73m and tested in laboratory air at R = 0.1 and f = 3 Hz. For these conditions, the crack growth rates in the axially loaded CLS specimens are almost identical for FM-73m and AF-55S adhesives. However, the $\Delta \mathscr{G}_{eff}$ variable fails to correlate the FM-73m data for the three different mode mixes (CLS, CB and WTB).

As an alternative to $\Delta \mathscr{G}_{eff}$, the following strain energy release rate parameter can be used:

$$\overline{\Delta \mathscr{G}} = \exp \left(-m \frac{\mathscr{G}_{I} \mathscr{G}_{II}}{\mathscr{G}^{2}}\right) \Delta \mathscr{G} \tag{26}$$

where m is an empirical constant. From the data in Figure 14, a best-fit value
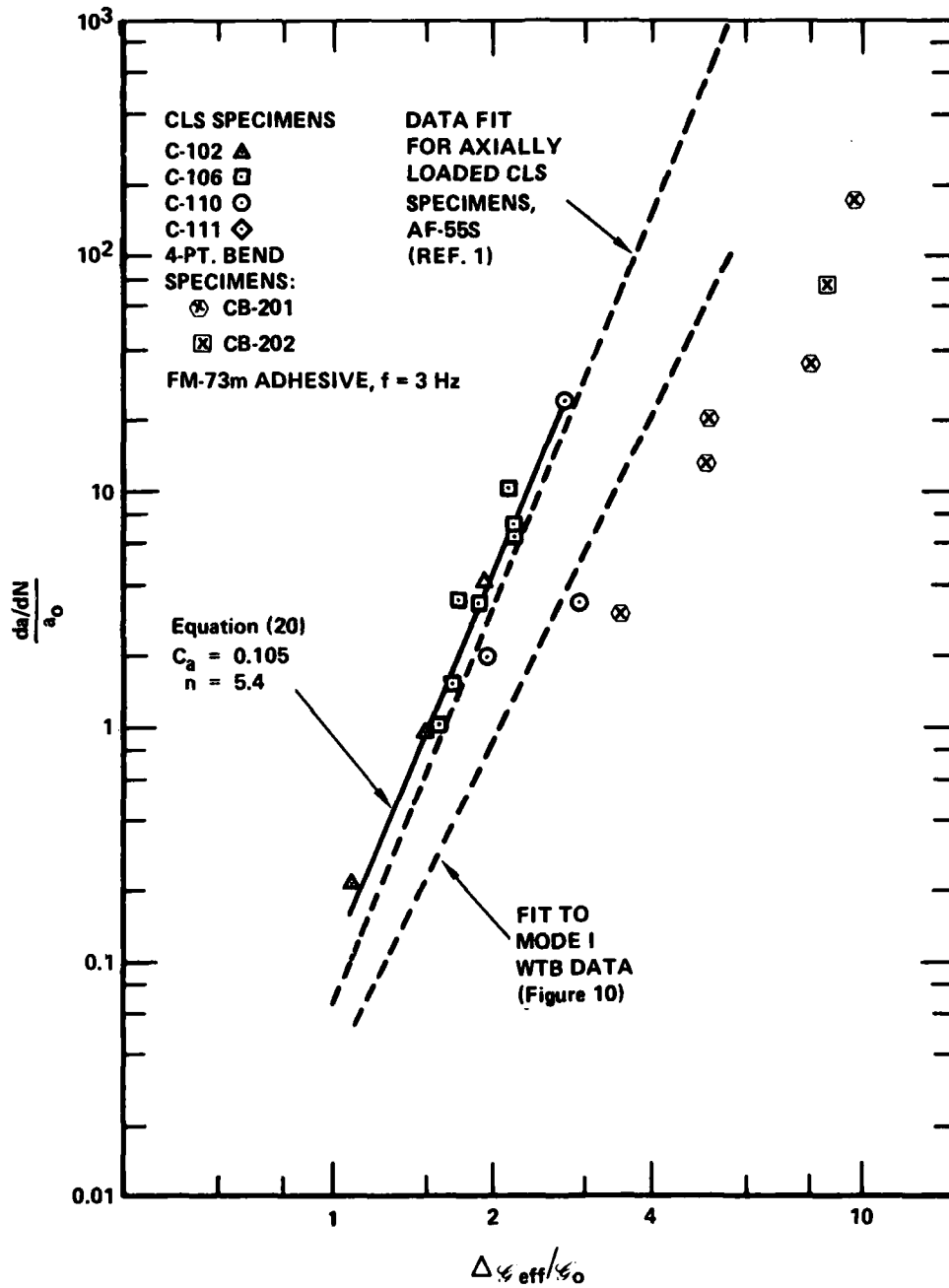
$$m = 1.0 \tag{27}$$

Figure 14. Mixed-Mode da/dN in Laboratory Air at R = 0.1

was obtained. Note in Figure 15 that, on the basis of $\overline{\Delta\mathscr{G}}$, the mixed-mode CLS specimen data from Figure 14 for both axial and bending loading coincide with the fit for the corresponding Mode I data from Figure 10.

AF-55S and FM-73m have essentially the same da/dN properties in laboratory air at R = 0.1 and f = 3.0 Hz, as measured on both the CLS and the WTB specimen. Therefore, all the mixed-mode data for both materials correlate to one scatterband, by use of $\overline{\Delta\mathscr{G}}$ as the abscissa, as shown in Figure 16.

A few data points were generated on CLS specimens in laboratory air at 3 Hz and a stress ratio of R = 0.6. These data are plotted as $\overline{\Delta\mathscr{G}}$ versus da/dN in Figure 17 and compared to the Mode I curve for R = 0.6. The parameter $\overline{\Delta\mathscr{G}}$ fails to correlate these data at R = 0.6.

Test data generated at high cyclic frequency, f = 15 Hz, are compared in Figure 18 to the corresponding data fits for f = 3 Hz. No significant effect of frequency can be concluded from these few data points. (The two points generated at R = 0.1 are within the scatterband of the data in Figure 16.)

2.3 Mode I da/dN Data in 333°K (140°F) Water

For AF-55S adhesive, immersion in 333°K (140°F) deionized water during fatigue cycling had caused a factor of 10 increase in da/dN at R = 0.1 and f = 3 Hz (Reference 1). A further increase in da/dN had been observed when the cyclic frequency was reduced to 0.25 Hz.

Two Mode I WTB specimens bonded with FM-73m adhesive were fatigue tested while immersed in 333°K (140°F) deionized water. One of these, specimen W-102, was presoaked in 333°K (140F) deionized water by virtue of a sustained load test which lasted 58 days without measurable crack growth.

Figure 19 is the da/dN plot of the Mode I environmental fatigue data for FM-73m adhesive. The data cover both R = 0.1 and R = 0.6 and are compared to the corresponding data fit lines for lab. air environment. Some points indicate increases in da/dN due to hot water immersion; some indicate reductions.
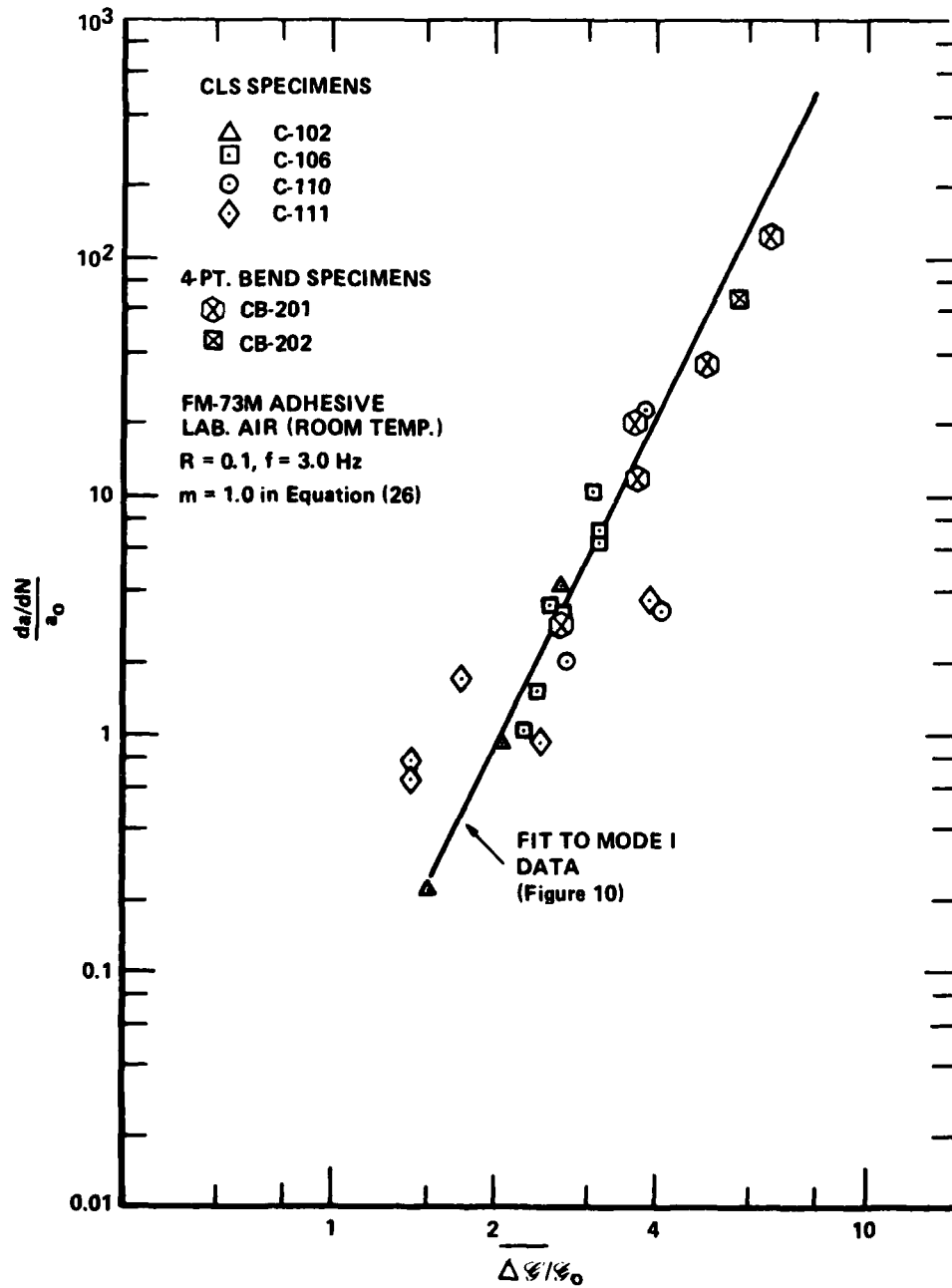
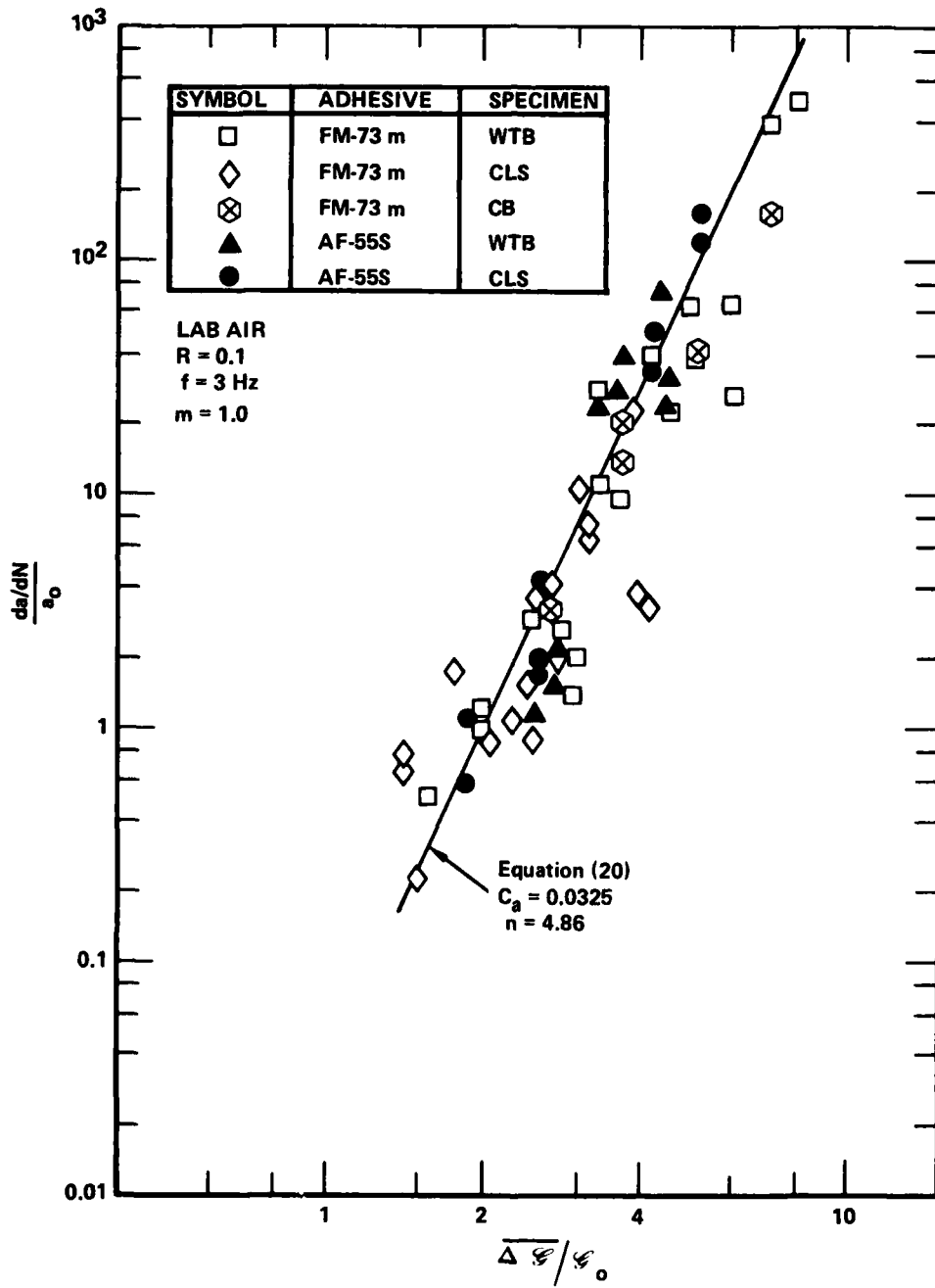Figure 15.   Use of $\overline{\Delta \mathscr{G}}$ for Mixed—Mode Data Fitting for FM—73m

50

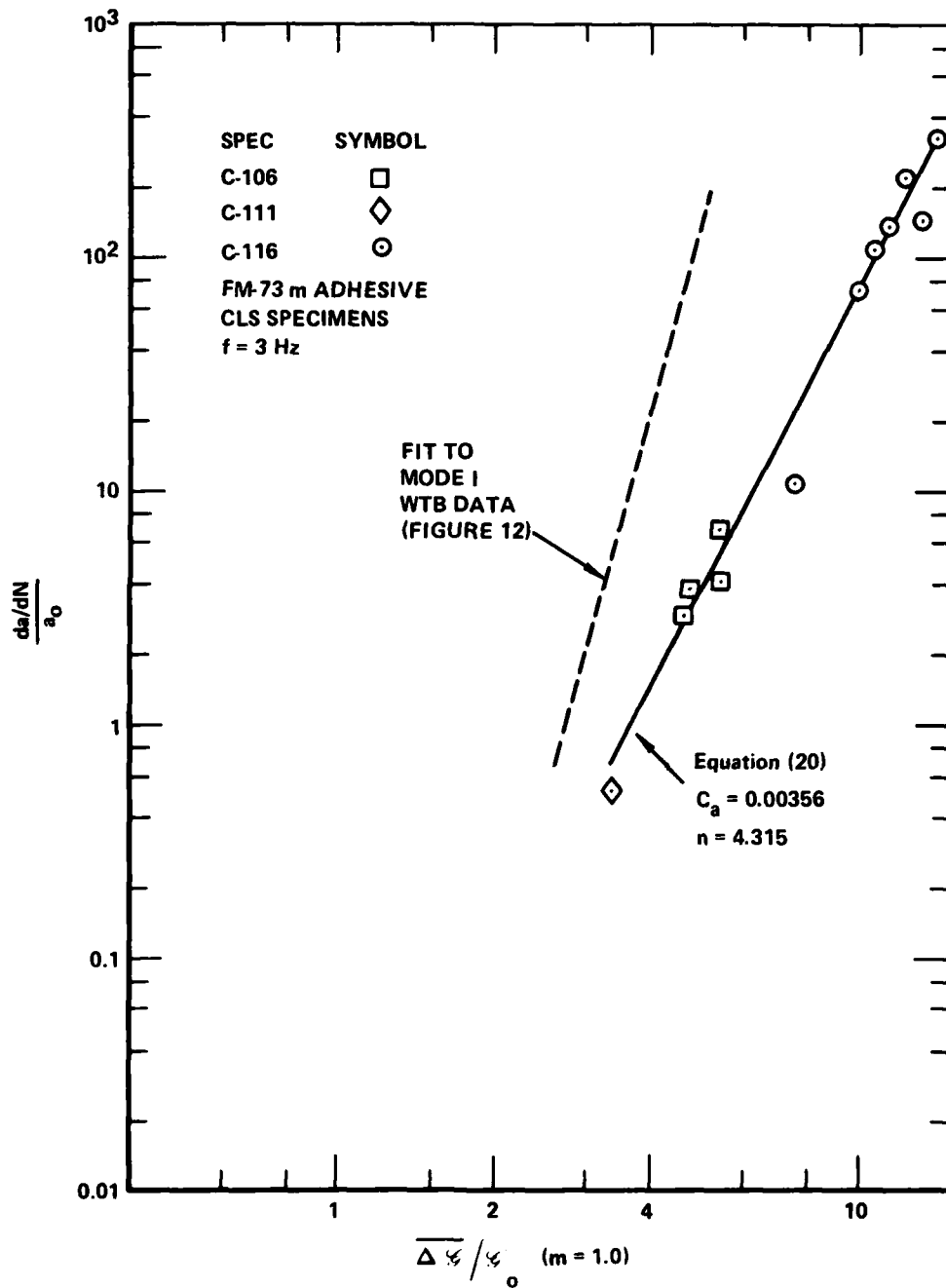Figure 16.   Correlation of FM-73m and AF-55S da/dN Data
for Pure and Mixed Modes

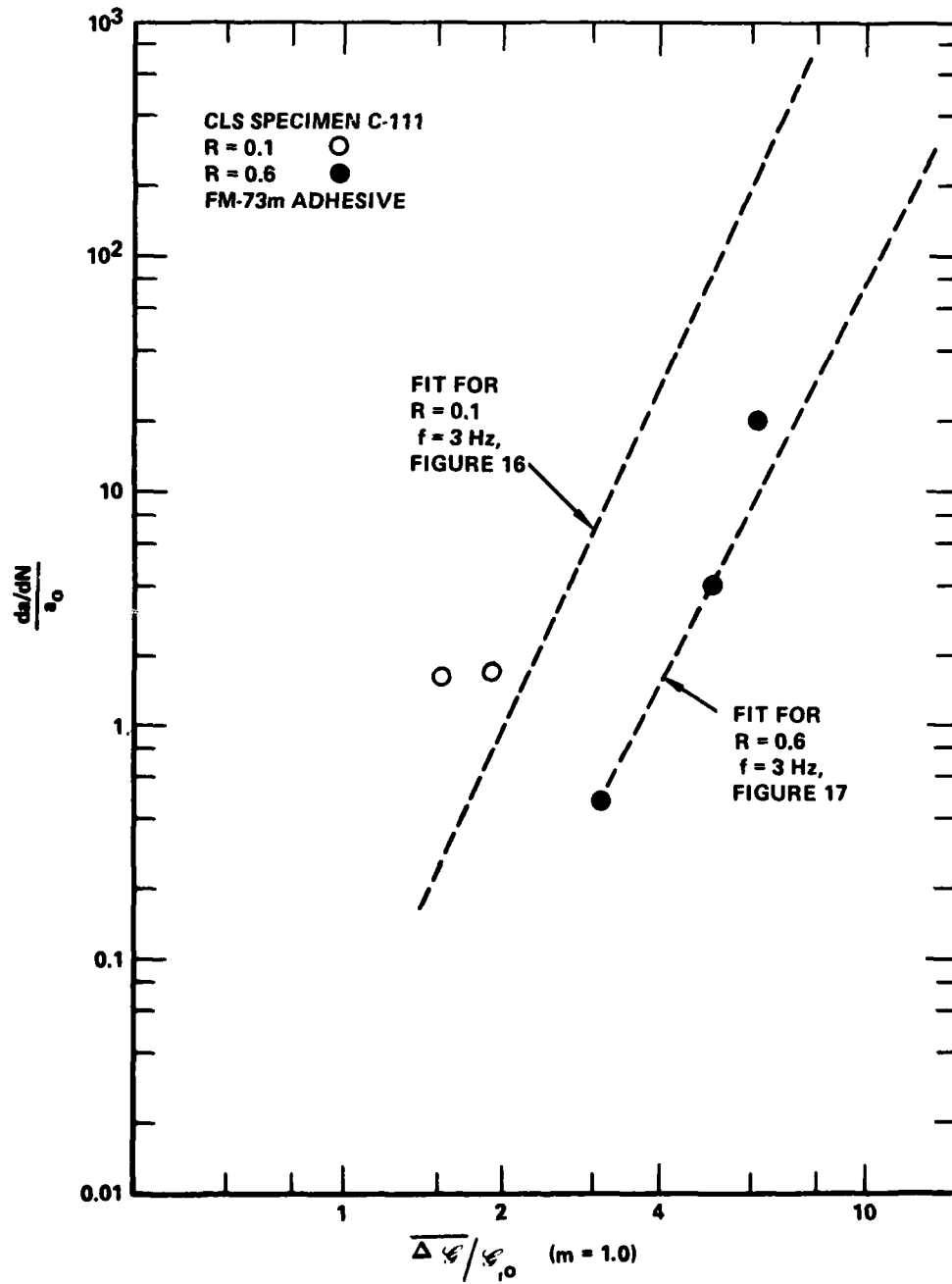Figure 17. Mixed-Mode da/dN in Laboratory Air at R = 0.6

Figure 18.   Mixed-Mode da/dN in Laboratory Air at f = 15 Hz

53

For each specimen, the data points in Figure 19 are numbered chronologically. With study, a trend with time and crack length becomes evident. The longer the test proceeds, the slower is the crack growth rate.

This trend is more evident when the data are replotted against time as in Figure 20. The ordinate, $\Delta\mathscr{C}_{EQV}/\Delta\mathscr{C}_{I}$, is the factor by which $\Delta\mathscr{C}_{I}$ would have to be multiplied to obtain, in a laboratory air environment, the value of crack growth rate observed in the hot-water immersion test. Mathematically, $\Delta\mathscr{C}_{EQV}$ is defined as:

$$\frac{\Delta\mathscr{C}_{EQV}}{\mathscr{C}_{o}} = \left(\frac{1}{C_a} \frac{da}{a_o dN} \right)^{1/n} \tag{28}$$

where C_a and n are the best-fit constants for the laboratory air data, given in Figures 10 and 12.

Figure 20 shows that, as fatigue testing of Specimen W-111 in hot water continued, the environmental effect gradually became beneficial rather than detrimental. Ultimately, after 600 hours of fatigue cycling in $333^{\circ}K$ ($140^{\circ}F$) water, the crack growth rate in hot water was slower than the corresponding rate for laboratory air environment by a factor of about 50. The data from Specimen W-102, which previously was sustained-load tested in hot water for 58 days, tends to show the same trend, but the test time effects are somewhat confounded by the fact that the cyclic frequency was reduced to 0.3 Hz for the last five data points.

For prediction for the structural specimens, a reliable da/dN curve was needed for FM-73m adhesive immersed in hot water and subjected to a fairly short-duration test. Therefore, two UDCB specimens which received no presoak were tested at high da/dN values, such that the total accumulated time that each specimen was being cyclically loaded was approximately 30 hours. The results from these tests (at R = 0.1 and f = 3 Hz) are plotted in Figure 21.
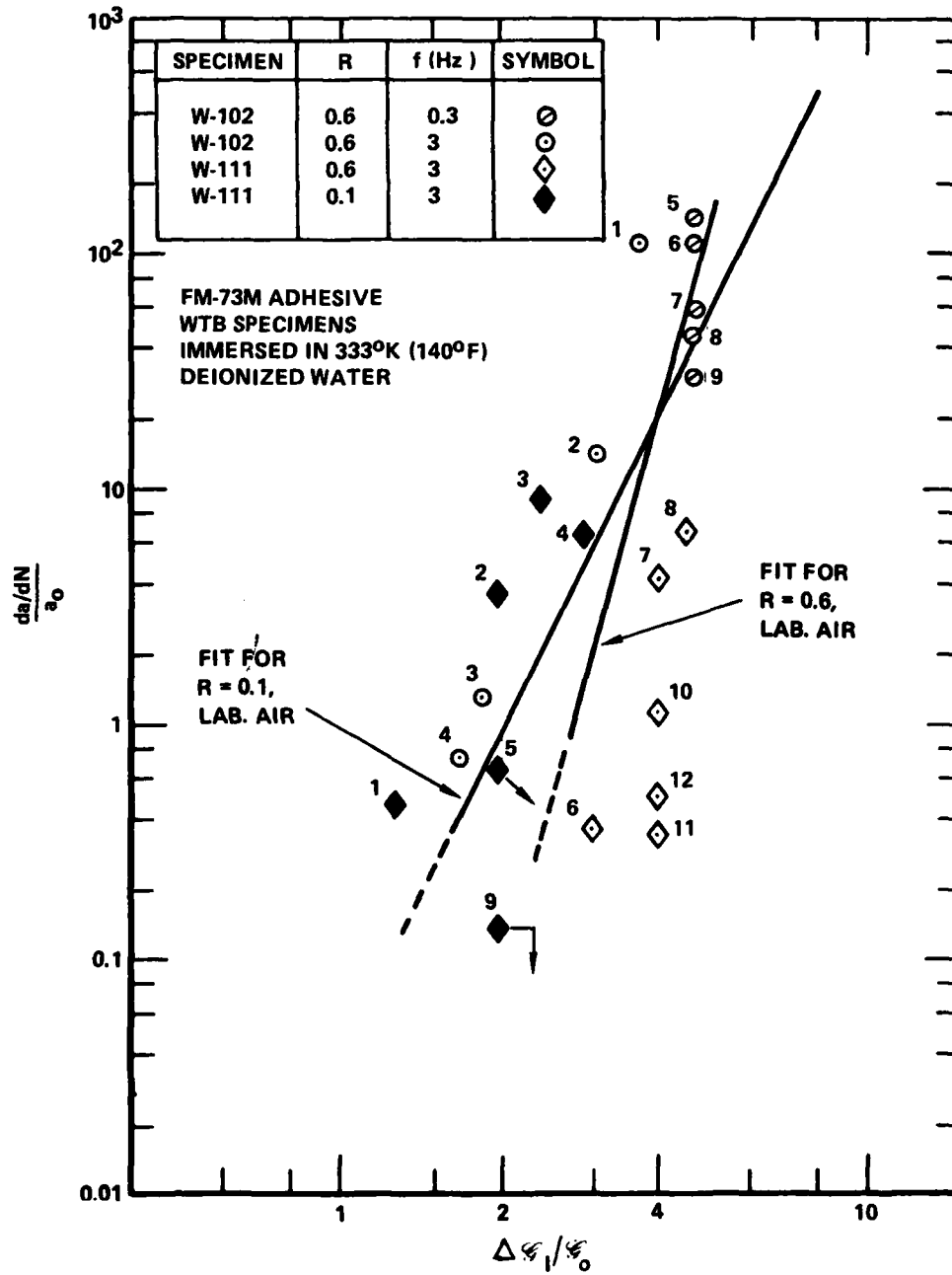
54

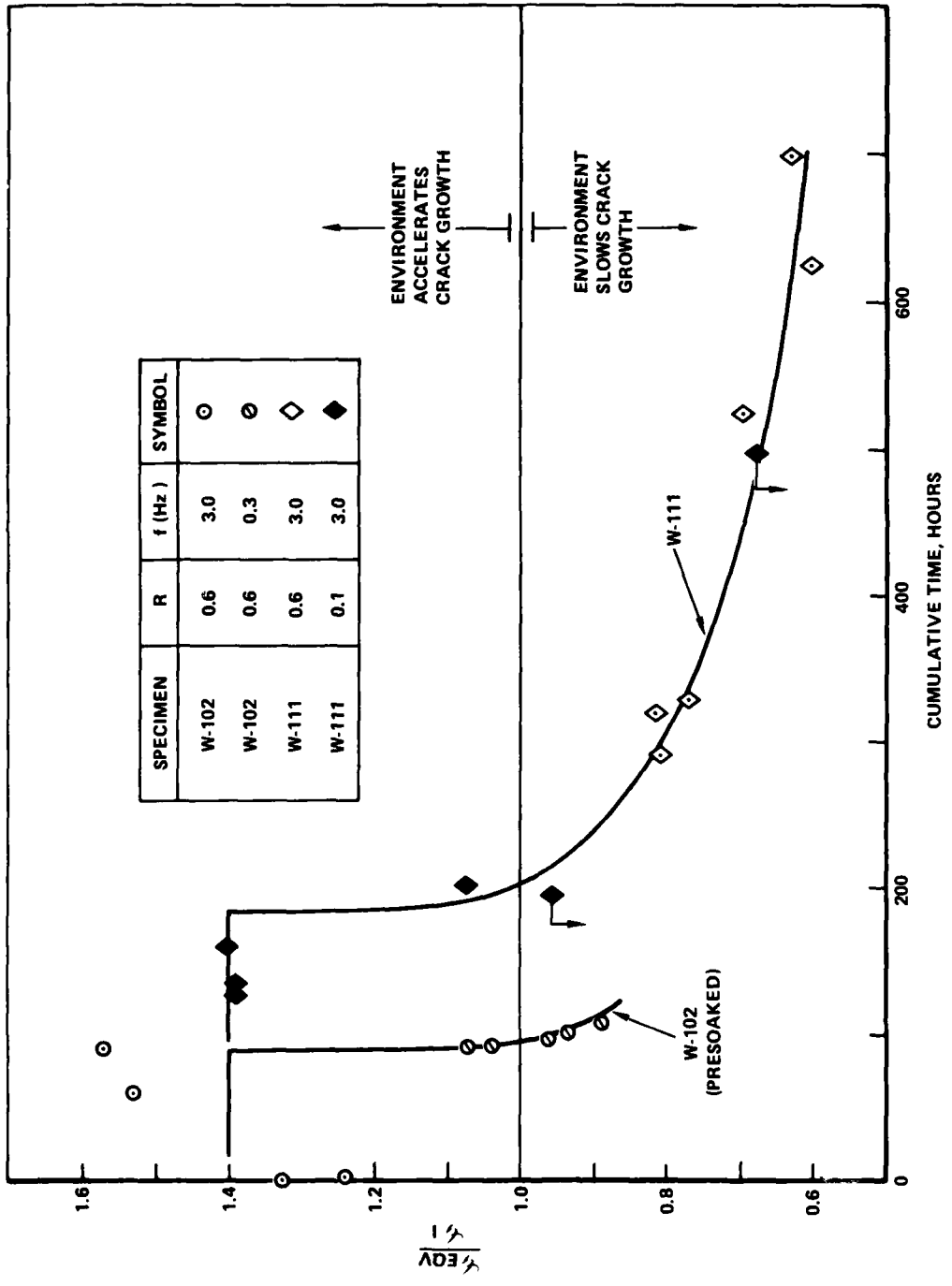Figure 19. Mode I da/dN in Hot Water

55

Figure 20. Effect of Fatigue Test Time on the Environmental da/dN Properties
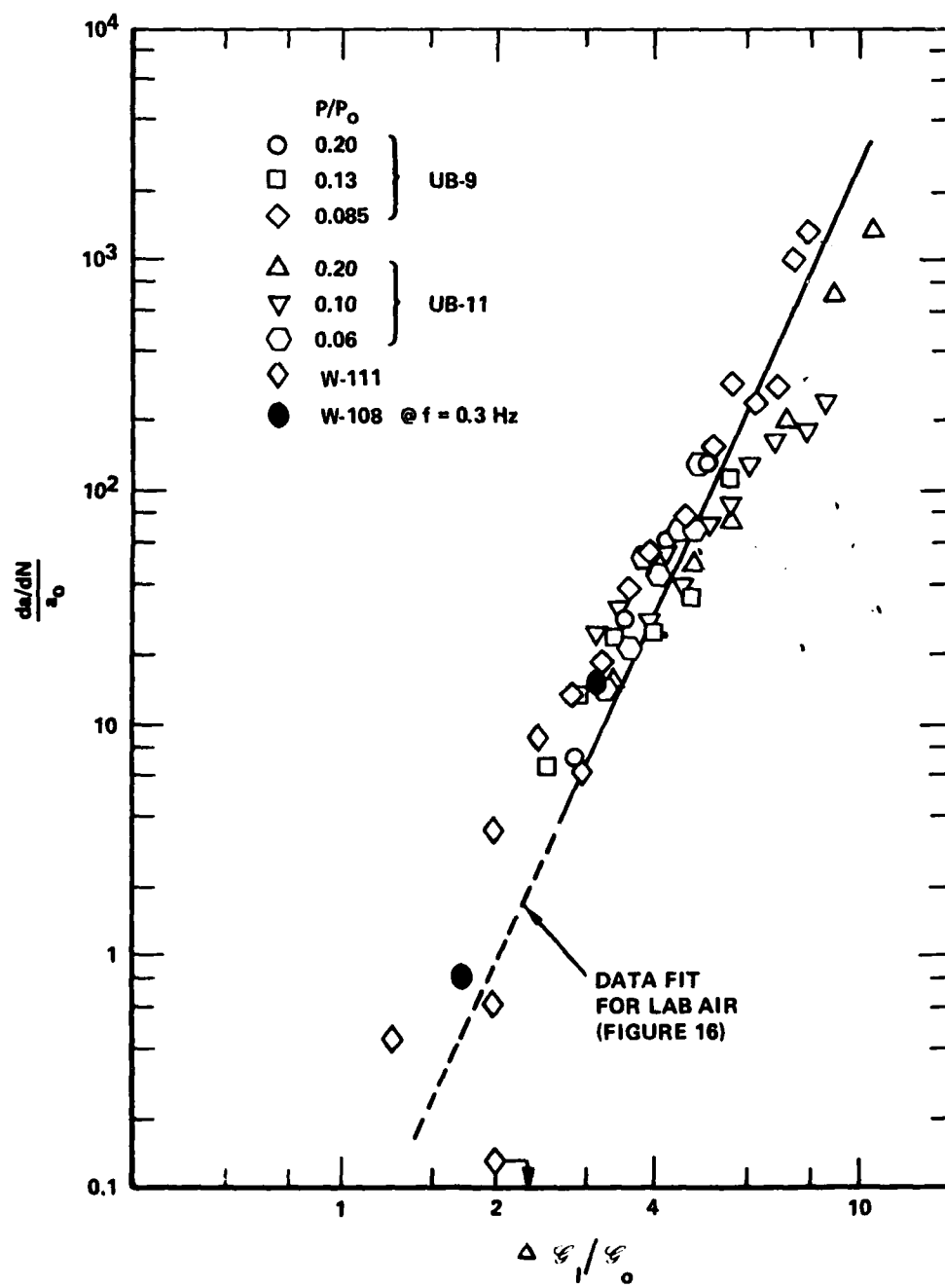of FM-73m in Pure Mode I

56

Figure 21.   Pure Mode I da/dN in 333°K $(140^{\circ}$F) Water
at R = 0.1 and f = 3 Hz

57

The crack growth rate is essentially the same in hot water and in laboratory air. Two data points obtained on WTB specimen W-108 at a lower cyclic frequency (f = 0.3 Hz) are within the scatterband of the f=3 Hz data.

A UDCB specimen was also tested in 333°K (140°F) water at a stress ratio of R = 0.6. The cumulative run time in this test was approximately 15 hours. The data are plotted in Figure 22. Again these data fall almost perfectly along the extrapolation of the data fit line for laboratory air from Figure 12, implying that there is no effect of the environment on the crack growth rate at R = 0.6 and f = 3 Hz in pure Mode I for short-term tests.

2.4 Mixed Mode da/dN Data in 333°K (140°F) Water

Three CLS specimens were side-notched and da/dN tested in 333°K (140°F) deionized water.

The data for a stress ratio of R = 0.1 and a cyclic frequency of f = 3 Hz are plotted in Figure 23. The abscissa is $\overline{\Delta\mathscr{G}}$, defined in Equation (26), with m = 1.0 as used to correlate the laboratory air data. The observed crack growth rates are slightly slower than those of the laboratory air data. Use of an m value in Equation (26) of 1.5 instead of 1.0 slightly shifts the CLS data without affecting the pure Mode I data. Thus, in 333°K (140°F) water at R = 0.1 and f = 3 Hz;

$$\overline{\Delta\mathscr{G}} = \exp\left(-1.5\frac{\mathscr{G}_I \mathscr{G}_{II}}{\mathscr{G}^2}\right)\Delta\mathscr{G} \tag{29}$$

This equation is used in Section IV for the crack growth analysis of the structural single lap joint specimens, along with the room temperature data fit from Figure 16, i.e.,

$$\frac{da/dN}{a_o} = 0.0325\left(\overline{\Delta\mathscr{G}}/\mathscr{G}_o\right)^{4.86} \tag{30}$$
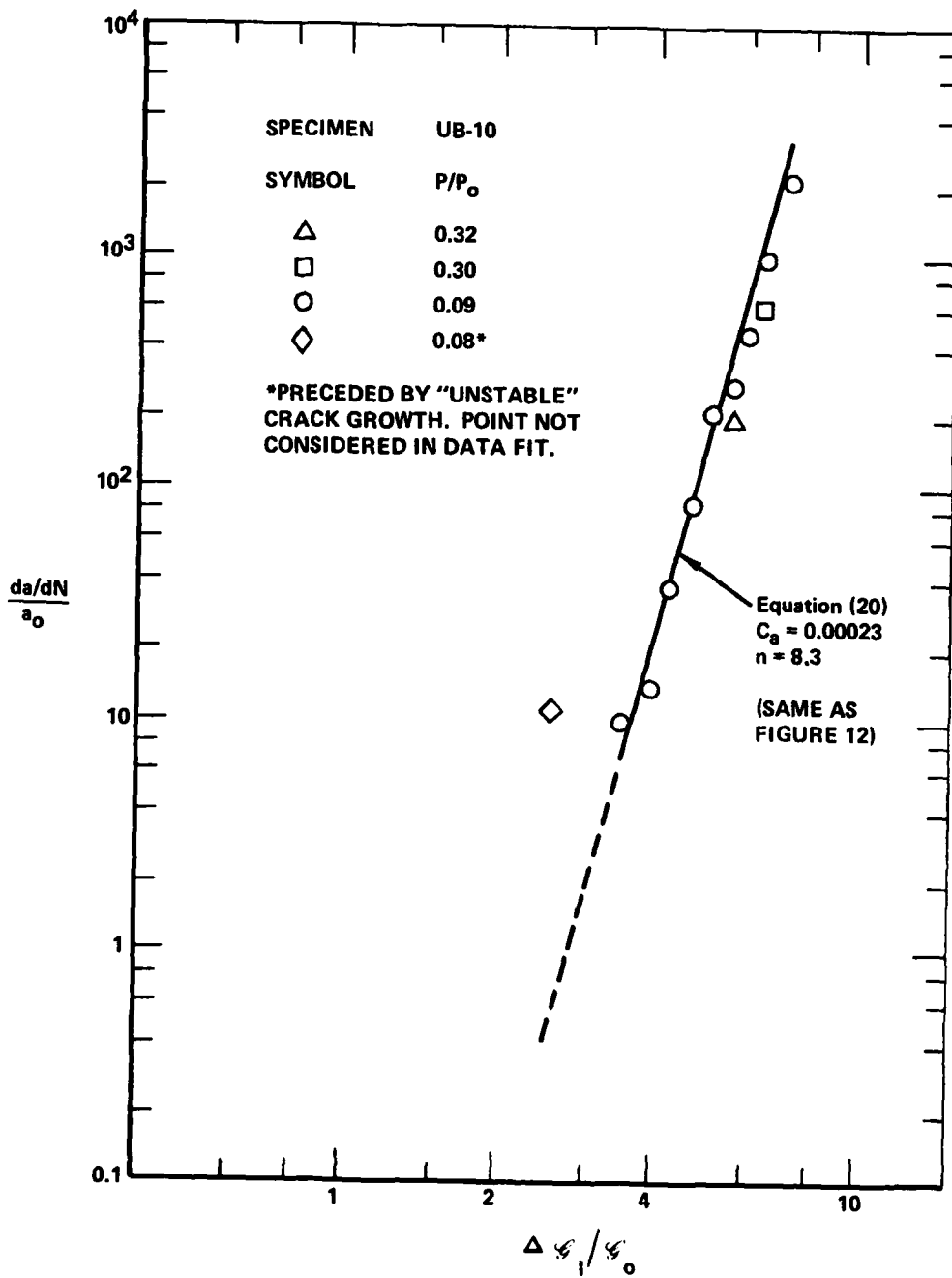
Figure 22.   Pure Mode I da/dN in $333^\circ K$ ($140^\circ F$) Water
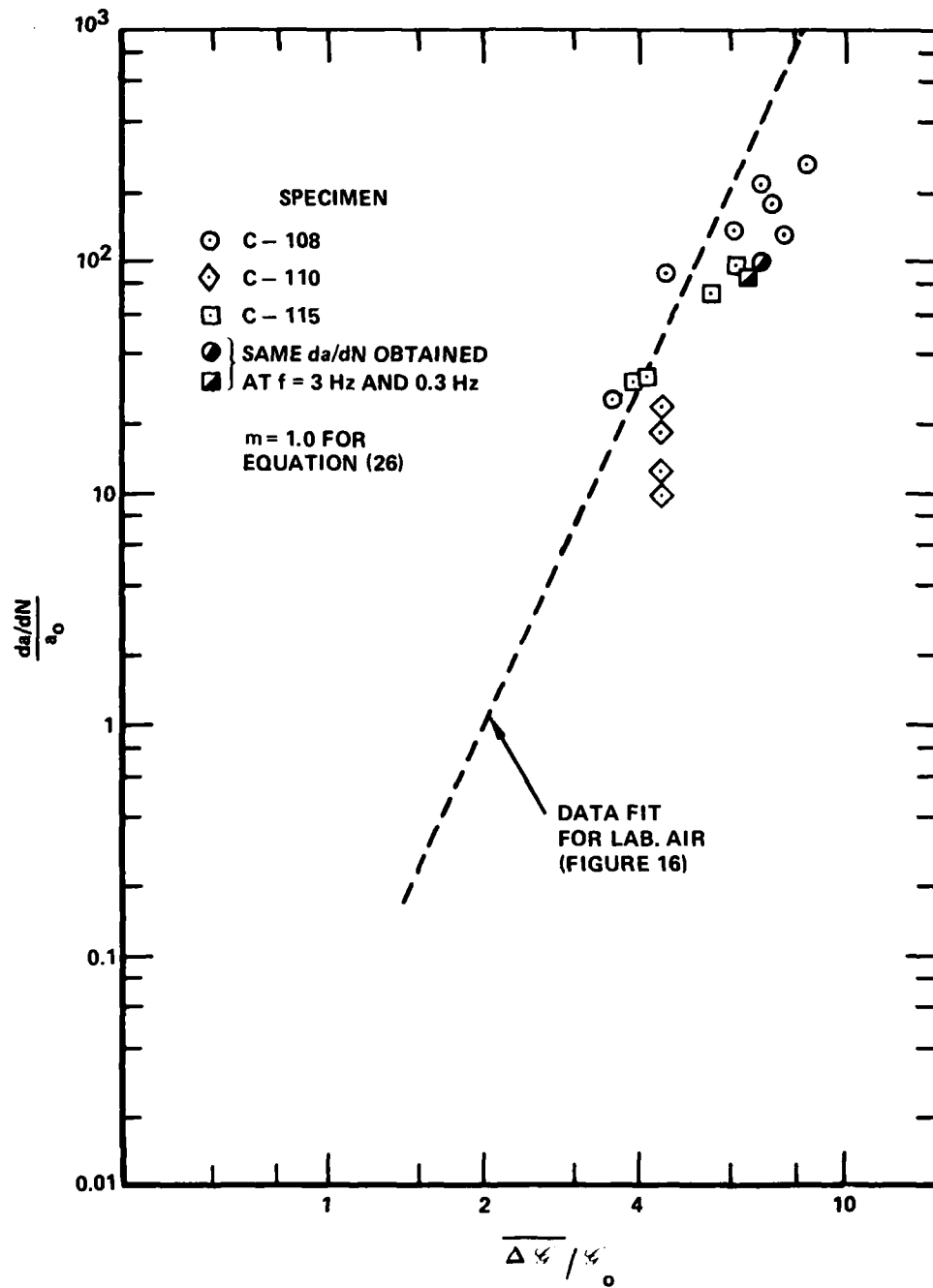at R = 0.6 and f = 3 Hz

Figure 23. Mixed-Mode da/dN in 333°K (140°F) Water
at R = 0.1 and f = 3 Hz

60

The last measurement of da/dN was repeated on both Specimens C-108 and C-115 at a lower cyclic frequency but with otherwise identical test conditions. In both cases, the crack growth rate at f = 0.3 Hz was within 10 percent of that measured at f = 3 Hz.

Additional data (besides those plotted in Figure 23) were obtained on specimen C-110 at R = 0.1, f = 0.3 Hz, and at R = 0.6, f = 3 Hz. These data are plotted in Figure 24. The data points are numbered sequentially. However, unlike that shown in Figure 22 for the WTB specimen, there appears to be no trends with time and crack length. This illustrates the type of unexplained scatter that plagued some of the baseline testing of this adhesive, unlike AF-55S.

2.5 Discussion of Baseline da/dN Test Results

In comparing the baseline da/dN data for FM-73m adhesive to those for AF-55S, two observations are strikingly clear:

- In laboratory air at R = 0.1 and f = 3 Hz, the crack growth rate curves for the two materials are identical.

- Immersion in 333°K (140°F) water causes da/dN in AF-55S to increase by more than an order of magnitude compared to the rate in laboratory air. In FM-73m, however, da/dN values in laboratory air and hot water are essentially equal.

The no-growth threshold for da/dN, $\Delta\mathscr{G}_{TH}$, is an important quantity. An engineering definition of $\Delta\mathscr{G}_{TH}$ (Reference 1) is the value of $\Delta\mathscr{G}$ for which da/dN is only 1 mm per year (1 in. per 25 years). These threshold values are calculated by extrapolating the data fit line on each data plot, using the equation

$$\Delta\mathscr{G}_{TH}/\mathscr{G}_o = \left(\frac{0.00127}{C_a f}\right)^{1/n} \tag{31}$$

The results for FM-73m are summarized in Table 10.

In diagnosing a bondline failure, it is useful to be able to easily distinguish between fracture surfaces created by different causes. This is

61

FM-73 ADHESIVE
CLS SPECIMEN C-110
IMMERSED IN 333°K (140°F)
DEIONIZED WATER

$\dfrac{da/dN}{a_o}$

10^3

10^2

10

1

0.1

0.01

13
12
15
16
7   14
13
5
4, 17
1
6
2
3
8
9
10

FIT FOR
R ≈ 0.1, RT
CLS SPEC.

FIT FOR
R ≈ 0.6, RT,
MODE I

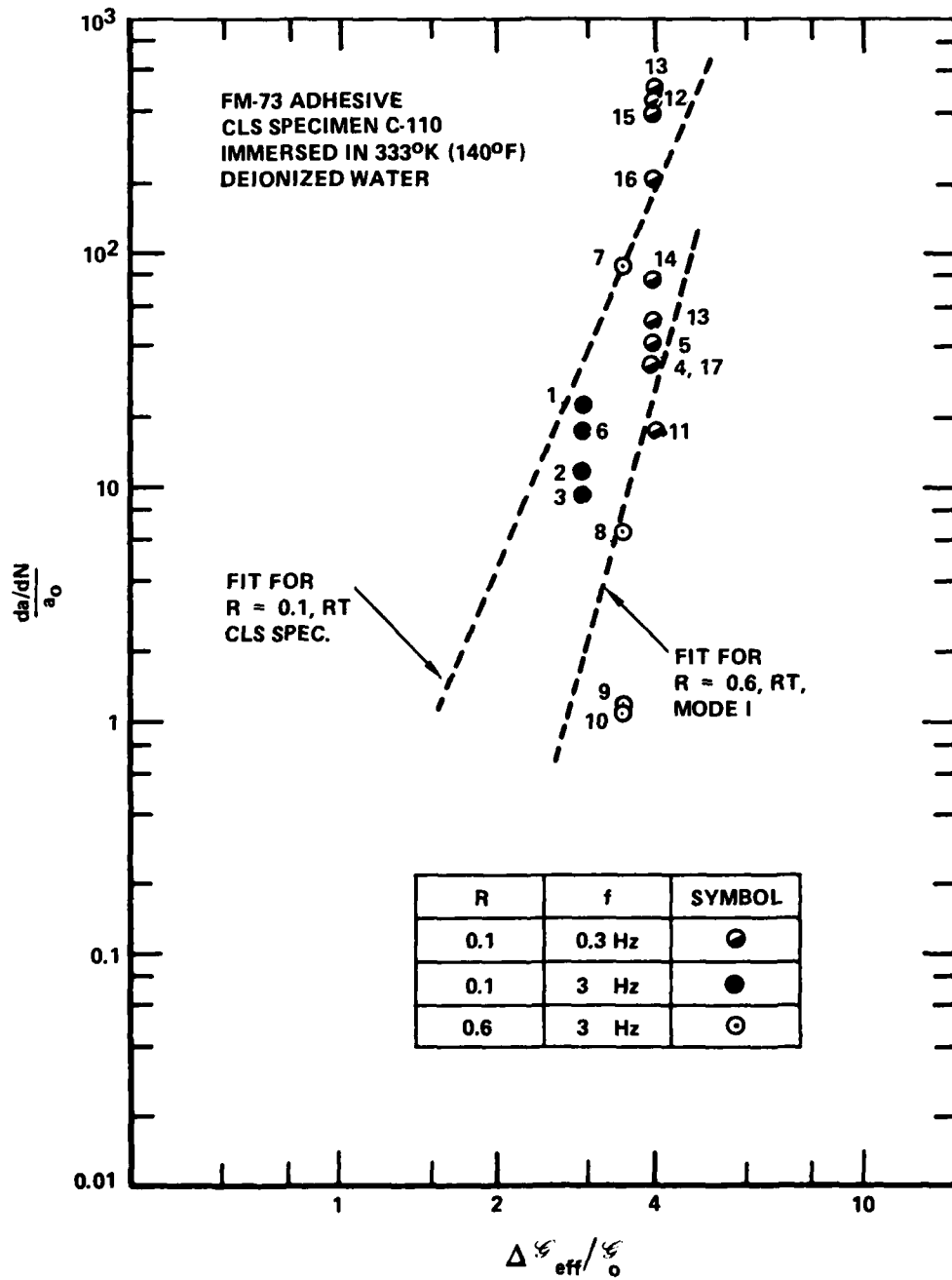| R	f	SYMBOL
0.1	0.3 Hz	◐
0.1	3 Hz	●
0.6	3 Hz	⊙

1   2   4   10

$\Delta \mathcal{G}_{eff}/\mathcal{G}_o$

Figure 24.   Mixed-Mode da/dN in Hot Water

62

TABLE 10. ENGINEERING VALUES OF da/dN THRESHOLD, FM-73m

| Test Conditions | | | | | | | | | | | | |
| Environment | | | | Frequency, Hz | | | Pure Mode I | Mixed Modes I & II | Data Plot, Figure No. | C_a | n | $\dfrac{\Delta\Psi_{ITH}/\Psi_o \text{ or}}{\Delta\Psi_{TH}/\Psi_o}$ |
R = 0.1	R = 0.6	Lab. Air	333°K (140°F) Water	0.3	3	15						
✓		✓	✓		✓		✓	✓	16	0.325	4.86	0.409
	✓	✓	✓		✓		✓		12	0.00023	8.3	1.076
✓		✓			✓	✓	✓		15	0.056	5.5	0.307
	✓	✓						✓	17	0.00356	4.315	0.610
	✓	✓				✓		✓	18	0.00356	4.315	0.420

63

possible for FM-73m, just as for AF-55S. An example is shown in Figure 25, a 10X view of the fracture surfaces of CLS specimen C-102. In this specimen, the mixed-mode fatigue cycling in laboratory air caused the crack to propagate primarily near the interface of one of the adherends, whereas the increasing-load fracture was primarily center-of-bond with the same inclined scales that characterized the mixed-mode failure of AF-55S (Reference 1).
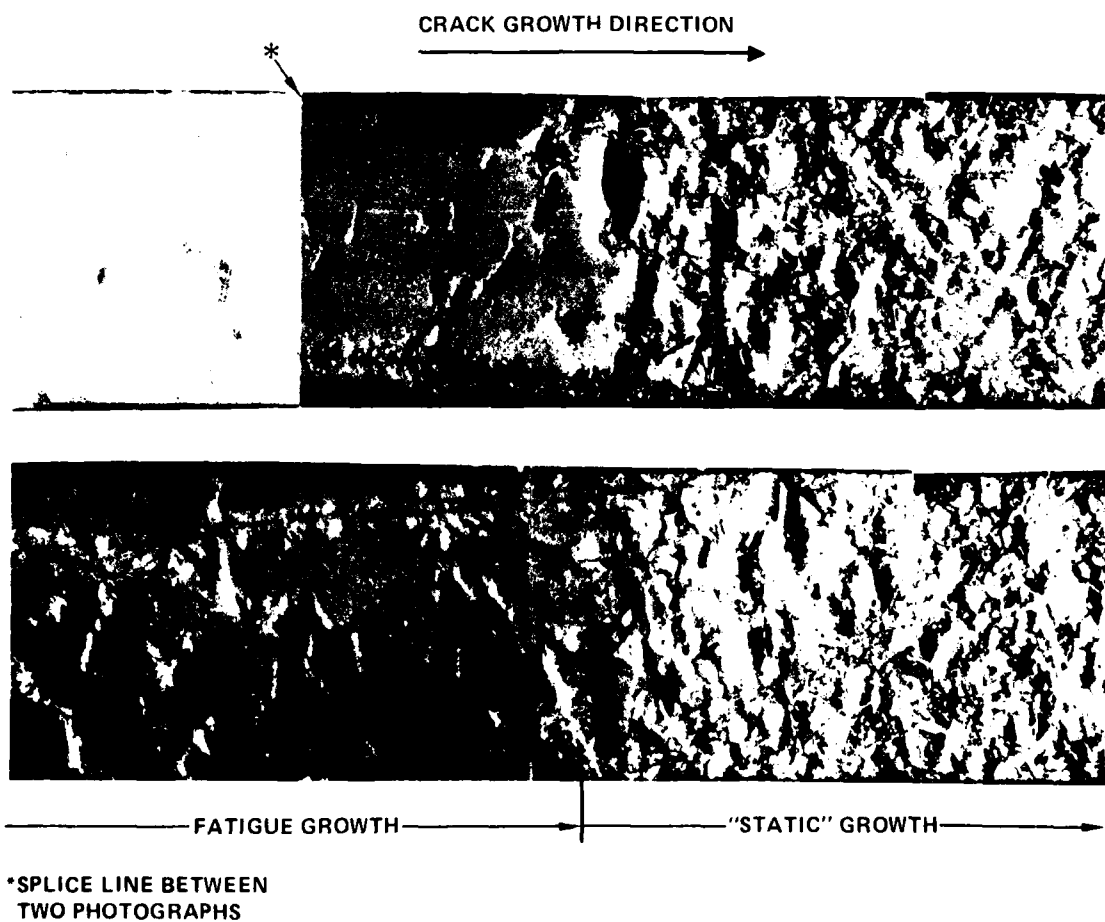
CRACK GROWTH DIRECTION

————————————FATIGUE GROWTH——————————▸◀——————————"STATIC" GROWTH——————————▸

*SPLICE LINE BETWEEN
TWO PHOTOGRAPHS

Figure 25. Mating Fracture Surfaces of CLS Specimen C-102 at
Transition from Fatigue to $\mathcal{G}_C$ Fracturing

SECTION IV

METHODOLOGY DEMONSTRATION

In Reference 1, six single-lap joint (SLJ) specimens with 3.1 mm
(0.125 in.) adherends bonded with AF-55S adhesive and containing bondline pre-
flaws were immersed in 333°K (140°F) deionized water and constant-amplitude
fatigue tested to failure. Baseline da/dN data from CLS and CDCB specimens
were used in conjunction with a finite-element-based strain energy release
rate analysis of the SLJ specimen to predict crack growth. The five appli-
cable experimental crack growth lives ranged from 48,297 to 58,338 cycles,
compared to a prediction of 118,000 cycles. (The sixth specimen failed pre-
maturely due to a machining defect in the metal).

That work was to be duplicated using the identical specimen geometry and
test conditions, but FM-73m adhesive instead of AF-55S. The purpose was to
show the extent to which the methodology for AF-55S is applicable to and
accurate for FM-73m. However, several improvements to the methodology were
made during this phase. These improvements led to the discovery that the
methodology that had been applied earlier to the AF-55 data had some large
inaccuracies which canceled one-another, leaving the net error of only about
a factor of two in the life prediction. The development of the improved
methodology, which corrects these inaccuracies, is described in this section.

1. STRUCTURAL TESTS

1.1 Test Specimen and Test Procedures

It was intended to test six SLJ specimens, as in Reference 1. Midway
through the testing of these specimens, however, it was discovered that the
surface preparation prior to bonding had probably been inadequate. Therefore,
some additional specimens had to be fabricated and tested.

The specimen, shown in Figure 26, has a width of 229 mm (9.0 in.). A piece of Teflon tape is attached to the primed skin just prior to layup and bonding. This creates a preflaw of prescribed size and location in the bond-line between the skin and the doubler.

The test conditions were identical to those of the previous SLJ specimens (Reference 1) bonded with AF-55S adhesive, so that the two adhesives could be compared. The specimens were constant amplitude fatigue cycled to a maximum axial tension load of 120.1 kN (27.0 kip) at a stress ratio of R = 0.1. Except for the final two tests, the cyclic frequency was 3 Hz. Lateral bending was constrained by flexures connected to a very stiff externally mounted beam. During cycling the test area was immersed in 333°K $(140^{\circ}$F) deionized water, pumped through a plexiglas tank that was bonded to the test specimen itself. Water temperature was controlled within about $\pm 1^{\circ}$K $(1.8^{\circ}$F). The 200-kip MTS machine at the Lockheed Rye Canyon fatigue laboratory was used for all tests. None of the specimens was presoaked prior to testing.

Crack growth was monitored during the test by a compliance technique. The test was stopped periodically and the water drained from the tank, so that a displacement gage could be placed across the gap of the joint. The displacement was correlated to crack length using the results of a finite element computation. The circle points in Figure 27 show this calculated result, assuming that only one crack propagates in the bondline, a uniform across-the-width crack originating at the gap of the joint. Later finite element analyses considered cases of multiple cracking. The darkened triangles show the first measurements on the initial test specimens (discussed in the next subsection). These tend to verify the finite element result.

1.2 Initial Tests

The crack growth results for specimens SLJ-101, -102, -105, and -106 are plotted in Figure 28. Specimens SLJ-101 and -102, which contained no initial bondline flaws, displayed substantial crack growth in the bondline (according to compliance measurements) before the metal adherends cracked and failed in the grip area at 33,668 and 42,551 cycles, respectively. Specimens SLJ-105 and -106, which contained widthwise Teflon tape initial flaws 7.6 mm (0.3 in.) deep, failed in the bondline at 49,186 and 27,309 cycles, respectively.
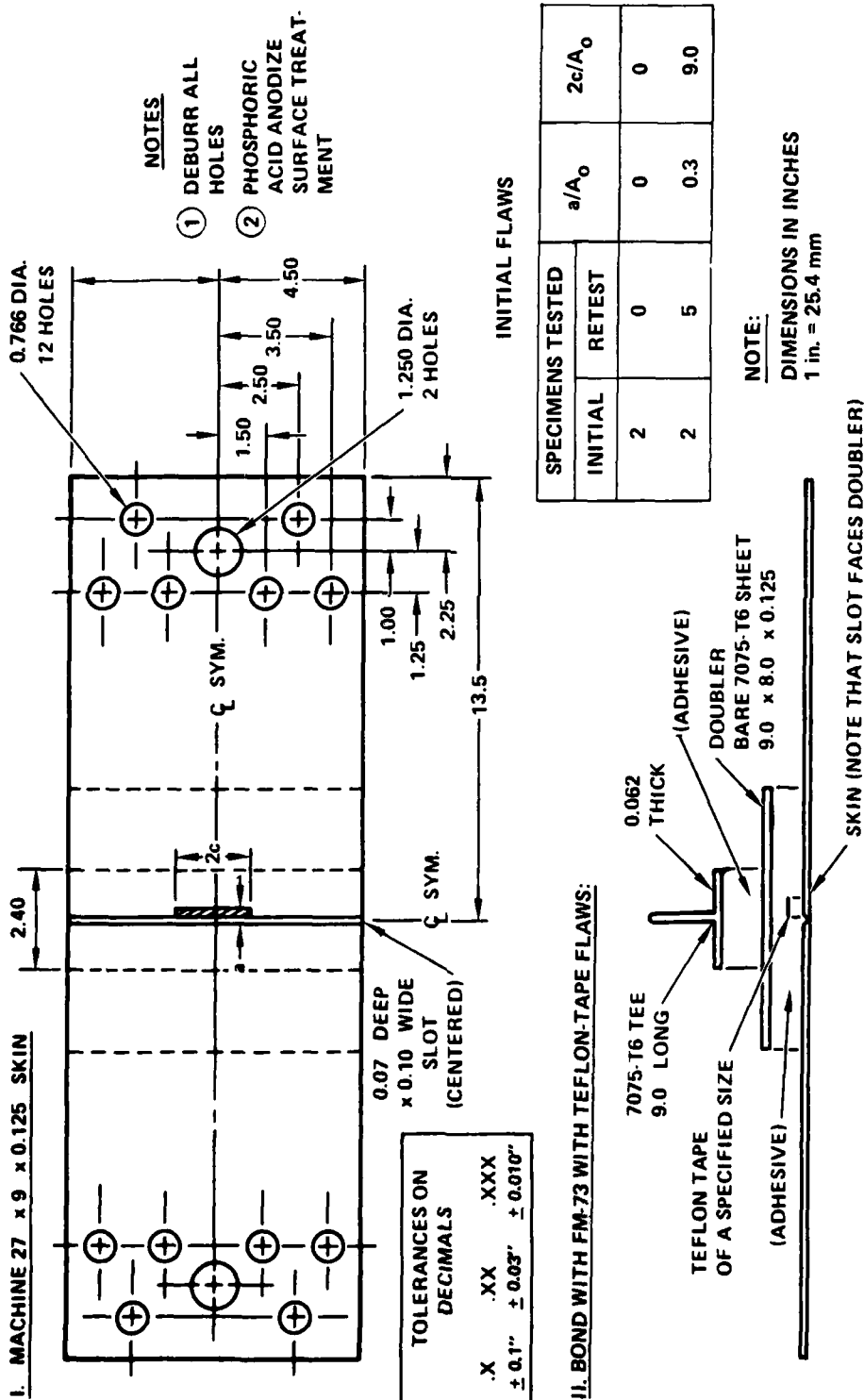
66

I. MACHINE 27 x 9 x 0.125 SKIN

0.766 DIA.
12 HOLES

1.250 DIA.
2 HOLES

0.766 DIA. ... 4.50
3.50
2.50
1.50

₵ SYM.

2.25
1.00
1.25

13.5

2.40

2c

0.07 DEEP
x 0.10 WIDE
SLOT
(CENTERED)

₵ SYM.

NOTES

① DEBURR ALL
   HOLES

② PHOSPHORIC
   ACID ANODIZE
   SURFACE TREAT-
   MENT

INITIAL FLAWS

SPECIMENS TESTED		a/A_o	$2c/A_o$
INITIAL	RETEST		
2	0	0	0
2	5	0.3	9.0

NOTE:
DIMENSIONS IN INCHES
1 in. = 25.4 mm

II. BOND WITH FM-73 WITH TEFLON-TAPE FLAWS:

7075-T6 TEE
9.0 LONG

TEFLON TAPE
OF A SPECIFIED SIZE

(ADHESIVE)

0.062
THICK

(ADHESIVE)

DOUBLER
BARE 7075-T6 SHEET
9.0 x 8.0 x 0.125

SKIN (NOTE THAT SLOT FACES DOUBLER)

III. AFTER BONDING, MACHINE SLOT THROUGH. FINAL CONFIGURATION IS A
SINGLE LAP JOINT TEST SPECIMEN WITH A BONDLINE FLAW BETWEEN
THE DOUBLER AND ONE SKIN MEMBER.

Figure 26. Single Lap Joint (SLJ) Specimen with Thin Adherends

67
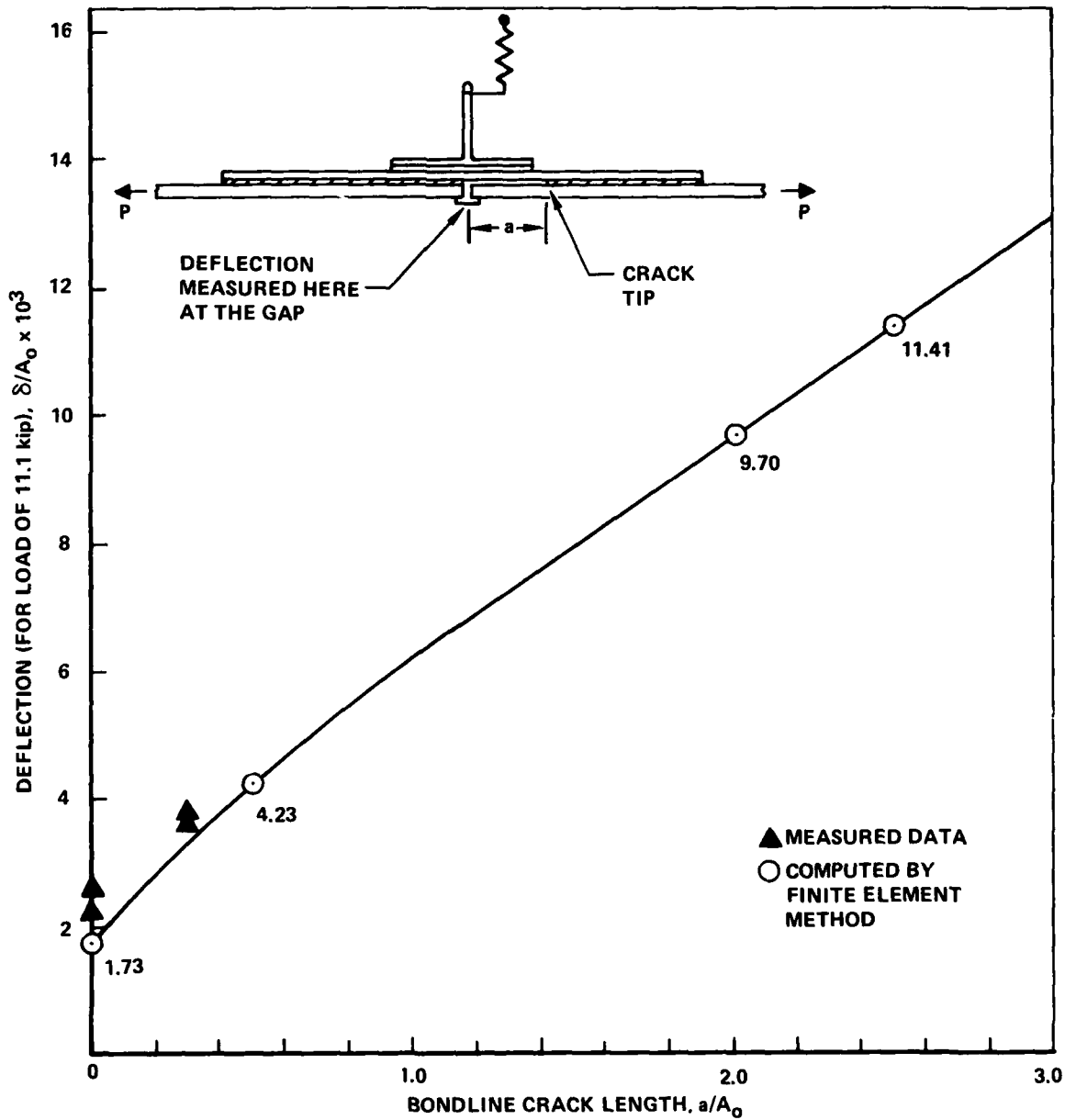
Figure 27. Gap-Opening Deflection of the SLJ Specimen for a Single
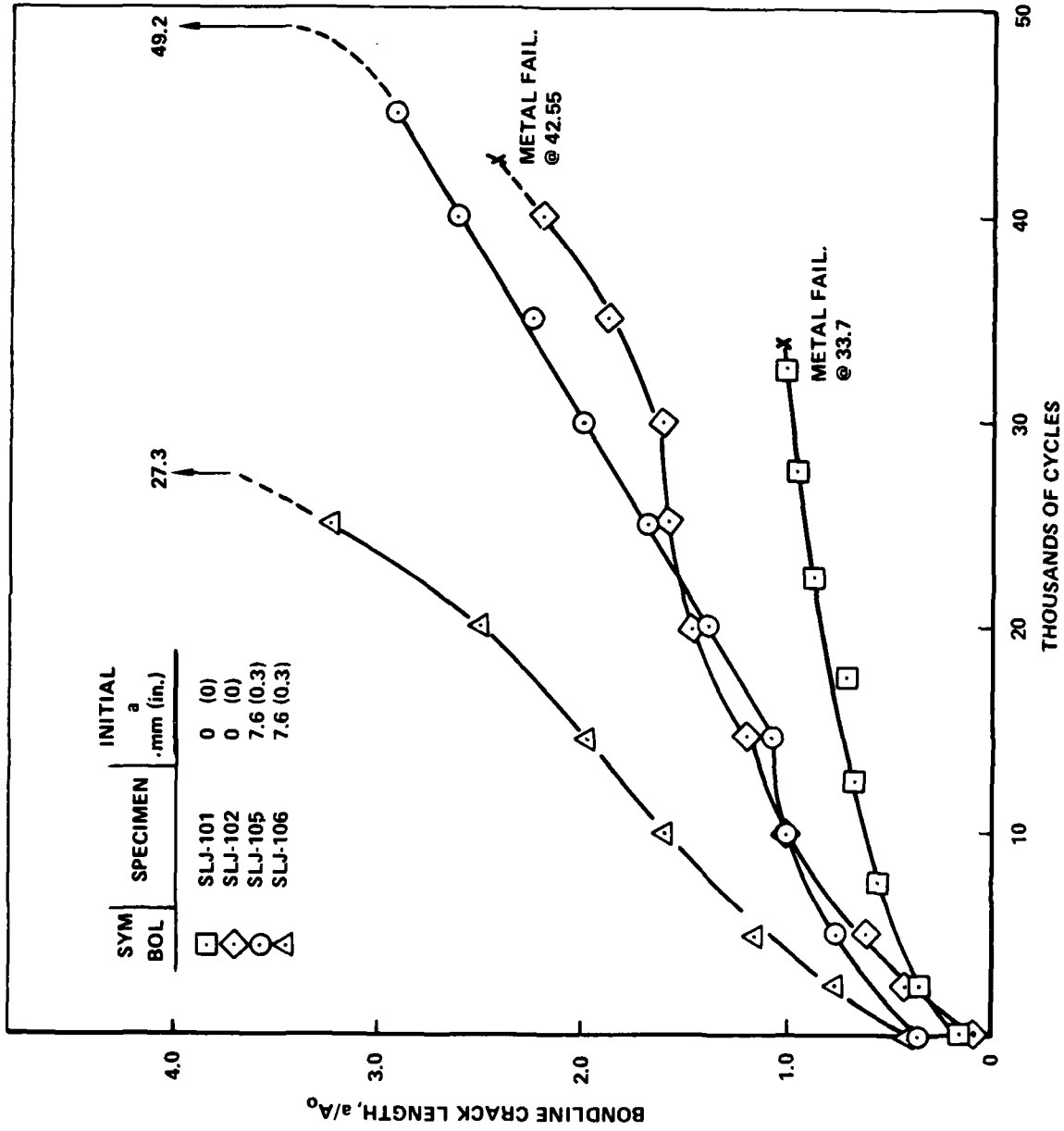Across-the-Width Bondline Crack

Figure 28. Crack Growth Data, Initial SLJ Specimens, FM-73m Adhesive

69

The primary failures of SLJ-105 and 106, however, were not within the adhesive layer, but at the interface between the primer and the metal. None of the baseline specimens had failed in this manner. Therefore, a fracture surface investigation was conducted to determine the extent and probable cause of the primer-to-metal-surface failure.

Each specimen has two skin-doubler bonded interfaces, only one of which became exposed when SLJ-105 and -106 failed, and neither of which was visible after metal failures in Specimens SLJ-101 and -102. The six remaining intact surfaces were examined ultrasonically for final crack profiles. Then a 25 mm (1 in.) wide strip of the skin was peeled away to confirm the ultrasonic measurements and examine the visible appearance of part of the fracture surface. In addition, Specimens SLJ-101 and -102 were chemically milled to expose patches of the adhesive for visual inspection.

Figures 29 through 32 show the results of the visual, ultrasonic, peel, and chemical mill examinations of the fracture surfaces for the four specimens. The ultrasonically detected flaws are outlined by dashed lines, chemical mill-detected by broken lines, and the others by solid lines.

The peel tests in Specimens SLJ-102, -105 and -106 revealed metal-primer interface cracks in the doubler on either side of the specimen centerline, where the hot water had access. Center-of-bond fatigue cracks occured at the end of the doublers, away from the hot water environment. The ultrasonic readings gave an adequate description of the crack profile but could not distinguish between interface and center-of-bond cracks.

The peel tests in Specimen SLJ-101 showed that both cracks were center of bond cracks. Note that da/dN was slowest in this specimen.

After the test, a drop of concentrated acid was placed on the external face of the doubler of Specimens SLJ-101 and -102 to remove the primer and expose the anodized metal surface. The golden hue indicating an anodized surface was obvious on SLJ-101. In contrast, little or no discoloration was present on SLJ-102. The test result was evidence of a problem with the anodize process affecting the doubler pieces on SLJ-102, -105 and -106 but not SLJ-101.
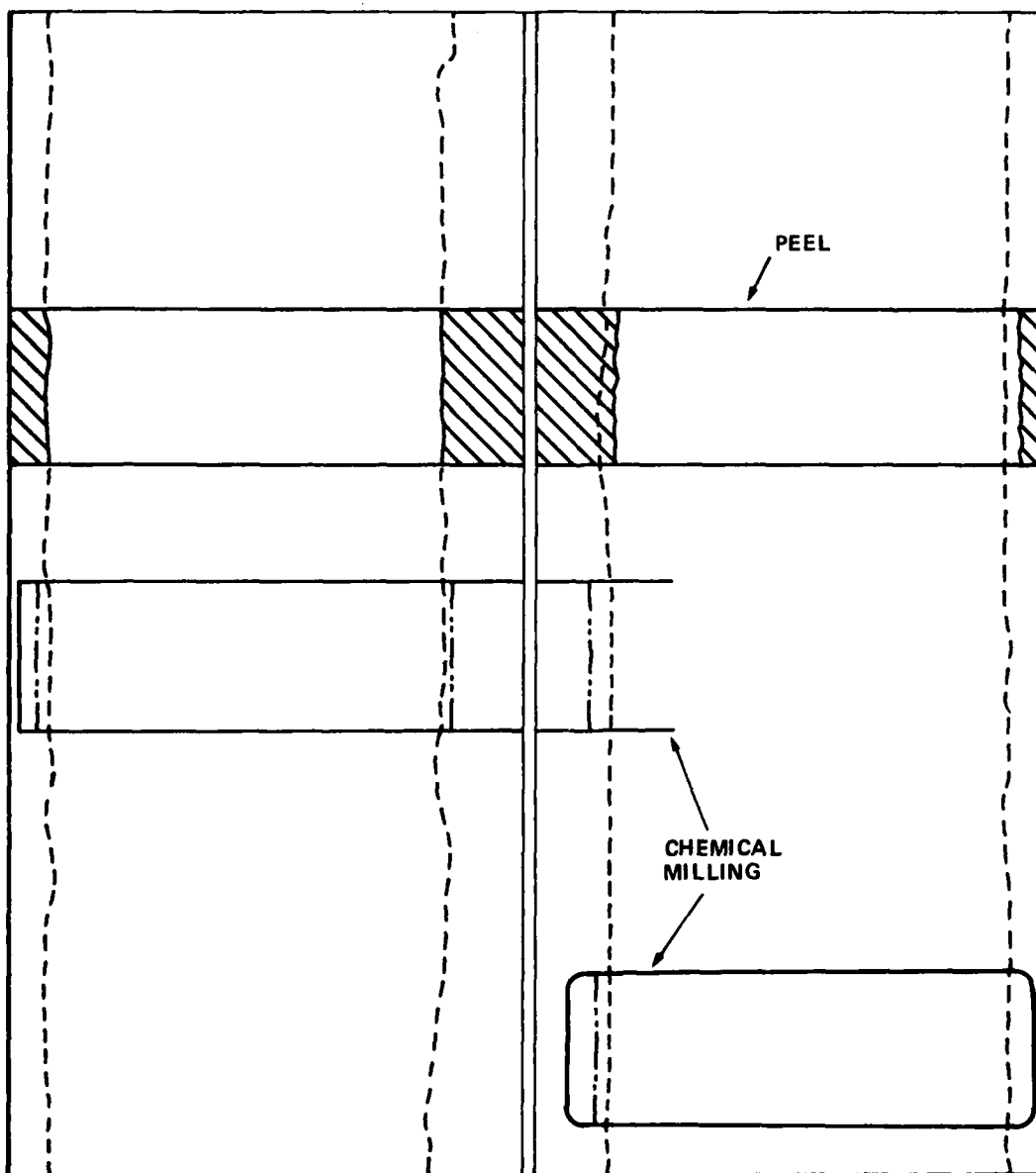
Figure 29. Fatigue Cracks on the Adhesive Surface of the Doubler on Specimen SLJ-101
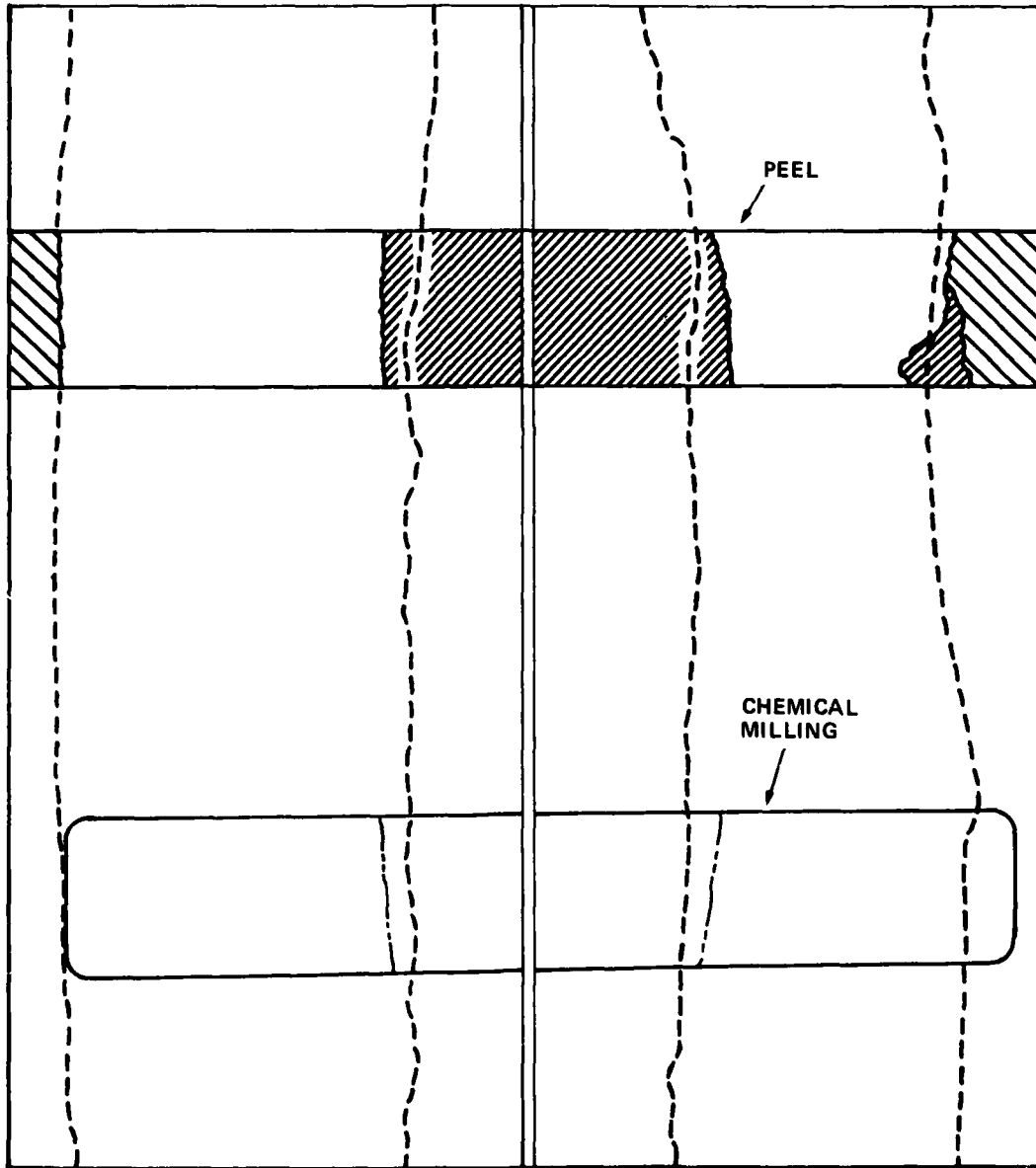
71

Figure 30. Fatigue Cracks on the Adhesive Surface of the Doubler on Specimen SLJ-102

- – – OUTLINE OF ULTRASONIC TRACE OF BONDLINE CRACK

CENTER OF BOND FATIGUE CRACK, VISUALLY OBSERVED

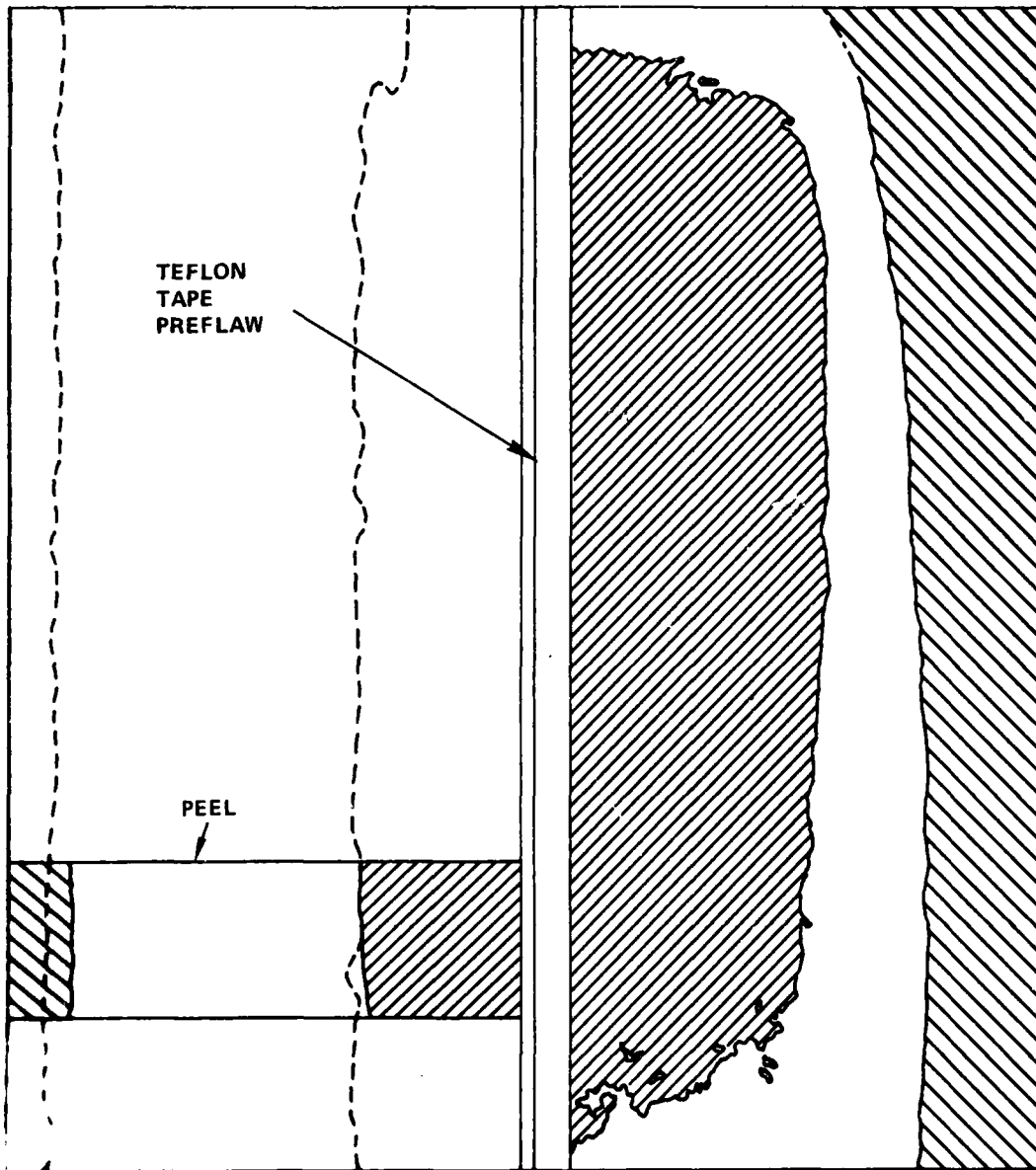METAL-PRIMER INTERFACE CRACK, VISUALLY OBSERVED

TEFLON
TAPE
PREFLAW

PEEL

racks on the Adhesive Surface of the
specimen CL -10

OUTLINE OF ULTRASONIC TRACE OF BONDLINE CRACK

CENTER OF BOND FATIGUE CRACK, VISUALLY OBSERVED

METAL-PRIMER INTERFACE CRACK, VISUALLY OBSERVED
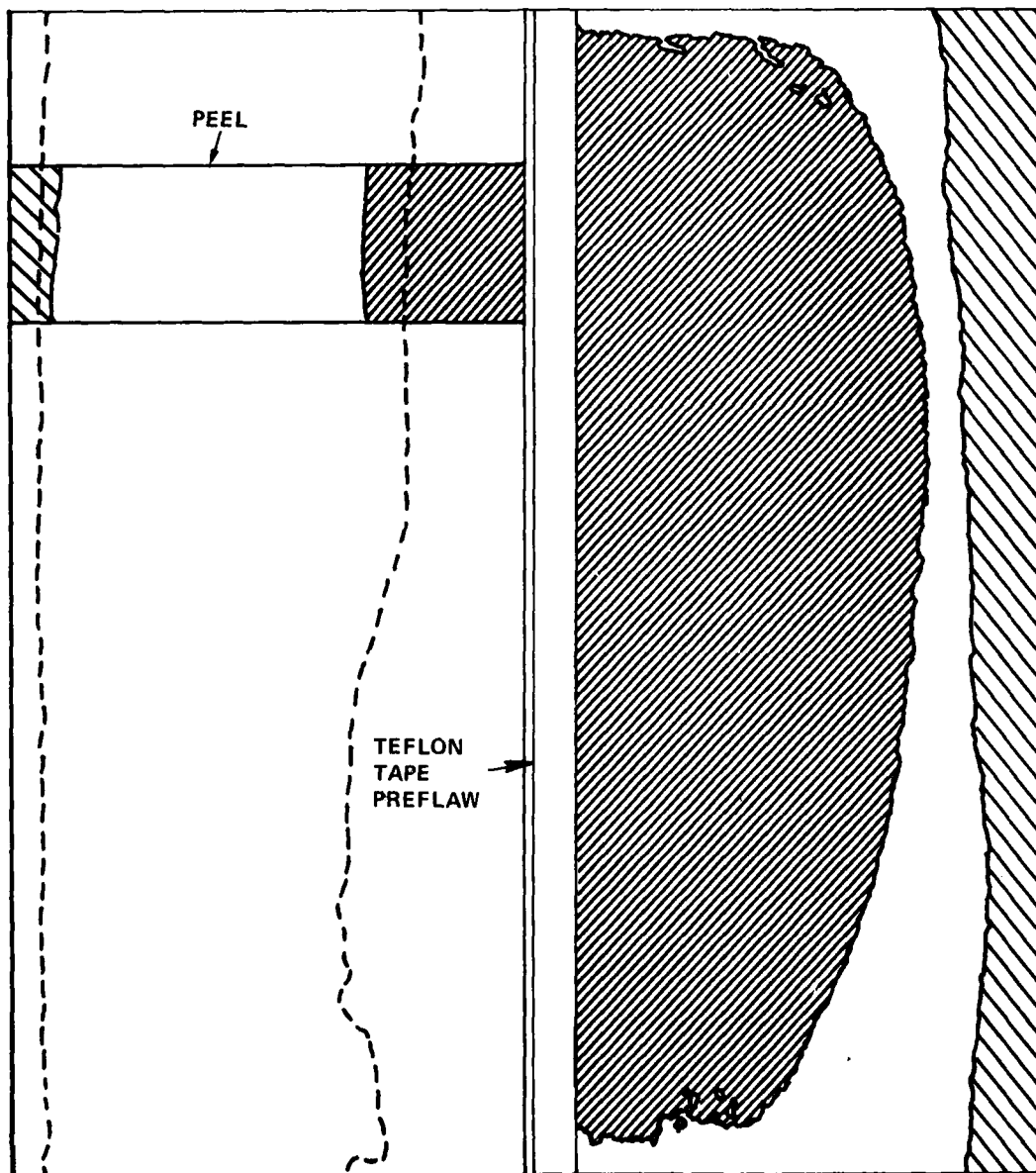
PEEL

TEFLON
TAPE
PREFLAW

Figure 32.   Fatigue Cracks on the Adhesive Surface of the
Doubler on Specimen SLJ-106

74

The purpose of testing the SLJ specimens was to check the fracture mechanics methodology for the fatigue growth of bondline flaws, using baseline data. All the baseline specimens had center-of-bond failures, even when tested in hot water. Therefore, the baseline data would be inapplicable to the interface failures of the SLJ specimens. For this reason, new specimens were prepared and the tests repeated.

1.3 Retests

New SLJ specimens SLJ-111 through 118 were machined to size and delivered to McDonnell-Douglas Company in Long Beach for surface preparation, priming, and bonding, using the PABST program system. A 7.6 mm (0.3 in.) deep, full-width initial defect was placed in each specimen, using Teflon tape just prior to layup and bonding.

Five of these specimens were tested. For Specimens SLJ-111 through 113, the test conditions were identical to those used previously. For Specimens SLJ-115 and 116, only the cyclic frequency was changed, f = 0.3 Hz instead of 3 Hz; otherwise, the test conditions were again identical.

Four of the five specimens failed in the bondline. The raw data, showing gap displacement (for the calibrated load of 63.4 kN (11.1 kip) versus time, are plotted in Figure 33.

The geometric mean crack growth life of the three SLJ specimens tested at 3 Hz was 84,200 cycles, compared to 54,900 for AF-55S (from Reference 1). At 0.3 Hz, the geometric mean life for FM-73m was 59,450 cycles, about 70 percent as long as at 3 Hz.

There is very little scatter in the deflection readings, which correspond to crack lengths. Furthermore, deflection readings for initial specimen SLJ-101, which apparently had the proper surface preparation and cracked within the adhesive up until the metal adherend failed, agree within a few percent with the deflection readings of Specimens SLJ-111 through 113.

A finite element analysis was used to relate the measured deflections to crack sizes. Four cracks were represented in the finite element model, one at
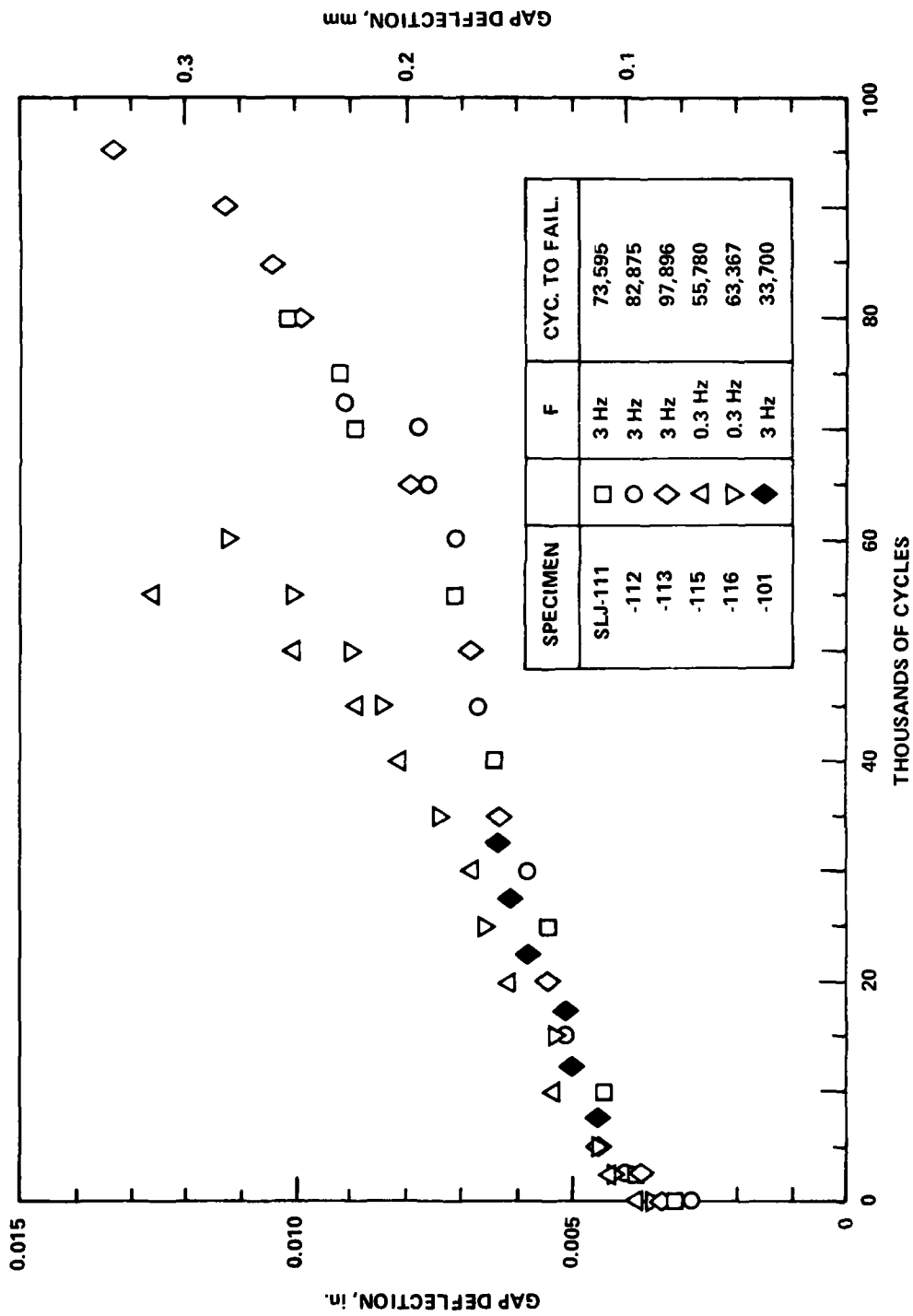
SPECIMEN		F	CYC. TO FAIL.
SLJ-111	□	3 Hz	73,595
-112	○	3 Hz	82,875
-113	◇	3 Hz	97,896
-115	△	0.3 Hz	55,780
-116	▽	0.3 Hz	63,367
-101	◆	3 Hz	33,700

Figure 33. Displacement—Time Plots for SLJ Retests

each end of the doubler and one on either side of the gap of the joint. The relative lengths of these cracks were estimated from the final crack sizes measured on broken specimens SLJ-111 through 113 after the tests.

As had been done with the initial specimens, the final crack sizes were measured by visual inspection of the exposed surfaces and ultrasonic inspection of hidden surfaces. To verify the ultrasonic measurements, 25 mm (1 in.) wide strips were peeled back to expose part of the hidden surfaces.

The fracture surface maps for Specimens SLJ-111 through 113 (tested at f = 3 Hz) are shown in Figures 34 through 36. The ultrasonically detected flaws are outlined by dashed lines and the others by solid lines. Near the gap of the joint where the cracks were accessible to the hot water, cracking occurred near the adhesive-primer interface, with some splitting of the primer. At the outer edges of the doubler, away from the hot water environment, cracking occurred within the adhesive. A distinct change in texture distinguished these fatigue cracks from the static fracture area caused either at the end of the test or when the strip was peeled back.

As shown in Figures 37 and 38, fracture surfaces of SLJ specimens 115 and 116 tested at f = 0.3 Hz contain substantial cracking between the primer and the anodized surface of the metal. This is a recurrence of the problem that occurred in the initial specimens, bonded at Lockheed and tested at f = 3 Hz. Recall that because of that problem, these new specimens were prepared at McDonnell-Douglas. It appears that the mode mix combines with the hot water-environment in these tests, attacking the interface and encouraging interface failures.

When the interface first failed on the initial specimens the problem was studied to decide if the major cause was specimen preparation or the severity of the test condition. The poor quality of the anodize on the initial specimens suggested a problem in the surface preparation of these particular specimens. However, having prepared the second set of specimens, using totally separate facilities, personnel and material batches, and having the same problem occur, leads now to the conclusion that the test condition is so severe that the problem can easily occur.

77

--- OUTLINE OF ULTRASONIC TRACE OF BONDLINE CRACK

[hatched box] CENTER OF BOND FATIGUE CRACK, VISUALLY OBSERVED

[hatched box] ADHESIVE – PRIMER INTERFACE CRACK, VISUALLY OBSERVED

PEEL

PEEL

TEFLON
TAPE
PREFLAW
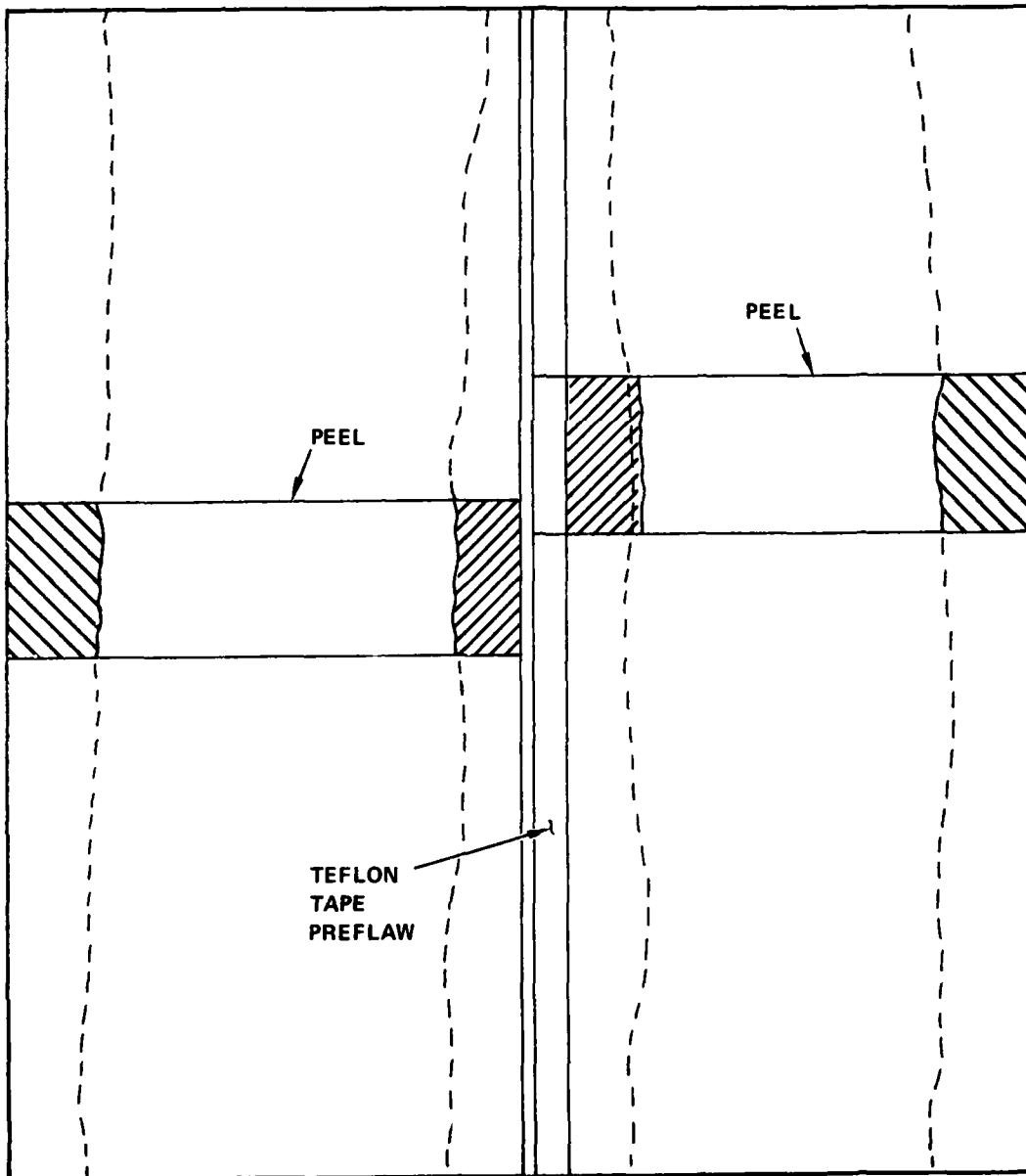
Figure 34. Fatigue Cracks on the Adhesive Surface of
the Doubler on Specimen SLJ-111

78

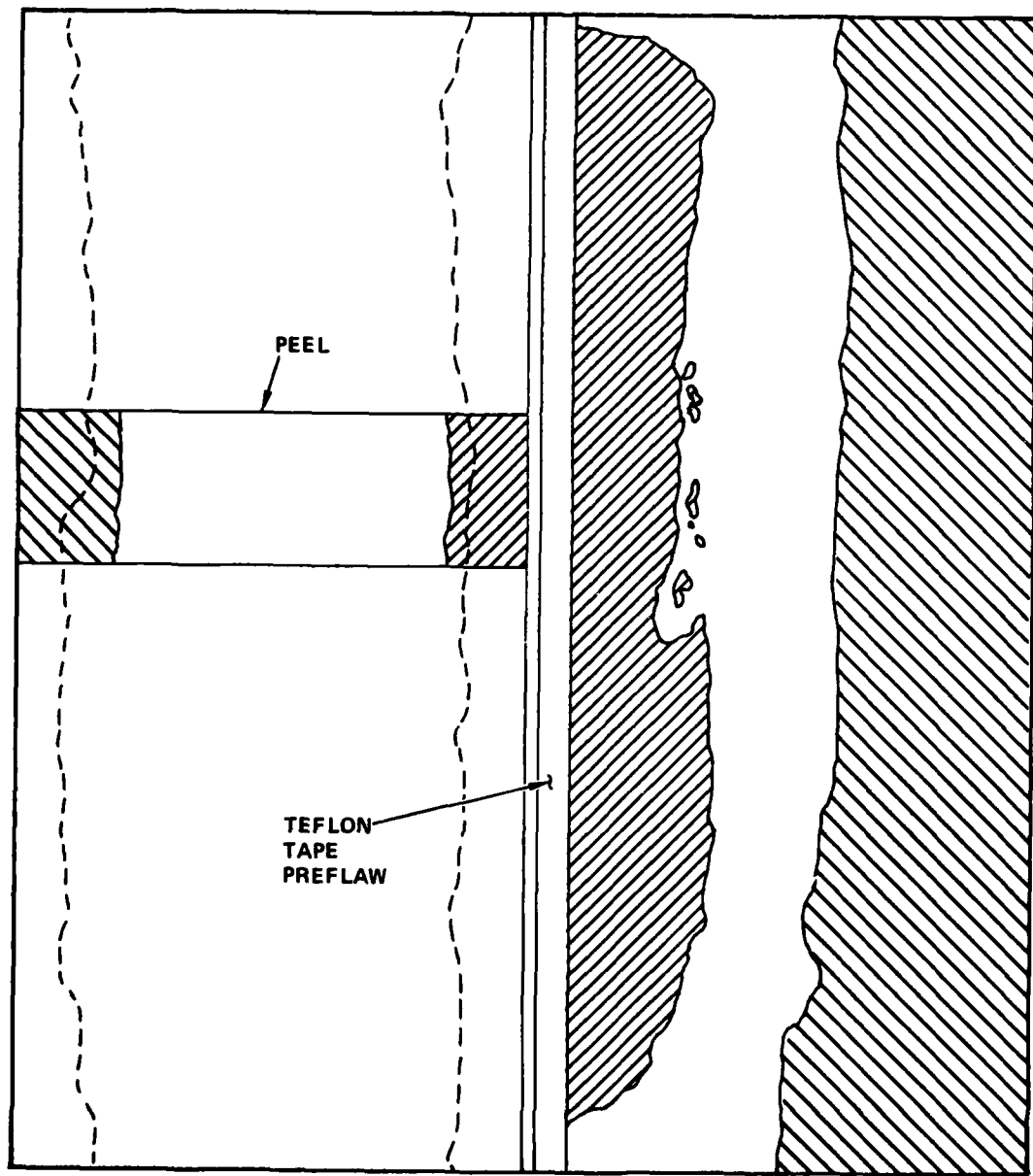Figure 35. Fatigue Cracks on the Adhesive Surface of the Doubler on Specimen SLJ-112

Figure 36. Fatigue Cracks on the Adhesive Surface of the
Doubler on Specimen SLJ-113

LEGEND:

- - - OUTLINE OF ULTRASONIC TRACE OF BONDLINE CRACK

CENTER OF BOND FATIGUE CRACK

ADHESIVE-PRIMER INTERFACE FATIGUE CRACK

PRIMER-METAL INTERFACE FATIGUE CRACK

CENTER OF BOND STATIC FRACTURE SURFACE
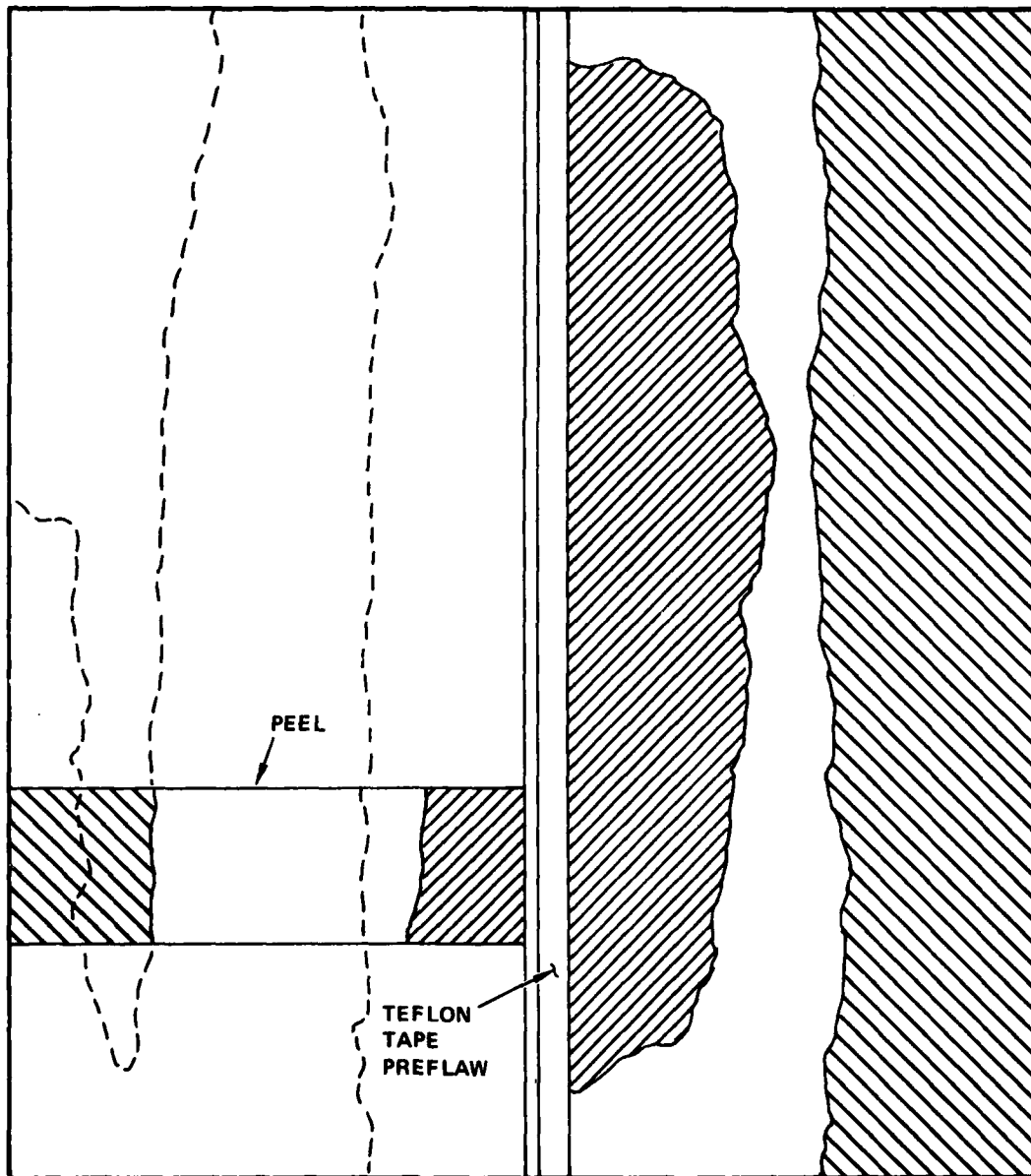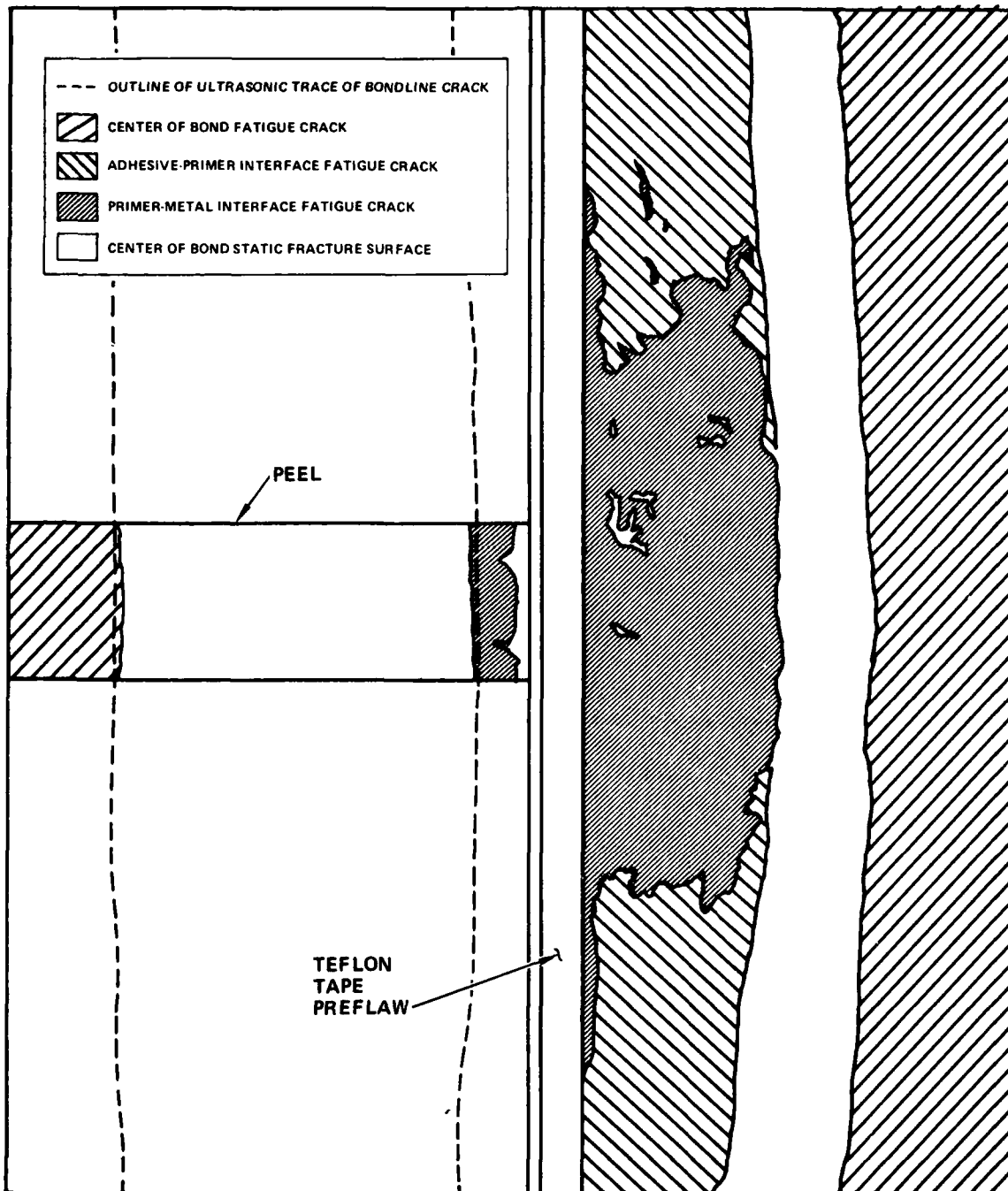
PEEL

TEFLON
TAPE
PREFLAW

Figure 37.   Fatigue Cracks on the Adhesive Surface
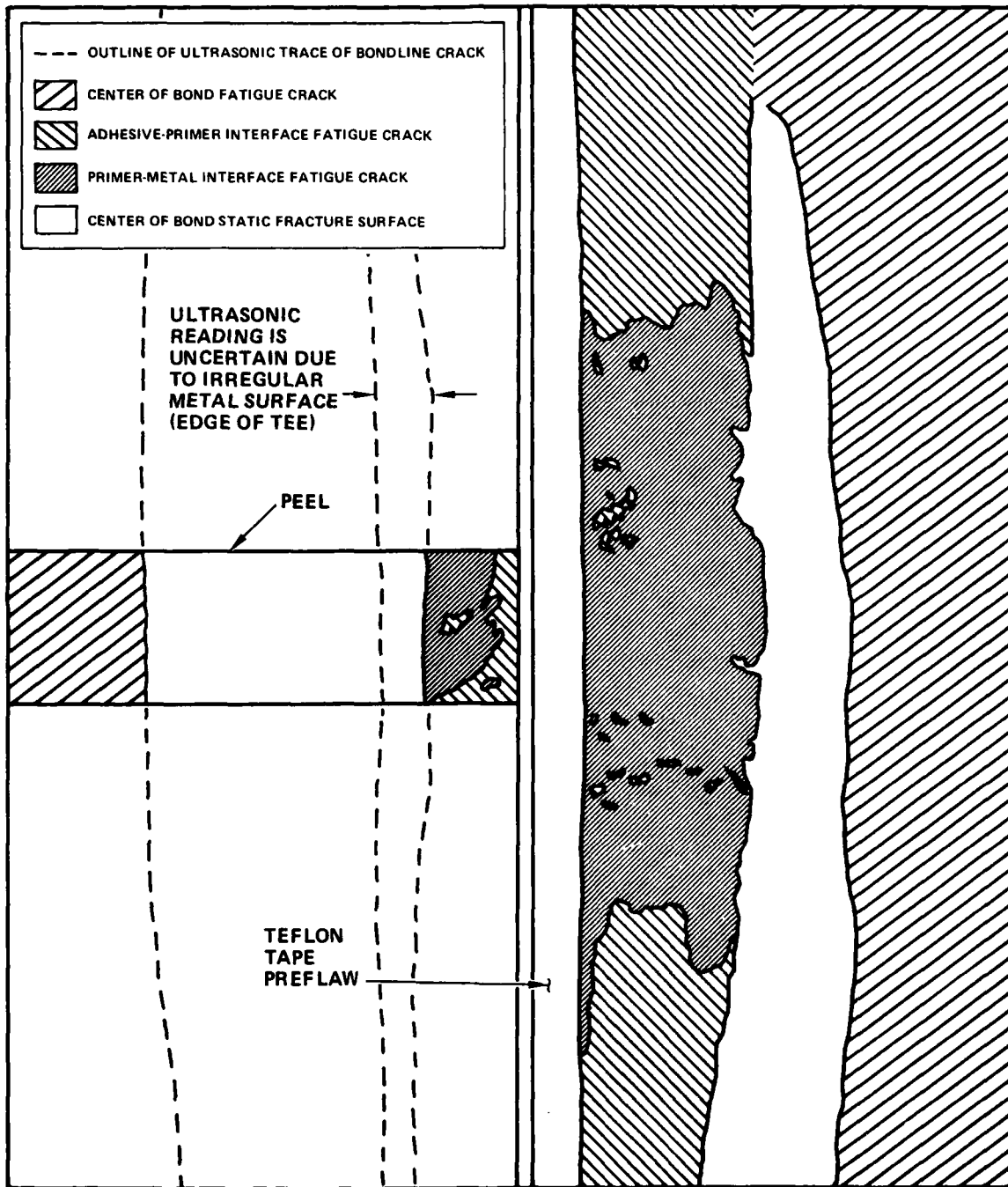of the Doubler of Specimen SLJ-115

81

Figure 38. Fatigue Cracks on the Adhesive Surface
of the Doubler of Specimen SLJ-116

Note that in all specimens, fatigue cracking occurred at all four edges. Figure 39 contains a side view sketch of the specimen identifying these four bondline cracks as a_1, a_2, b_1, and b_2. The final lengths of these cracks (length equals crack area divided by specimen width) are plotted as points in the figure. The linear fits provide values of a_2, b_1, and b_2 for any value of a_1 for any of the three specimens tested at f = 3 Hz, beginning with their initial values of zero when a_1 equals 7.6 mm (0.3 in).

A nonlinear finite element model used as an element in the theoretical analysis was also used as a tool in the experimental monitoring of crack length. Crack growth monitoring in the tests was accomplished indirectly by monitoring the opening deflection across the gap of the joint for a fixed load of 49.4 kN (11.1 kip). The nonlinear finite element model provided the relationship between crack sizes and the gap opening, shown as a solid line in Figure 40. The dashed lines in Figure 40 are the results of other non-linear finite element calculations using other assumed combinations of crack sizes, that are different from the empirical crack sizes of Figure 39.

2. ANALYSIS OF STRUCTURAL TESTS

2.1 Analysis Approach

The analytical procedure for estimating crack growth for the SLJ specimens was essentially the same as used in Reference 1 for the AF-55S adhesive specimen. As part of this procedure, two different methods were used to obtain strain energy release rates, an approximate estimation using equations from Reference 1, and an exact computation using the singular crack tip finite element. Correspondingly, two crack growth estimates were obtained and compared to one another and the data for specimens SLJ-111, 112, and 113.

The first step in the analytical procedure is a stress analysis of the entire specimen for a sequence of assumed bondline crack sizes. The specimen is geometrically nonlinear, so a nonlinear finite element program was used.

As seen in Figures 34 through 36, four bondline cracks grew simultaneously in the test specimens. These data on relative crack sizes, plotted
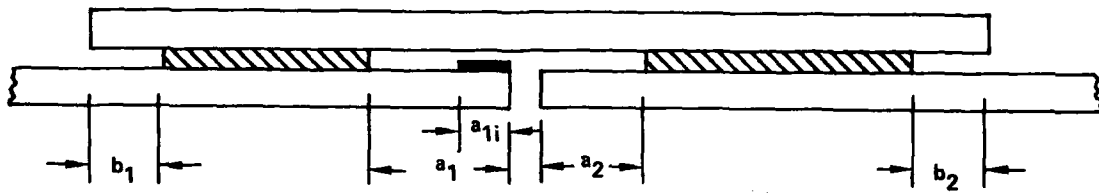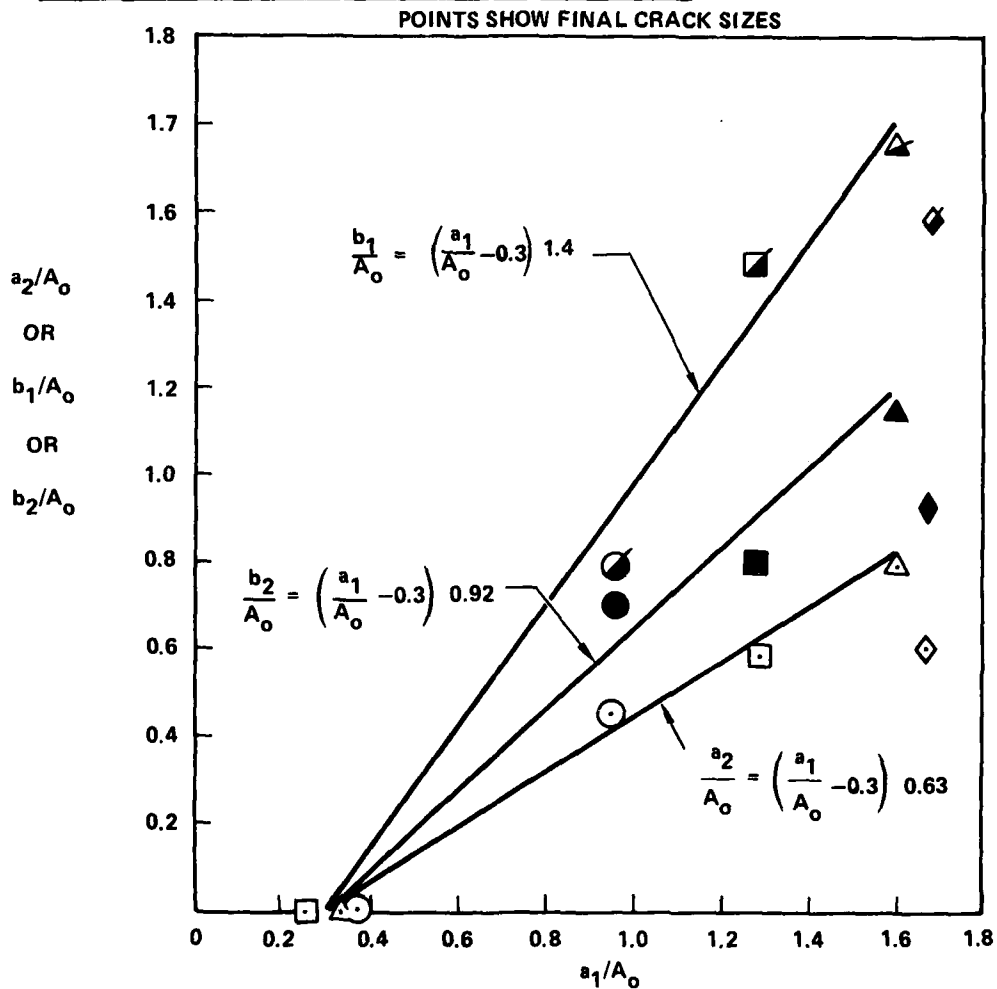
Figure 39. Final Crack Condition of Specimens SLJ-111 through 116 and Assumed Crack Length Relationships During Testing at 3 Hz
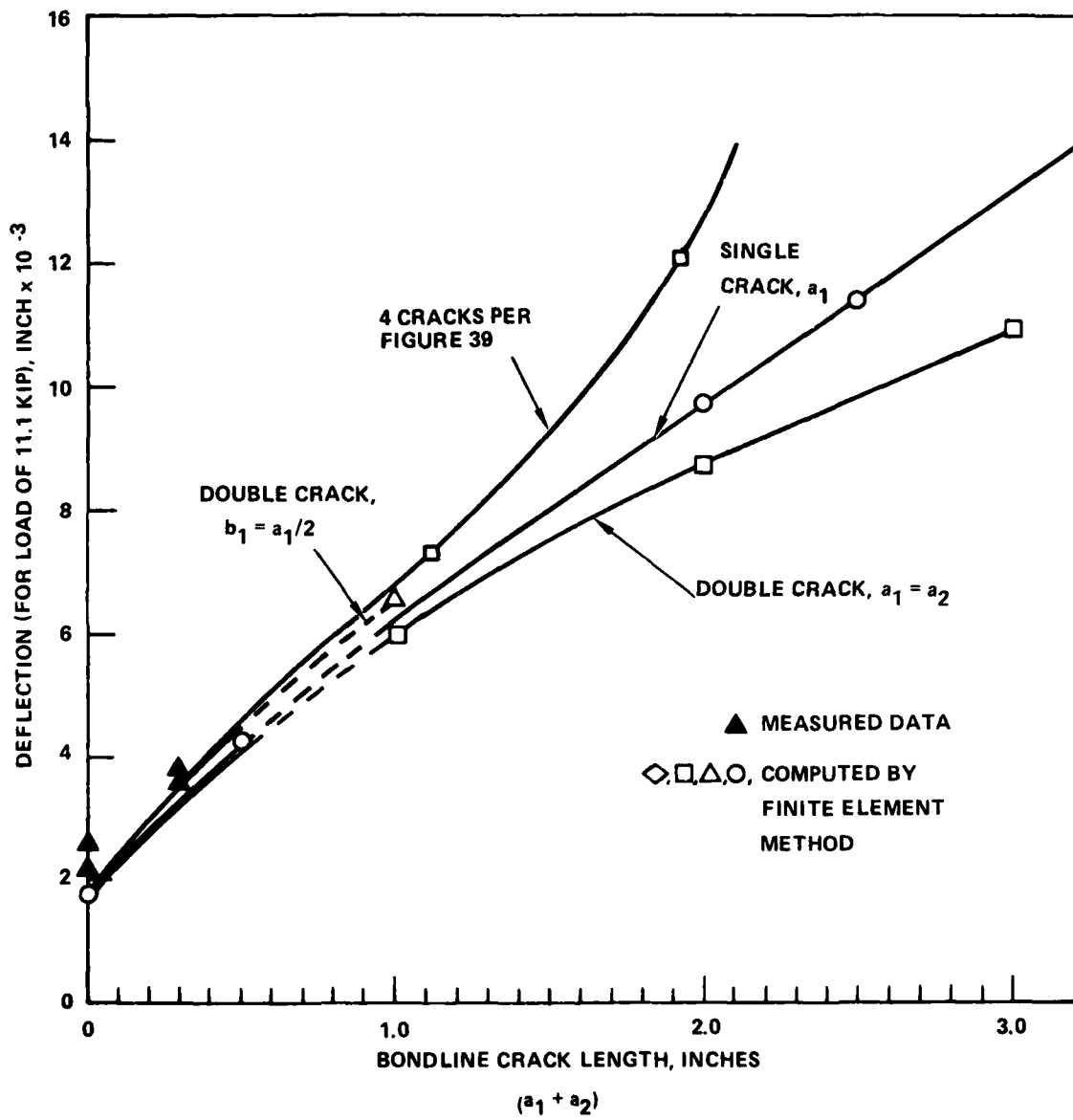
Figure 40. Deflection of the Thin-Adherend SLJ Specimen

in Figure 39, were used to define across-the-width crack sizes for the analysis. Three nonlinear finite element analyses were conducted, using the crack conditions summarized in Table 11. The initial and final crack sizes were known, but the relative crack lengths for the intermediate case had to be estimated by assuming the linear crack length relationships shown in Figure 39.

Internal forces, deformations, and bending moments were obtained from the nonlinear finite element analyses. These provided the basis for calculating $\mathscr{G}_I$ and $\mathscr{G}_{II}$, the components of strain energy release rate.

The approximate estimation of $\mathscr{G}_I$ and $\mathscr{G}_{II}$ utilizes the computed axial force P and bending moment M at the crack tip. Let $\bar{y}_o$, $(EA)_o$, and $(EI)_o$ be the location of the centroid and the tensile and bending stiffnesses of the skin-doubler laminate. Let $\bar{y}_2$, $(EA)_2$, and $(EI)_2$ designate the centroid location and tensile and bending stiffnesses of the doubler for cracks emanating from the gap between the skin pieces, or of the skin for cracks emanating from the edge of the doubler. Let b_N designate the width of the joint. For conciseness, define

$$Y = \sqrt{\frac{(EI)_2}{(EI)_o}} \tag{32}$$

The approximate expressions for $\mathscr{G}_I$ and $\mathscr{G}_{II}$, based on the algebraic analysis of the CLS specimen discussed in Section 2, are *

$$\mathscr{G}_I = \frac{2M^2 (1 - Y^2)}{7b_N (EI)_2} \tag{33}$$

---

*There is a component of $\mathscr{G}_{II}$ due to the axial force P and a component of $\mathscr{G}_{II}$ due to the induced bending moment M. The total $\mathscr{G}_{II}$ is not the sum of these two components, as erroneously stated in Reference 1, but rather the square of the sum of their square roots, as given in Equation (34). Equation (34) is correct because stresses acting in the same direction add linearly, and stress is proportional to the square root of strain energy release rate. It is important to reaffirm, however, that the total $\mathscr{G}$ is the linear sum of the components; i.e., $\mathscr{G} = \mathscr{G}_I + \mathscr{G}_{II}$.

86

TABLE 11.

ASSUMED CRACK SIZES FOR NONLINEAR FINITE ELEMENT ANALYSIS
OF THE SLJ SPECIMEN

| | Analysis Number | | |
	1	2	3
a_1/A_o	0.30	0.80	1.30
a_2/A_o	0	0.32	0.63
b_1/A_o	0	0.70	1.40
b_2/A_o	0	0.46	0.92

$$\mathcal{G}_{II} = \left\{ \sqrt{ \frac{P^2}{2b_N} \left[\frac{1}{(EA)_2} - \frac{1}{(EA)_o} - \frac{(\bar{y}_2 - \bar{y}_o)^2}{(EI)_o} \left(\frac{1-\gamma}{1+\gamma} \right) \right] } + \sqrt{0.75\,\mathcal{G}_I} \right\}^2 \qquad (34)$$

For the exact computation of $\mathcal{G}_I$ and $\mathcal{G}_{II}$, a linear finite element model of each crack tip neighborhood can be constructed, containing the singular crack tip finite element. The finite element modeling procedure follows that described for the CLS specimen in Subsection 1.2 of Section II. Each crack tip region model is similar to that shown in Figure 3 of Section II. The boundary conditions are derived from the internal forces, moments, and deflections of the nonlinear model of the entire specimen. Geometric linearity is achieved in the crack tip region model by selecting a sufficiently small length-to-thickness ratio. This linearity allows the use in the finite element model of the singular crack tip finite element, which contains the correct theoretical elastic stress field in the crack tip neighborhood and provides $\mathcal{G}_I$ and $\mathcal{G}_{II}$ directly as output.

Using $\mathcal{G}_I$, $\mathcal{G}_{II}$, and $\mathcal{G}$ as estimated approximately or computed exactly, the effective strain energy release rates for fatigue crack growth can be calculated from Equation (26), using $m = 1.5$ for cracks a_1 and a_2 which were

accessible by the hot water, and m = 1.0 for cracks b_1 and b_2 which were
outside the hot water immersion tank. Equation (30) relates $\Delta \mathscr{G}$ to the crack
growth rate (da/dN) for both environments. Thus, by integration of da/dN,
the crack growth computations can be completed and compared to the experimental
results.

2.2 Analytical Results

Strain energy release rates were calculated by both methods for the
two cracks on the precracked side of the doubler. Figure 41 shows the cal-
culated effective strain energy release rates at the tip of the primary
crack, a_1, and a secondary crack, b_1. The open points were obtained by the
approximate analysis method using Equations (33) and (34). The closed
points were computed more exactly using the special crack tip finite element.

The approximate and exact analyses yielded substantially different
results. First, the approximate analysis for primary crack a_1 indicated a
slight drop in $\Delta \mathscr{G}$ followed by a sharp increase as the crack became longer.
In contrast, the exact analysis showed $\Delta \mathscr{G}$ to continually decrease for crack
a_1. Secondly, (except for a_1 at crack sizes above $a_1 + b_1$ = 38 mm (1.5 in))
the approximate strain energy release rates tend to be lower than the exact
results by 40 to 80 percent. This difference corresponds to underestimates
of crack growth rate by factors ranging from 5 to 17 when the approximate $\mathscr{G}$-
estimates are used.

The crack growth rates were estimated for cracks a_1 and b_1 using the
exact strain energy release rates plotted in Figure 41. Figure 42 shows a
comparison of the estimate with the crack growth data from Specimens SLJ-111,
112, and 113. The solid line is the analytical estimate and consists of the
sum of the dashed lines, which were calculated separately for the individual
cracks a_1 and b_1, out to a preselected final total crack length of
$a_1 + b_1$ = 68.6 mm (2.7 in.), which was about average for the three test
specimens.

2.3 Discussion of Analytical Results

Good agreement is shown in Figure 42 between the crack growth data and
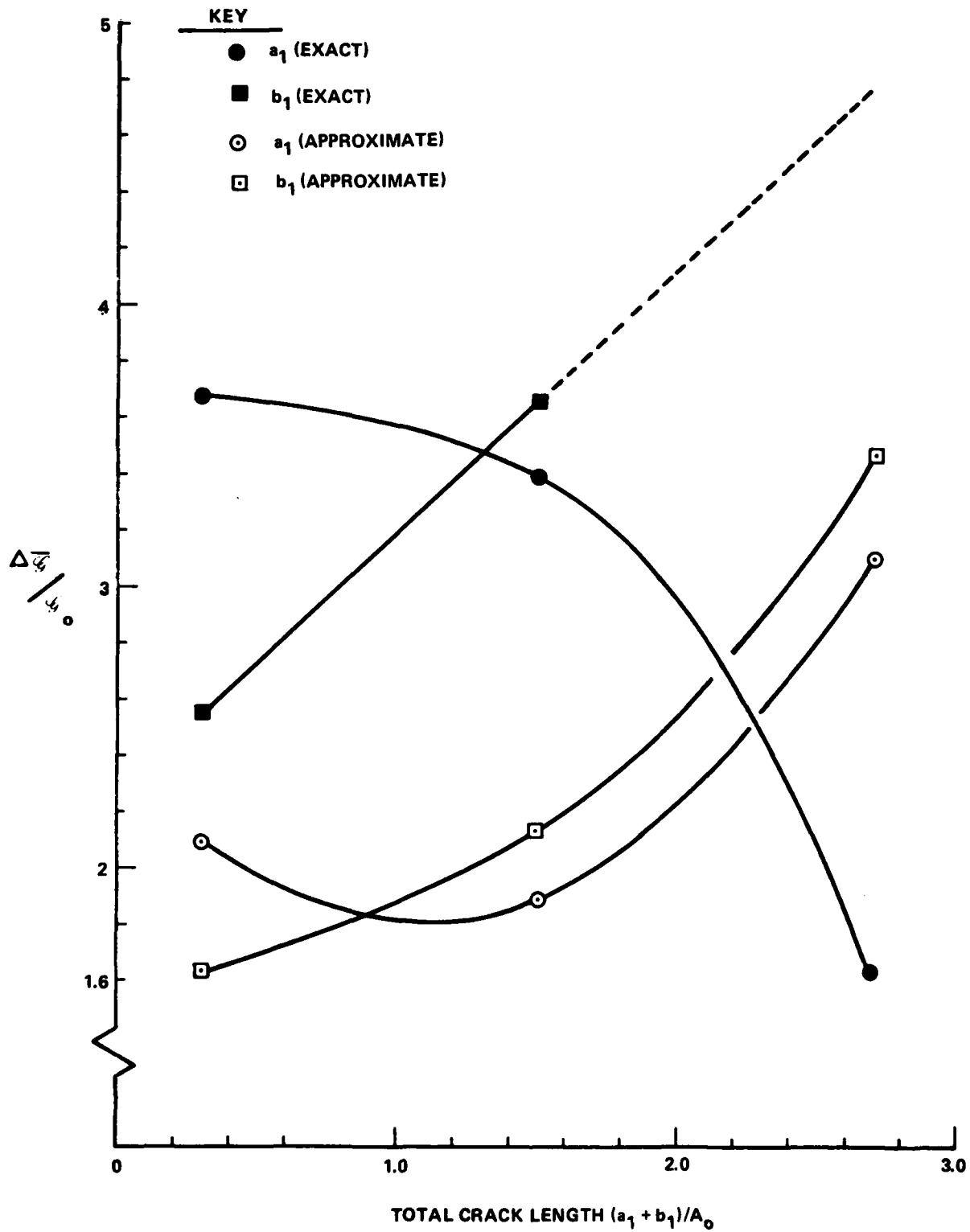the analytical estimate. Not only is there close agreement in the growth

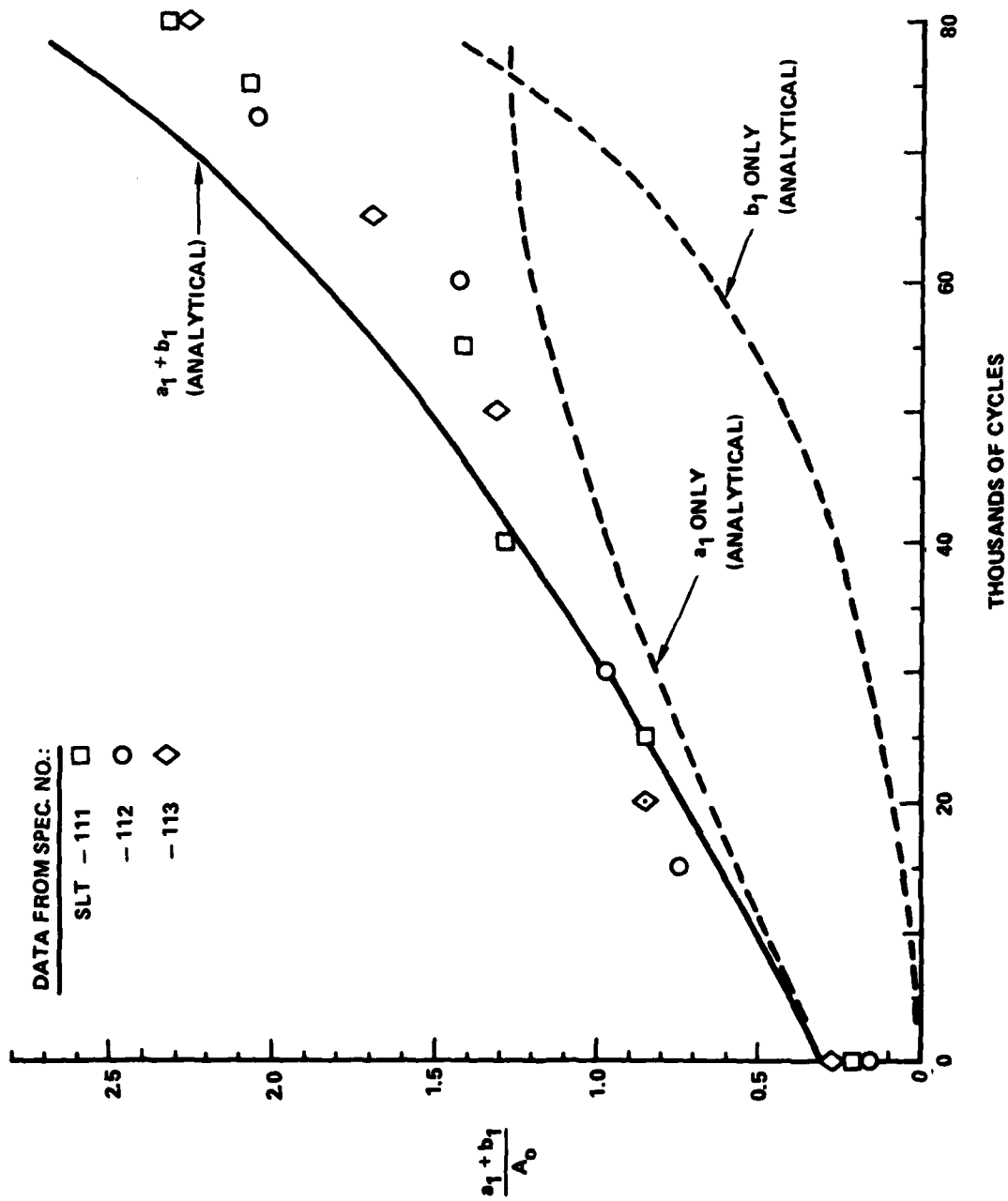Figure 41. Effective Strain Energy Release Rates for the SLJ Specimen

Figure 42. Crack Growth Data Comparison for Specimens SLJ-111, -112, and -113

rates of the total crack $a_1 + b_1$, but also for the calculated final relative crack lengths a_1 and b_1. For the preselected final total length of $a_1 + b_1 = 68.6$ mm (2.7 in.), the data-fit line in Figure 39 dictates that $a_1 = 33$ mm (1.3 in.) and $b_1 = 35.6$ mm (1.4 in.). The analytical estimates of a_1 and b_1 are within 1.6 percent of those experimental values.

This verification of linear elastic fracture mechanics theory is encouraging. However, the failure of the approximation equations (33) and (34) to adequately estimate strain energy release rate is unfortunate in view of the expense and complexity of having to use the crack tip finite element. Further study is needed to understand why the approximate method is so inaccurate and to develop more general approximation techniques.

In Reference 1, the approximate calculation method was used to predict crack growth lives. The predicted growth rates were about half the experimental growth rate values.

Here, several new developments were introduced into the approximate analysis approach for the SLJ specimens bonded with FM-73. These included

- Use of improved baseline da/dN equations

- Consideration of multiple cracking

- Correction of an error in the approximate equation for $\mathcal{G}_{II}$.

Although intended to improve the reliability of the analytical procedure, these developments led to a much larger discrepancy between actual and estimated crack growth rates when the approximate method of estimating $\mathcal{G}_I$ and $\mathcal{G}_{II}$ was used, necessitating the second, more exact, finite element analysis. Had these new developments been implemented for the AF-55S specimens, the error of the approximate method would also have been much larger than that reported in Reference 1.

The crack growth estimates for FM-73m specimens are not really predictions, because they were carried out after the tests had been completed. Had they been obtained prior to testing, one detail in the procedure would have changed, requiring more computer calculations but not substantially changing the analytical result. The procedure change would have resulted

from the lack of prior knowledge of relative sizes of the four cracks a_1, a_2, b_1, and b_2. Only initial crack sizes would be known a priori.

The rigorous analysis would begin with a nonlinear finite element computation for the specimen in its initial condition. Then $\Delta \overline{\mathscr{G}}$ would be calculated for all four cracks (a small crack, perhaps 0.8 mm (0.03 in.) would be assumed at initially uncracked locations) and the relative crack growth rates estimated. Based on these relative rates, relative sizes of the cracks after an increment of growth would be selected for the next complete analysis. This calculation process would be repeated until the static failure condition is reached.

The rigorous computation method requires a large number of finite element runs. The crack size assumptions made in the above analysis reduce the computational efforts without changing the crack growth rate estimates by more than a factor of about 1.5. This factor is estimated based on comparisons between the assumed relative crack sizes shown in Figure 39 and the analytical crack sizes shown in Figure 42.

SECTION V

CONCLUSIONS AND RECOMMENDATIONS

Linear elastic fracture mechanics methods can provide reliable estimates of fatigue growth rates of bondline cracks in structural joints. The reliability of the crack growth estimates depend upon the reliability and applicability of the baseline data and the structural analysis of the joint. The following guidelines were used in this program and are recommended:

- The bonding methods and materials for the baseline test specimens should be identical to those of the structure. If the structure consists of large area bonds, then the baseline specimens should be machined from large area bonded panels.

- The strain energy release rate analysis of the baseline specimens should be accurately known.

- The mode mix ratios ($\mathcal{G}_I/\mathcal{G}$) that are tested should cover the mode mix range of the structure to be analyzed. If possible, three levels of $\mathcal{G}_I/\mathcal{G}$ should be tested to increase the accuracy of interpolation

- The environment, cyclic frequency, and stress ratio should cover the range of anticipated fatigue service usage for the structure. If the structure will be subjected to spectrum loading, spectrum testing of the baseline specimens is recommended, since little is known about load interaction effects in structural adhesives.

- The method used to compute the strain energy release rate components ($\mathcal{G}_I$ and $\mathcal{G}_{II}$) for each bondline crack in the structure should be accurate and should include the consideration of potential multiple cracks and their interaction effects.

The four baseline fracture mechanics specimens used in this effort are recommended for general use in obtaining baseline data for large-area bonded structure. These are the long Cracked Lap Shear (CLS) specimen loaded in axial tension, the CLS specimen in four-point bending, the Mode I Width Tapered Beam (WTB) specimen, and the Mode I Uniform Double Cantilever Beam (UDCB) specimen. Development efforts with these specimens resulted in the following conclusions:

93

- The closed-form expressions for $\mathscr{G}_I$ and $\mathscr{G}$, developed in Reference 1, for the CLS specimen loaded axially or in uniform bending are accurate, since they agree closely with the results of an exact finite element analysis.

- Four-point bend fatigue tests of the CLS specimen provide data at an intermediate value of $\mathscr{G}_I/\mathscr{G}$ (0.57) between that of the pure Mode I specimen (1.0) and the axially loaded CLS specimen (0.2). The specimen is simple to make, the load requirements are low, the $\mathscr{G}$-analysis for pure bending is exact, and the data are valuable for improving the interpolation equation for mode mix effects.

- Mode I specimens machined from large-area bonded panels can have different da/dN properties than the Contoured Double Cantilever Beam (CDCB) specimen (see Figure 8). The CDCB specimen should not be used as a baseline specimen for large-area bonded structures.

- Compliance calibration of the Width Tapered Beam (WTB) specimen verifies that $\mathscr{G}_I$ is nearly constant for the configuration shown in Figure 5. There appears to be a slight dependence on crack length, negligible for most purposes, as shown in Figure 7. This dependence could be virtually eliminated by moving the loading holes, but to do so would require a recalibration and is not recommended.

- The variable $\mathscr{G}$ Uniform Double Cantilever Beam (UDCB) specimen is a viable alternative to the WTB specimen for da/dN testing. The two specimen configurations produced the same da/dN curve (Figure 11). Crack tunnelling, which makes the crack length somewhat ambiguous, can be minimized because the UDCB specimen need not be as wide as the WTB. Consistent da/dN data for FM-73m adhesive were obtained on the UDCB specimens immersed in hot water, whereas WTB data suffered from high scatter in these tests.

Using the baseline specimens and test procedures developed, fracture mechanics data were obtained for the selected PABST adhesive, FM-73m. These data enable a number of quantitative conclusions about the fracture mechanics properties of this adhesive:

- Static fracture mechanics properties of FM-73m are similar to those measured in Reference 1 for AF-55S. Average $\mathscr{G}_{IC}$, measured in 36 tests, was 2.38 kJ/m^2 (13.58 lb/in). Measurements of the Mode I component of $\mathscr{G}_c$ in increasing load tests of a CLS specimen were within 11 percent of this value. Limited sustained load testing in 333°K (140°F) water indicates that the crack growth resistance of FM-73m is as good or better than that of AF-55S. Because these static properties are so good, the usual critical condition for this adhesive (like that of AF-55S) will tend to be fatigue crack growth.

- The following empirical expression for effective strain energy release rate can accurately account for mixed-mode loading at R = 0.1 and f = 3 Hz:

$$\overline{\Delta\mathcal{G}} = \exp\left(-m\ \frac{\mathcal{G}_I\ \mathcal{G}_{II}}{\mathcal{G}^2}\right)\Delta\mathcal{G} \tag{34}$$

where m = 1.0 in laboratory air and m = 1.5 immersed in 333°K (140°F) deionized water. When da/dN is plotted against $\overline{\Delta\mathcal{G}}$, the data from all baseline specimens coincide, regardless of mode mix. Equation (34) is strictly empirical, so for other adhesives or test conditions a somewhat modified definition may apply.

- The da/dN properties of AF-55S and FM-73m (as measured on CLS and WTB specimens machined from large-area bonded panels with 9.5 mm (3.76 in.) aluminum adherends) in laboratory air at R = 0.1 and f = 3 Hz are all identical and can be fitted with the single da/dN curve as shown in Figure 16.

$$\frac{da/dN}{a_o} = 0.0325\left(\overline{\Delta\mathcal{G}}/\mathcal{G}_o\right)^{4.86} \tag{35}$$

This equation also applies for FM-73m in 333°K (140°F) water.

- As observed in Reference 1, the slope of the da/dN curve is steep compared to that of cracks in metallic materials. This means that small changes in stress cause large changes in crack growth rate. Furthermore, small errors in estimated stress cause large errors in estimated crack growth life, which makes it difficult to design for finite life. Crack growth threshold values can be estimated by extrapolating the linear data fits of log(da/dN) versus log($\overline{\Delta\mathcal{G}}$) down to a value of 1 mm per year (1 in. per 25 years). The da/dN scatter detracts from the confidence level of these estimates, since the best-fit line is not always clearly defined. Nevertheless, this procedure gives usable threshold values, by virtue of the steepness of slope of the da/dN curves.

- An apparent interaction between the effects of test duration and immersion in 333°K (140°F) water on da/dN was discovered to be present in FM-73m. In the short term, the hot water immersion had anywhere from a small beneficial effect to a detrimental effect on da/dN. In long-term tests, immersion in hot water had a beneficial effect, decreasing the da/dN compared to its corresponding value in laboratory air. Although these effects are not fully understood, FM-73m is clearly superior to AF-55S in resisting fatigue crack growth in 333°K (140°) water.

95

The crack growth testing and analysis of preflawed structural Single Lap Joint (SLJ) specimens led to the following conclusions concerning failure surfaces, quantitative crack growth results, and crack growth analysis capabilities for bondline cracks in structural adhesive joints:

- Mixed-mode fatigue loading during immersion in hot water tends to drive the cracks from within the adhesive layer toward the interface. Twice in the structural Single Lap Joint (SLJ) fatigue testing, the portion of the failure surface that had been immersed in hot water failed at the primer-metal interface. In the first set of specimens, fabricated at Lockheed and tested at $f = 3$ Hz, the failure mode was tentatively blamed on the fact that the phosphoric acid anodizing was inadequate. The second set of specimens appeared to be properly anodized by PABST program personnel at McDonnell-Douglas, and at $f = 3$ Hz, no primer-metal interface cracking occurred. However, the last two specimens from the second set, tested at $f = 0.3$ Hz, failed primarily near or at the metal-primer interface in the water-immersed region. The causes and consequences of these interface failures need to be investigated further.

- Multiple cracking occurs in the SLJ specimens. There were cracks emanating from all four transverse edges on all specimens bonded with FM-73m, even though no more than one initial Teflon tape preflaw was introduced.

- Scatter was minimal in the data obtained from SLJ specimens, especially in the specimens fabricated at McDonnell-Douglas. Test lives for these specimens (in cycles to failure) were shorter at $f = 0.3$ Hz than at $f = 3$ Hz by a factor of 0.7. The lives of these FM-73m specimens were longer by a factor of 1.5 than the corresponding lives of specimens bonded with AF-55S (Reference 1).

- Crack growth in SLJ specimens was monitored by the compliance technique used in Reference 1. In addition, unexposed bond surfaces of all specimens were inspected ultrasonically before and after testing, and a 25 mm (1 in.) wide strip of one adherend was peeled after testing to expose part of each unfailed surface to determine final crack configurations. There is a clear difference between the visual appearance of a fatigue-induced crack surface in FM-73m and one caused by monotonic loading.

- A number of improvements were introduced into the prediction methodology used in Reference 1. Baseline Mode I data from large-area bonded WTB specimens was used, rather than from CDCB specimens. The interpolation equation was improved by including an intermediate mode mix baseline fatigue test condition, the four-point bond test of the CLS specimen. The nonlinear finite element analysis of the specimen

96

and the calculation of crack growth simulated the true multiple cracking conditions. The strain energy release rates were estimated two ways, indirectly from algebraic approximations relating $\mathscr{G}_I$ and $\mathscr{G}_{II}$ to the crack tip bending moments and axial loads, and directly by use of a supplementary linear finite element model of the crack tip region in which $\mathscr{G}_I$ and $\mathscr{G}_{II}$ are the exact output from a special singular crack tip finite element. The approximate method of estimating $\mathscr{G}_I$ and $\mathscr{G}_{II}$ proved unreliable and led to an order of magnitude error in the predicted crack growth rates. The direct method with the singular crack tip finite element is accurate, but it may be too costly for general design use, especially for cases requiring growth rate predictions for interacting multiple cracks. Research is recommended to develop improved approximate methods for estimating strain energy release rates for bondline cracks in structures.